2018

Testing the Capability of Close-Range Photogrammetry to Document Outdoor Forensic Scenes With Skeletal Remains Using Mock Scenarios

Kevin Gidusko
University of Central Florida

TESTING THE CAPABILITY OF CLOSE-RANGE PHOTOGRAMMETRY TO DOCUMENT OUTDOOR FORENSIC SCENES WITH SKELETAL REMAINS USING MOCK SCENARIOS

by

KEVIN A. GIDUSKO
BA Anthropology University of Central Florida, 2011

A thesis submitted in partial fulfillment of the requirements
for the degree of Master of Arts
in the Department of Anthropology
in the College of Science
at the University of Central Florida
Orlando, Florida

Summer Term
2018

Major Professor: John J. Schultz

ABSTRACT

More rigorous methodological protocols are needed to document outdoor forensic scenes containing skeletal remains. However, law enforcement protocols rarely provide specific guidelines for processing these scenes. Regardless, the need to preserve contextual information at crime scenes is of paramount importance and it is worth exploring new technological applications that will allow for better documentation. Close-range photogrammetry (CRP) is one option for outdoor scene documentation, more prominently utilized in archaeological contexts, that may provide forensic archaeologists with a tool to better document these scenarios via 3D modeling. To test the efficacy of CRP as documentation tool three mock scenarios representing common outdoor scenes were created using faux osteological material: a close scatter of osteological remains in a pine flatwood setting, a wide scatter of osteological remains in the same setting, and the partial excavation of skeletonized remains. Images were collected using a digital camera and processed using Agisoft Photoscan Professional. A series of variables were tested in successive iterations of data capture for each scenario to determine best practices for overall accuracy: camera images captured by hand versus fixed to a tripod, scale bar positioning, and number of images captured. Accuracy was determined via final root mean square error values and through a comparison between real-world to virtual measurements. Results show that CRP is a cost and time-effective method of documenting contextual data at a scene via the creation of 3D models and scaled orthomosaic images. This method is most useful for the documentation of excavations owing to the controlled and contrasted sub-surface in comparison to the subject material. The two scatter scenarios offered additional challenges due to the complexity of the ground covering, however models nonetheless provided accurate contextual detail and errors may be mitigated through proper data capture. There was little difference in the

variables for image capture, scale bar placement, or number of images. Instead, the quality of images, image capture method, and post-processing operations proved to be more important. Due to the ease of use and the ability to convey best practices for data capture, the utilization of CRP for outdoor scene documentation is recommended as a valuable addition to current forensic documentation protocols. Future research should focus on the utilization of actual osteological material as a proxy for forensic scenarios as well as study the applicability of CRP to assist in documenting taphonomic modifications.

To my mother, who put me on this path.
And to Patty, who chose to travel this path with me.

ACKNOWLEDGMENTS

While the work of putting together a thesis often feels like a solitary task, it is anything but. I owe great amounts of appreciation to the many people who helped me complete this work. Thank you to my advisor, Dr. John Schultz, for his dogged persistence and support through the years as well as his commitment to working with a non-traditional student who was trying to have a career on the side. He is undoubtedly one pillar of my success. Thank you to my committee members, Dr. John Walker and Dr. Scott Branting; both of whom offered incisive views on my research which allowed me to expand the scope of what I was trying to accomplish. Thank you to Mason Guinto and Lexie Jones, fellow graduate students who made field work a possibility. Much appreciation also goes to Mr. Wayne Harrod, who provided access to the research site used for data collection. For much of the time I was in graduate school I had the pleasure of working at the Florida Public Archaeology Network under Sarah E. Miller. A special thanks to her for consistently ensuring I could fit grad school into my work schedule and for her care and concern about my well-being through it all. Perhaps most importantly, thank you to two astounding women in my life: my mother, Nancy Gidusko, and Patrisha Meyers, my future wife. Both provided unparalleled support to me throughout this process and are the other pillars of any success I have attained. I would not have begun nor would have I persisted without them.

TABLE OF CONTENTS

LIST OF FIGURES

LIST OF TABLES

CHAPTER ONE: INTRODUCTION

The preservation of evidence at outdoor crime scenes can pose a challenge to law enforcement professionals and forensic anthropologists. Several variables (weather, animal disturbances, various taphonomic processes, etc.) may act upon the crime scene, which can create confusion in interpretation or the loss of data vital to the investigation. Recent trends in forensic anthropology highlight the importance of applying more rigorous methodological approaches on-site and emphasize the necessity of determining and documenting context in crime scene scenarios (Dirkmaat 2008). However, law enforcement protocols often lack specific guidelines for processing outdoor crime scenes containing skeletal remains. As Dirkmaat (2012:48) notes, this may be due to the belief that the myriad ways in which an outdoor crime scene might be impacted engenders the belief that evidence loss is a forgone conclusion. Meticulous, forensic documentation of outdoor crime scenes can be considered as overly time-consuming with little payoff.

New methods of field documentation exist, however, that allow for quicker, more precise preservation of crime scene evidence than current standard practice allows. One newer method of data capture that allows for fast and accurate preservation of crime scene information is the utilization of 3D-modeling technology. The use of 3D modeling methods in the anthropological sub-disciplines of archaeology and biological anthropology is fast establishing its place as an integral data collection technique (Kuzminsky and Gardiner 2012, Forte 2014, Green et al. 2014, Howland et al. 2014, Prins 2016, Remondino and Campana 2014, Sapirstein 2016, Wallace 2017). At its most basic, 3D modeling, in this context, is the creation of an accurate, digital representation of a real-world object using a variety of data-capture techniques in such a way that

the subject's scale is maintained when digitally reproduced. The use of 3D modeling in forensic investigations has so far largely been focused on indoor crime scene reconstruction (Komar et al. 2012;

2013) and tissue/bone trauma analysis (Fourie et al. 2011, Kettner et al. 2011). Additionally, most 3D modeling research in a forensic context has utilized laser-scanning as the means of data acquisition. Laser-scanning, or terrestrial LiDAR, as a 3D modeling technique is highly accurate, though costly, and data processing requires intensive knowledge. Laser scanning is currently a benchmark data collection option, albeit one not readily available to those wishing to implement 3D modeling into their site documentation processes. A far more cost-effective and readily available option is close-range photogrammetry (CRP).

Considering the exigencies of outdoor crime scene documentation, this thesis will demonstrate the use of a relatively quick and cost-effective 3D modeling technique which may prove to be an invaluable tool in the preservation of contextual information at a forensic scene: CRP. Here, photogrammetry is a data collection technique that relies on digital photographs and specialized software using structure-from-motion (SfM) and multi-view stereo (MVS) visual computing algorithms to allow for reality capture (Douglass et al. 2015). Digital images are easy to produce and all law-enforcement agencies have access to digital cameras for scene documentation (Robinson 2010). Specialized computing hardware is not always needed as most commercially available computers are capable of producing 3D models. While software packages and specialized hardware represent the costliest aspects of creating 3D models via CRP, there are open-access options available. As such, CRP offers the ability to create high-

quality 3D data using tools and materials already commonly available to the forensic archaeologist that are far more affordable than laser scanning.

The purpose of this research is to determine the methods in which terrestrial CRP applications might be brought to bear on outdoor forensic scenes with skeletonized remains that improves scene documentation and later investigatory practices. Specifically, this research will examine the use of CRP in common Florida outdoor environments: pine flat woods and oak hammocks. A corollary of this research will be to discuss best practices for forensic archaeologists or other law enforcement professionals so that data collection moves towards standardization and consistency. Three mock scenarios were created that represented common scenes a forensic archaeologist might encounter: a clandestine burial excavation, a small (lightly scavenged) scatter of skeletonized human remains, and a wide (heavily scavenged) scatter of skeletonized human remains. This was accomplished using plastic teaching skeletons to mimic actual human osteological material. As will be discussed further, the mock scatters share greater similarities in the lessons learned regarding the application of CRP than does a comparison between the mock excavation and the scatters. As such, these scenarios will be discussed separately to better define the capabilities, shortcomings, and best practices between the application of CRP to exhumations and scatters.

The scenario comprised of a mock excavation of skeletonized human remains is discussed in Chapter 2. The controlled, careful excavation of human remains most closely resembles the work of bioarcheologists currently employing CRP methods. As such, this chapter will more closely draw from current efforts in the discipline of archaeology to integrate CRP methods into documentation protocols. Here, CRP is adept at capturing the static, defined

features of archaeological sites with excellent results. Similarly, CRP offers an excellent solution to the documentation of partially excavated human remains in a forensic context with the additional benefit of preserving larger aspects of the scene and thus possibly preserving additional evidence for later evaluation.

The scenarios comprised of small and wide scatters are discussed in Chapter 3. These surface scatters of skeletonized human remains represent a more common scenario for the forensic archaeologist. Surface scatters are due to a number of taphonomic processes (time, weather, scavenging) and in every way represent a more complex data capture process for CRP. Here, scenes may be poorly or irregularly defined, cover a wide area, and be within significant vegetation. Each individual factor represents a challenge to CRP; the combination of factors thus necessitates a more individualistic approach to scenes than discussed in Chapter 2. While these challenges may limit the applicability of CRP data capture for scatter scenes, Chapter 3 discusses its capability as a field documentation tool in light of the shortcomings inherent in documenting potentially complex scenes.

To address the research questions for these scenarios, an overview of current trends in forensic archaeology in the United States as well as literature relevant to these objectives will be discussed. A short discussion on the process of CRP will be followed by an overview of the materials and methods to be used in each portion of this research. Finally, the 3D results of each of these scenarios will be compared and contrasted relative to each other with a discussion of best practices and an exploration of intractable caveats. A comparison between all three scenarios will be discussed in the final section.

CHAPTER TWO: THE APPLICATION OF CLOSE-RANGE PHOTOGRAMMETRY TO OUTDOOR FORENSIC EXCAVATIONS OF SKELETONIZED REMAINS

Introduction

Traditionally, forensic anthropology has been a lab-focused endeavor. Typical forensic investigations may be compartmentalized into three stages of data acquisition: 1) at the scene 2) during autopsy and 3) in the lab (Dirkmaat 2012:49). This places the work of the forensic anthropologist towards the end of the larger-scale data acquisition process. Increasingly, however, the forensic anthropologist may bring a wider array of investigative techniques to bear upon a crime scene. Forensic anthropologists might specialize in field data collection processes, or may even be involved in the process of searching for human remains, such as in the use of ground penetrating radar to locate clandestine burials (Schultz 2012), the collection of surface scatters of skeletonized material (Lewis et al. 2017), or in the excavation of the aforementioned burials (Connor 2007). This shift places the forensic anthropologist at the forefront of evidence collection and requires a corresponding, but separate set of skills. That is, the application of archaeological techniques to the documentation of a crime scene, or forensic archaeology (Dirkmaat 2012, Dupras et al. 2012). A forensic anthropologist may or may not be trained as a forensic archeologist and vice versa (Dirkmaat 2012:55; Dupras et al. 2012:5). Forensic archaeology may be thought of as a unique sub-discipline within archaeology, one that requires a specialized methodology and knowledge base with a need for flexible field excavation methods (Hoshower 1998). One of the most integral responsibilities of the forensic archaeologist at a scene is to accurately map and document the scene in situ prior to excavation or removal of

evidence. This is typically accomplished via digital photography and hand-mapping. Hand mapping can be a time-consuming task, even for experienced practitioners, and the results are dependent on the skill-level of the individuals completing the task. One newer piece of technology that is fast gaining a foothold in other anthropological sub-disciplines may offer a superior alternative to traditional site documentation of forensic scenes: close-range photogrammetry (CRP). The use of 3D documentation is not new to the field of anthropology, having found itself utilized in archaeology and bioarcheology with an increasing frequency for several years (Anderson 1982, Douglas et al. 2015, Forte 2014, Sapirstein and Murray 2017). More recently, however, the capability and relative low cost of CRP as a 3D documentation method has made it an increasingly viable choice for site documentation, one that has not been widely applied to forensic excavations thus far, despite the readily apparent overlap in purpose between its use in bioarcheological and forensic excavations. While the capabilities of CRP are not such that this suite of technology will immediately replace hand-mapping, the capabilities are such that they provide an invaluable additional tool to better document a scene in situ, with more context preserved than via other, more mediated methods of documentation.

The purpose of this chapter is to discuss and demonstrate the applicability of CRP as a data-capture tool in the documentation of partially excavated skeletal remains at a forensic scene as well as to provide recommendations for how to integrate CRP data capture at outdoor forensic excavations. The use of CRP to document partially excavated skeletal remains is most like its application in bioarchaeological as well as general archaeological contexts. This is largely due to its excellent capability to accurately model static, well-defined features with contrasting elements within a site or scene. In the scenario discussed in this chapter, the partially excavated remains

were in the context of a controlled test unit, with a homogenous surrounding sub-surface. Series of digital photos were captured to determine best practices for field documentation and subsequent post-processing. In this chapter a brief background of forensic archaeology and of 3D documentation in archaeology will be discussed. Additionally, a brief background to CRP will be provided to place it in context to its more recent and widespread adoption. Finally, this chapter will provide an overview of the process of field data collection, post-processing, and data-sharing capabilities of CRP with a discussion of what this process might offer the forensic archaeologist.

Background

Forensic archaeology as a distinct approach to evidence collection in a forensic context has been an aspect of the larger forensic methodological discussion since the 1980s (Lovis 1992; Morse et al. 1983; Sigler-Eisenberg 1985). The application of archaeological excavation methods to forensic scenarios came after the larger coalescence of forensics into a distinct discipline. During this period, there was a recognition that better evidence collection in the field would provide the forensic anthropologist with a more robust amount of data with which to conduct analyses. Additionally, larger-scale contextual information concerning a crime scene could be accurately documented, which also allows for better analysis of the crime scene and frees the forensic anthropologist from relying solely on osteological material. Indeed, the use of archaeological techniques in a forensic context has been shown to provide better control of evidence in crime scene processing than traditional post-scene autopsy or lab investigations alone (Blau and Ubelaker 2009, Dirkmaat 2012, Dupras et al. 2012).

The forensic archaeologist operates within a medico-legal framework, which differs from the more traditional archaeological research process (Dupras et al. 2012) Generally, archeological investigations are research-oriented and follow similar methodological steps. The principle investigator in a traditional archaeological scenario is oftentimes the instigator of the research and the one who will manage the data collected through all stages of analysis. The forensic archaeologist must reorient themselves within the larger data collection process, however, one in which they may or may not manage analysis after field data collection. Moreover, the forensic archaeologist must not only undertake sound archaeological methodology, but may also contend with issues of extreme time constraints, legal constraints, the needs of law enforcement officials, the media, and an array of problems that traditional archaeological research does not regularly encounter (Dupras et al. 2012:5; Skinner et al. 2003). Thus, the forensic archaeologist fulfills a role complimentary to the work of the forensic anthropologist, but in particular focuses on five main responsibilities: Locating and eliminating suspected areas of interest; interpreting scene context; scene mapping; excavation of remains; and collecting remains and evidence (Dupras et al. 2012:5-9). Certainly, the responsibilities of the forensic archaeologist may expand given different circumstances (see Skinner et al. 2003 for further discussion), but the fundamental attributes which define the work of archaeological applications in a forensic scenario are those that serve to provide a controlled collection of evidence in situ to aid in further analysis and interpretation.

The use of 3D modeling as a means of capturing an accurate depiction of a crime scene falls under the scene mapping responsibilities of a forensic archaeologist. Mapping a forensic scene is standard practice for all situations. Forensic anthropologists utilize standards of practice

regarding the collection of evidence from human skeletal remains, though the forensic archaeologist must work in more varied situations where the standardized application of methods is not feasible (Buikstra and Ubelaker 2010; Bass 2005).

CRP and 3D Applications in Archaeology

Photogrammetry is, "the art, science, and technology of obtaining reliable information about physical objects and the environment through processes of recording, measuring, and interpreting photographic images and patterns of recorded radiant electromagnetic energy and other phenomena" Wolf (1983:1). Digital photogrammetry then may be understood as the recreation of a real-world object or scene in a digital space via the capture of a series of 2D digital images. More specifically, CRP is defined as data collected at less than 300m between the camera and the subject (Mathews 2008:5).

The application of CRP falls within a suite of technologies and methodological techniques collectively termed high-density survey and measurement (HDSM). Types of HDSM hardware and software include global navigation satellite systems (GNSS), global positioning systems (GPS), laser scanning devices (LiDAR), total stations, unmanned aerial vehicles (UAV), structured light, and CRP, or structure from motion (SfM) software (Forte 2014; Opitz and Limp 2015). The use of these technologies in the discipline of archaeology is relatively new and represent what Opitz and Limp see as, "a fundamental shift in how we create and engage with the archaeological record" (2015:348). Indeed, the utilization of HDMS might be better thought of as a sea-change event in archaeology, one of many (often technological) innovations which do not just push archaeological methodologies forward, but which also allow for new, broader questions to be posed to archaeological data sets. As a collective whole, HDSM allows for the

quick and precise measurement of archaeological resources in a digital, shareable, and reproducible format (Forte 2014, Berggren 2015). This can be achieved at a scale that stretches from the individual artifact to site-wide data capture (Ioannides 2014). At its most basic, the technologies associated with HDSM record x,y,z spatial data points which can be digitally represented, and which contain enough data (individual points) that the digital reproduction of the item or place exists as a nearly one-to-one 3D model. These points may also be given spatial geometry and incorporate color data in 3D outputs. These 3D models can in turn be the source of continued investigations and research long after field data collection. For a destructive science, such as archaeology, or forensic archaeology, where evidence can only be collected once, the ability to reconstruct a site or scene after initial investigations is of paramount value. The ability to model the contextual data of a scene as it exists, rather than through the mediated form of note-taking, hand-mapping or digital photographs, allows for that scene to be re-engaged with by other researchers at later times; this is as close to providing a more total amount of raw data to one's colleagues as may be possible in archaeology or forensic archaeology. As such, the utilization of CRP methods at a forensic scene (or archaeological site) enhances the scientific process by making raw data digitally replicable in a 3D virtual space.

An aspect of most incipient instances of HDSM research and development is that much of it traditionally occurred in Europe. This trend continues today. Only recently has research from North America begun to move at the pace of European counterparts (Opitz and Limp 2015). This can be attributed to several factors: early adoption and utilization by heritage management professionals in Europe despite initial unwieldiness, the prevalence of historic monumental architecture in need of constant observation, and funding programs via the

European Union that invested in HDMS technological advances (Ioannides et al. 2014; Opitz and Limp 2015:350). However, as proof-of-concept studies aggregate from European colleagues, the lure of technologies which promise increased precision and speed of data capture is proving hard to ignore by North American anthropologists. Opitz and Limp (2015:351) note that the preponderance of HDSM literature to date deals heavily with the mechanics of methodological processes; that literature which makes the leap to interpretation, analysis, and new archaeological arguments remains in the minority. The aim here is to move towards further application of HDSM technology as its capabilities are well-documented. Moving forward, these further applications may also impact the manner in which we interpret data/evidence.

While the focus of HDSM research thus far is largely concerned with the methodological components of associated hardware, software, and field techniques, the creation and utilization of 3D digital data brings with it new methodological approaches as well (De Reu et al. 2014, Galeazzi 2016, Opitz and Limp 2015). The process of on-site abstraction (such as stratigraphy profiling, planimetric drawings, creation of site maps, etc.) in archaeological data collection requires by its very nature an interpretation of the information at hand. While this information is collected by trained professionals, it is nevertheless often an abstraction through the lens one or few individuals. Opitz and Limp (2015:359) site the work of Simons and Chabris (1999), specifically noting the tendency for "inattentional blindness" given dynamic events. Inattentional blindness occurs when we "see what we are prepared to see," or it is the tendency to simplify complex sensory data into easily definable chunks based on our prior experience and understanding of the scenario in which we find ourselves. The ability to more truly abstract data/evidence acquisition via 3D modeling methods is, in this manner, an opportunity to engage

in a more recursive interaction with whole data sets. That is, information can be shared as given actualities, not interpreted notes, thus allowing us (and others) to engage with the original information repeatedly. In this way, we may limit the impacts of possible inattentional blindness on interpretation processes. This greatly benefits archaeological research, though the implications for forensic archaeology offer a great deal more.

3D Applications in Forensics

The use of 3D modeling techniques in the field of forensics is currently focused on examining the manner in which this new technology might prove useful to current and future research efforts (Sansoni et al. 2009:541). While some law enforcement agencies can incorporate laser-scanners into forensic investigations, this is by no means the norm across all agencies. Cost, required expertise, and necessity are all factors that determine this technology's use at this time. In short, it is not a core component of forensic investigations yet.

While 3D modeling techniques are gaining popularity in other sub-disciplines within anthropology, its use in forensics has been slow to take hold. Despite its obvious impact in the realm of archaeology, as above, and more specifically in the realm of bioarchaeology to understand why this technology should be more fully integrated into standard forensic field investigations. While traditional hand-mapping techniques are not ready to be entirely supplanted by 3D technology just yet, it is worth recognizing the glaring fact that any scene documentation is the "mediated expression" of that given site (Morgan and Wright 2018). That is, regardless of how skilled the collector of site data is, that information is mediated via that individual or the group's capabilities at that time; field notes are only as good as the person taking notes, the mapping is only as good as those drawing the maps, etc. This is the crux of archaeological or

forensic interpretation: the application of experience to derive the essential components of information that will be then conveyed to others (Dirkmaat 2012, Dupras and Schultz 2008). This has broader applications as well: digital documentation has the capability to gather data in a more complete form, to gather data that one may not intend to. This includes information about light waves, soils, or other extraneous information not recognized as pertinent at the time. However, as was noted by Simons and Chabris (1999), we have a tendency to focus in on the intended data points: our inattentional blindness (here, an unintentional dismissal of details when focused on a task one is trained for) can prove detrimental to the goal of collecting all important data or evidence at a site. As it is applied in current bioarchaeological work, the use of 3D modeling techniques allows for near-total scene preservation (Forte 2014), the ability to perform intensive analysis without impacting osteological material (Kuzminsky 2017), and its ability to integrate with other spatial mapping software such as a geographic information system (GIS) means that complexity can be managed and excavations can be "reversed" (Berggren 2014). Any of these capabilities would be an advantage to the work of forensic archaeology. Taken together they represent a logical future direction of forensic scene documentation as they provide more, and more accurate, preservation of evidence for later investigatory purposes. Despite this, 3D applications in forensics have been less applied and less examined.

A review of literature discussing 3D modeling applications in a forensic context demonstrates that the current focus of research can broadly be categorized into two foci: forensic scene reconstruction and the examination of soft-tissue/bone trauma data from a fleshed body. Much less research has been conducted concerning both outdoor forensic scenes and, more specifically, outdoor forensic scenes with skeletal remains. These are not distinct categories and

should be considered as broad and inter-related; the utilization of 3D imaging techniques has not yet reached a stage in the discipline where extreme niche applications are apparent. Rather, the research relies heavily on lateral applications of the technology within the field and across several different scenarios (Table 1). A common thread at this stage for research in this vein is the two-part question: Does it work? How well does it work?

Table 1. A selection of main research focusing on 3D applications in forensic crime scene analysis. Note the two foci: indoor scene reconstruction and tissue/bone analysis, also the lack of focus on outdoor scenes.

Year	**Foci**	**Research Subject**	**Reference Information**
2003	*Tissue Trauma*	*Utilized early photogrammetry coupled with CAD to model injuries from instruments.*	Brüschweiler et al.
2003	Tissue/Bone Trauma	Structured light used in conjunction with CAD to digitize skin and bone injuries.	Thali et al.
2009	Tissue/Bone Trauma	Laser scanning applied to lesion documentation in accidents/homicides.	Sansoni et al.
2011	Tissue Trauma	Tested the accuracy and reliability of three different 3D scanning systems; laser scanning, cone beam computed tomography, and photogrammetry.	Fourie et al.
2011	Bone Trauma	Discussion of 3D printing of scanned material for trauma analysis.	Kettner et al.
2012	Indoor Scene	Indoor crime scene laser scanning for later investigation.	Buck et al.
2012	*Outdoor Scene*	*Handheld laser scanner to document crime scenes and during autopsy.*	Komar et al.
2013	Indoor Scene	Computer tomography and computer visualization tools to aid in crime scene depiction and bullet trajectory analysis.	Colard et al.
2015	Tissue Trauma	Applying photogrammetry to pathology documentation during autopsy.	Urbanová et al.
2015	Indoor Scene	Photogrammetry applied to indoor crime scene reconstruction.	Zancajo-Blazquez et al.
2016	Indoor Scene	3D documentation of bloodstains for later analysis.	Hołowko et al.
2016	Indoor Scene	Indoor scene reconstruction using 3D visualization.	Costantino et al.
2017	Outdoor Scene	Photogrammetry via drones for scene documentation.	Urbanová et al.
2017	Outdoor Scene	Drone mapping of scattered, scavenged remains.	Lewis 2017

The use of 3D modeling applications in crime scene reconstruction and analysis is a fruitful endeavor thus far. One good example is the work of Constantino et al. (2016) who showed that there are multiple lines of evidence that might be investigated as a result of 3D data capture at a crime scene. This study utilized laser and CRP scanning to capture information at a staged crime scene. From the collected data, the authors made valid assumptions about bullet trajectory and velocity, measurement information from shoe and finger prints, and created a visual representation of the scene for use as a display to non-experts, such as a jury. Blood spatter analysis is another area of study within this category: Holowko et al. (2016) demonstrate the advantages of utilizing 3D laser scanning to preserve blood spatter evidence at a crime scene as well as its use in the later analysis. The 3D model of the blood spatter provided an added dimension to analysis, one which could be conducted in a virtual state and with results that were more easily shared. The authors note, however, that though laser-scanning provided good, precise results, there are still limitations in its use most directly owing to its cost and required expertise to operate. A last example of research utilizing 3D data to reconstruct crime scenes evidence is Komar et al.'s (2012) use of laser-scanning to collect ephemeral evidence at the crime scene. Here, the authors identify perhaps one of the most impactful applications of this technology, its ability to capture aspects of the scene that are not capable of easily being documented or recovered. The authors identify a number of different applications including use in documenting information from clandestine graves, footprints, mass graves, at fire scenes, and any other evidence that might be resistant to traditional casting methods. In collecting 3D data for several of these scenarios the authors demonstrate the value of being able to better visualize and analyze ephemeral evidence using laser-scanning technology.

Some recent research seeks to utilize 3D data capture techniques to preserve evidence that may be extant on a human body in a forensic scenario before decomposition potentially masks or obliterates evidence. In these situations, the goal is to capture 3D visualizations of trauma so that precise metric analysis can be done. An example of this is the work of Bruschweiler et al. (2003) which describes attempts to collect CRP models of the damaging effects of items on tissue; teeth marks, hammer blows, tire treads, etc. all leave distinctive patterns which can be digitally captured and accurately measured. In this way, the potential instrument of damage can be better defined for investigators and, if found, measured against a detailed 3D model of the marks. Similar to this research was that of Thali et al. (2003), who demonstrate the capabilities of CRP to capture morphological data from skin trauma. In this case, CRP was used to accurately recreate the shape of the weapon used against the deceased. By capturing a 3D model of the skin trauma, the authors were able to reverse engineer the shape of the item which caused that trauma. In this instance, a 2D overlay of the 3D models was created which demonstrated the type of gun muzzle which left the skin trauma. Urbanova et al. (2010) describe the utility of integrating CRP as a component of postmortem examinations. Citing the accuracy and ability to collect information about lesions, skin markings, tattoos, and cause of death information (in the case of a suicide by hanging), the authors suggest the increasing ease of use should be exploited during future autopsy examinations. Finally, Fourie et al. (2011) demonstrate the accuracy and reliability of utilizing 3D data capture (laser-scanning, cone beam computed tomography, and CRP). Comparisons of anthropometric measurements were made on 3D models of a male face for each 3D modeling technique. All techniques were found capable of producing accurate and reliable data for research.

Less discussed in the wider literature 3D modeling and forensic scene documentation is research which focuses on outdoor scenes, especially those which contain skeletonized material. Some focus on skeletal material has achieved positive results thus far. Ebert et al. (2011) discuss the application of 3D modeling and rapid prototyping (here, 3D printing) technologies. Skeletal abnormalities and trauma can be imaged and printed for educational purposes, or to provide better demonstration material in a courtroom setting. Similarly, Kettner et al. (2011) utilize 3D modeling and reverse engineering to recreate skeletal material that has undergone extreme trauma. In this case, the authors demonstrate the capabilities of 3D modeling to allow for reconstruction of a cranium which was mostly shattered due to trauma. The 3D model and subsequent reverse engineering in this case allowed for a reconstruction of the point of impact, one which could be completed without the need for the body. Missing from the wider discussion is the application of CRP on outdoor skeletonized remains, especially in the context of a scavenger scatter. One foray into this subject was the recent work by Lewis et al. (2017) who document the capabilities for unmanned aerial vehicles (UAVs) to document skeletal scatters with 3D mapping. A similar line of research by Urbanova et al. (2017) examined the use of UAVs to collect 3D documentation on-site for hard-to-reach bodies. While drones may prove to be a useful tool in scene documentation they are costlier and less versatile than a standard digital camera used at a forensic scene. Additionally, the downdraft of air caused by propeller rotation could actually impact evidence at the scene. Certainly, in the case of documenting a partially excavated individual a drone would be more hindrance than help.

Material and Methods

Faux Skeletal Material

For the purposes of creating a mock excavation, a plastic teaching skeleton was used to mimic actual human osteological material. The plastic material in this case was of a homogenous, white color that was somewhat reflective due to the material. While morphological traits readily evident on actual human bone were apparent in the faux skeletal material, the manufacture of this material was not of a sufficiently high level to accurately mimic human bone. Prior to burial, the skeletal material was measured according to standards for human osteological data collection (Buikstra and Ubelaker 1994). For the purposes of testing final model accuracy, this research focuses on testing the precision of measurements for the humeri and femora, two of the longest bones and two that might offer the most distortion during post-processing owing to their length and linearity. The humeri were measured at the maximum length (ibid. 81) points and femora were measured at the maximum bicondylar length points (ibid. 82).

Research Site

This mock scenario was conducted in Brevard County, Florida on private property. A 1 x 2m test unit was dug to an approximate depth of 30 centimeters into a common soil type for the area, a Copeland complex: poorly drained, loamy fine sand with a limestone substrate (USDA 2018). Prior to test unit excavation the area was cleaned, and any brush or grass was cut back to effectively denude the site immediately surrounding the area to be utilized, a common practice before forensic excavation. At 30 cm, the faux skeletal material was placed in anatomically correct positioning to represent a body dumped into a shallow grave. Soil was placed on top of the teaching skeleton and then excavated to the point of documentation (Figure 1).

Figure 1. Overview of mock excavation scenario. The faux skeletal remains are arranged to mimic a hasty, shallow burial. Scale bars with coded targets surround the excavation unit. Here, the camera is being set for data collection. Out of shot is a tent which provides shade over the scene thus allowing even lighting during data collection.

Hardware

Data was captured using a Canon EOS Rebel T5i digital camera, affixed with an 18-55mm kit lens. Generally, photogrammetry is best captured using a wider focal length; the adjustable kit lens common on many entry-level digital cameras is thus a good option for documenting variable scenes (Douglas 2015, Sapirstein and Murray 2017). This digital single-lens reflex (DSLR) model is a standard, entry-level digital camera that captures images at 18 megapixels. For a portion of the data collection, a standard tripod was used as well as a remote

shutter release. Scale bars produced by CHI (2018) were used both for test unit measurement and due to the inclusion of photogrammetric control markers (also called coded targets or coded markers) on the bars themselves (Figure 1). Each marking is unique and each marker is recognized by photogrammetry post-processing software. The utilization of markers in a photogrammetry project allows for faster post-processing and better control of scale and image alignment in the final model output (Sapirstein and Murray 2017). It is possible to conduct CRP data collection without the markers, or even without any scale present in images. However, this is not suggested; accuracy of the final model suffers without the use of either scale bars, control markers, or both (Douglas 2015). Additionally, the use of control markers and scale allows for the imposition of real-world coordinate systems on to the model via GPS and GIS systems. Without this, the final 3D model exists in a local coordinate system bereft of a connection to an actual spatial coordinate system (Douglas et al. 2015, Liew et al. 2012, Soler et al. 2017).

Data Collection

As in archaeological data collection, there is currently no one, perfect method of collecting data for a CRP project. Rather, there exists a selection of best practices and discussions on appropriate data collection parameters to utilize (Douglas et al. 2015, Galeazzi 2016, Sapirstein and Murray 2017). The methods described below are a distillation of practices the author received training in from several resources that range from engaging with other researchers in the field utilizing CRP for projects to attending an intensive scientific photogrammetry training with Cultural Heritage Imaging (CHI 2018). The general workflow process discussed below is the result of two years of trial and error utilizing CRP to document cultural resources, archaeological sites, and historic structures. More specific to the current

research, the workflow described here concerned with the documentation of outdoor forensic scenes is the result of testing 45 example scenarios, pre-processing roughly 17,000 images, processing 80 models, and with over 700 hours of processing time invested. Even with the significant time investment described here, the process below is only a best practices overview given a specific situation. These practices will naturally need to adapt as scene variables change.

To define the best method of CRP as a documentation technique for forensic excavations a series of four image data sets were captured using the CHI scale bars. Two of these data sets were collected by holding the digital camera in the hand and two were collected with the digital camera mounted on a tripod with a remote shutter release. This was to test whether the stability of a tripod had an impact on the final accuracy of the 3D model outputs. Additionally, for each of these data sets, handheld and tripod, the scale bars were placed around the excavation at surface level and within the excavation to determine whether placement of the scale bars provided better final accuracy (Table 2). In those sets where the scale bars were placed within the excavation unit, one scale bar was placed upright along the excavation wall (Models 2 and 4) to test whether additional z-value point data affected the final model accuracy. A photography color card should also be included in at least one shot for later white balancing.

Table 2. Overview of data capture parameters for the four models.

	Scale Bars	**Shooting Method**	**Camera Setting**	**Number of Images**
Model 1	Outside of excavation	Handheld	Aperture Priority	84
Model 2	Inside of excavation	Handheld	Aperture Priority	86
Model 3	Outside of excavation	Tripod	Aperture Priority	92
Model 4	Inside of excavation	Tripod	Aperture Priority	73

Photogrammetry requires overlapping look-angles at different levels around the entirety of the subject to be documented (Douglas et al. 2015:140). Generally, the more points of intersection between images, the better the final model. These points of intersection are mapped in and between individual images by matching pixel neighborhoods (Agisoft 2018). A general workflow (Figure 2) for data collection of shallow burials should look similar to the following: Images should have at least an 80% (or 2/3) overlap and the camera should move at a set level for each 360-degree circuit around the subject with at least 3 levels of full data collection (Agisoft 2018, CHI 2018, Douglas et al. 2015). For example, if the first entire circuit of images was taken at a low angle with roughly 10 degrees of movement (or enough to give sufficient overlap between images) around the subject then when the original point was returned to the camera would be raised enough to give 80% overlap of images in a vertical direction and the data capture would continue with another circuit of 80% overlap until the starting point was reached again. This would be repeated at least one more time, though depending on the subject size or other variables additional circuits may be required. At the beginning of each circuit the camera would be rotated to one of three different positions for the entirety of that circuit: landscape, shutter trigger up, or shutter trigger down (CHI 2018). As auto rotate was disabled, this will preserve the view of the images collected in each position which assists the software in tie point matching. The number of images per scenario for this research ranged from 73-86 images. While the number of images is important, far more important is the quality of the image being collected; CRP software can create a better model with a few technically proficient images than with many blurry, poor quality images.

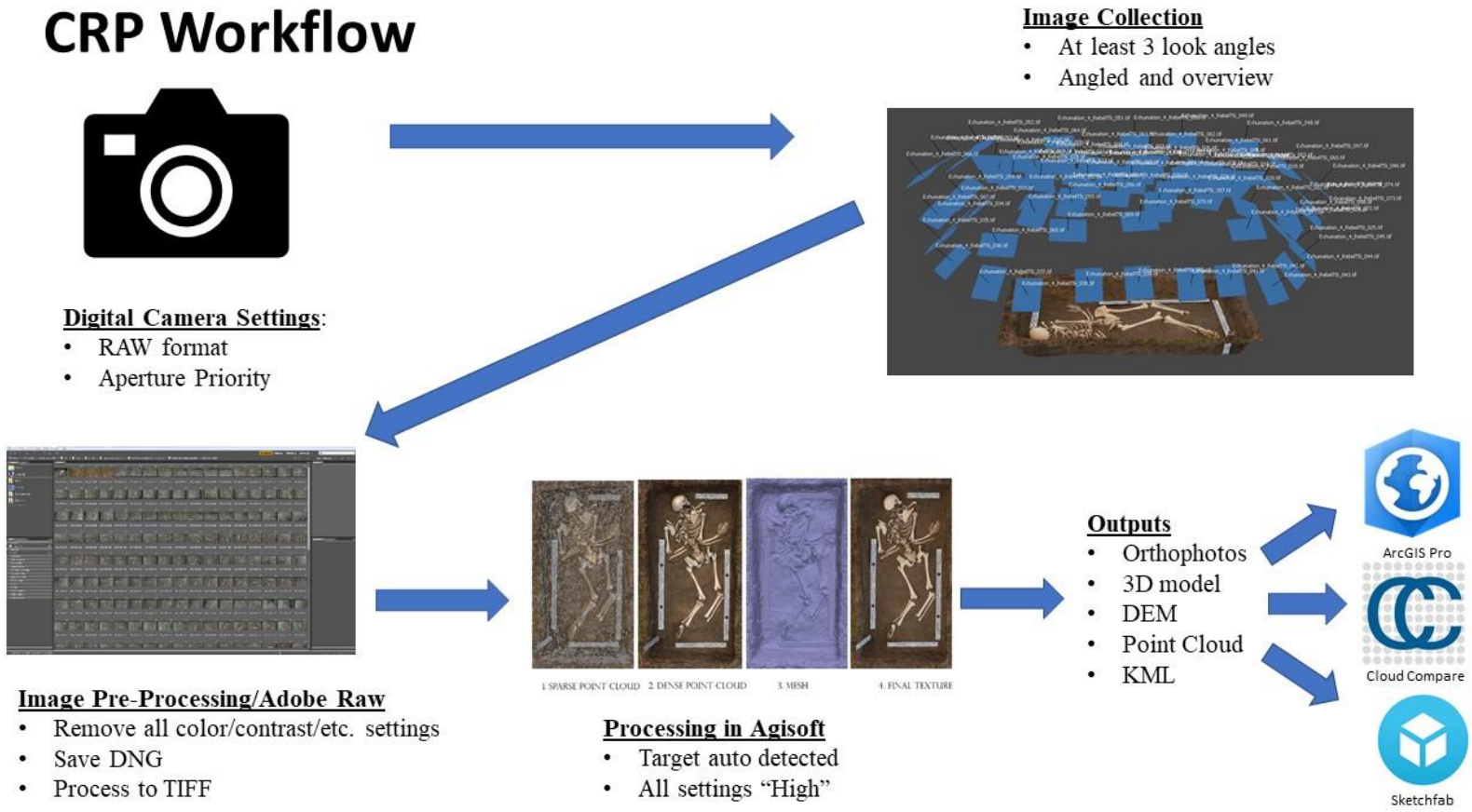

Figure 2. A general workflow for documenting a shallow excavation with CRP. Note that images are collected around the entirety of the subject with at least 80% overlap at 3 different angles. Images are pre-processed in Adobe Camera Raw to correct for color and lens distortion. Next, images are processed in Agisoft Photoscan, which allows for a variety of outputs.

All images were captured in .raw format to preserve as much sensor data as possible (Agisoft 2018, CHI 2018). In order to maintain similar standards across each scenario a few key choices were made when capturing images with the digital camera: the focal length was set to 18mm and taped in place; all images were collected in the automatic aperture priority setting; image stabilization and autofocus was disabled on the kit lens; and autorotate was turned off as a setting on the camera. These settings provided standardization across data collection circuits and are recommended settings for CRP projects (BLM 2008, CHI 2018). Importantly, the static setting of the focal length allows for better post-processing error assessment as points are triangulated in space via one focal length only, instead of a variation of focal lengths as might occur with autofocus enabled (CHI 2018, Douglas et al. 2015, Sapirstein and Murray 2017). Preparing the camera to acquire data in this way allows for high-quality images that are optimized for photogrammetry post-processing. Additionally, providing a standard set of camera settings may assist in educating forensic archaeologists or other law enforcement officials in general best practices for data acquisition whether the images will be post-processed or not.

One final word on acquiring image data for photogrammetric projects: Special care was taken to limit any instances of poor-data images: These include images with blur, reflective objects, bright objects, and moving objects which are nearly impossible for photogrammetry software to process. Special care was taken to maintain circuit distance around the mock excavation scenarios to maintain focus as the autofocus was disabled and the lens was taped to mimic a prime lens at 18mm. Images with poor data may be used in post-processing, may be removed, or may be edited prior to processing to remove portions with poor data. However, if

proper field data collection techniques are followed, this will facilitate a more streamlined workflow for the creation of 3D model deliverables.

Pre- and Post-Processing

Each image data set for each scenario was pre-processed similarly. While almost any digital image processing software would allow for the pre-processing steps discussed here, this project utilized Adobe Camera Raw to further prepare the image sets for photogrammetric processing. Within the program, the images may be batch processed to account for desired changes in contrast, sharpness, or any other application needed to assist in producing good pixel data for processing. Regardless of personal choices about the images, the most important components of pre-processing are white balancing of images and the removal of lens distortions. White balancing is conducted via the white balancing tool (common in all image processing software) and can be conducted by using the tool on an image that contains the photography color card. Removal of lens distortion is an option within the program and is automatic if engaged. Image metadata will contain information for the program to determine the camera lens used and an automatic function adjusts for that lens's distortion. Image data was saved in two formats: 1. Images were saved in a digital negative format (.dng) for archiving and 2. Images were then processed to .jpegs for use in Agisoft Photoscan Professional (Figure 3).

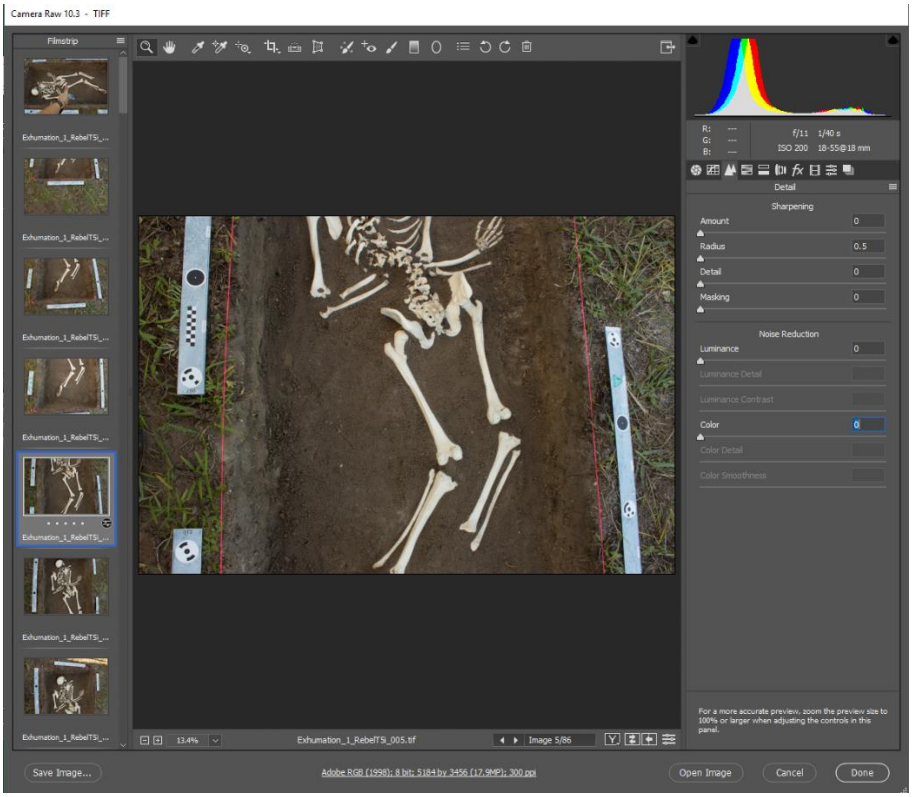

Figure 3. Pre-processing .raw image files for use in Agisoft Photoscan in Adobe Camera Raw. The goal is to produce an image that is as representative of the actual object as possible. This includes removing color corrections and applying lens corrections. Here, an image is being pre-processed and these settings will be applied to every picture in the image folder.

All data sets were processed to 3D models using Agisoft Photoscan Professional, primarily within v.1.3.4 though with some later work conducted in v.1.4. There are currently several SfM/MSV-contingent photogrammetric software packages available to the consumer and as open source software. Photoscan remains one of the most popular of these photogrammetric packages, however, largely due to its interoperability and the amount of control users have over processing steps (Bolognesi et al. 2014:114).

At each stage of processing within Photoscan, the user may define the level of computational effort expended on that step (Figure 4). Values range from low to high and within these options additional decisions may be made to define the output. Deciding which array of

processing options to use is a matter of defining beforehand what the purpose of the final output is and having a sound understanding of the computer's image rendering capabilities. Larger data sets will require more computational effort and similarly a desired accuracy will require more effort and time. As the goal of this research was to digitally replicate the mock excavation scene as accurately as possible, "high" values were chosen at each step discussed below.

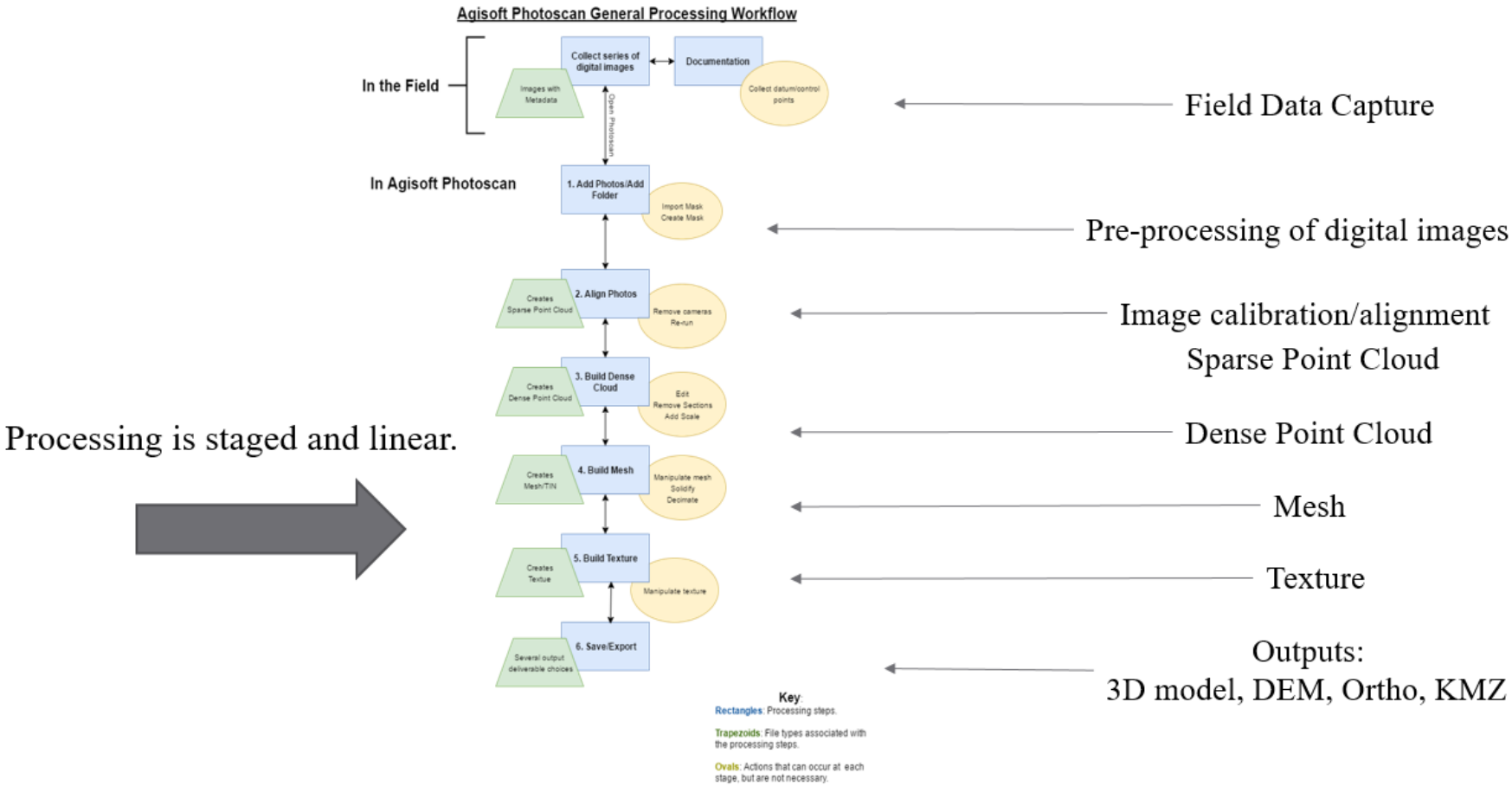

Figure 4. Generic overview of photogrammetry processing stages with a selection of outputs.

After loading pre-processed cameras into the Photoscan software, the first step is to align the camera angles. Here, the term camera applies to each individual image and is used to denote the image and its corresponding metadata as one entity. It is at this stage that the SfM algorithm is used to define camera locations in space in relation to one and other as well as to the subject to be modeled (Agisoft 2018, Douglass et al. 2015:138). The result of alignment is the sparse point cloud (SPC) which depicts for the user the general outline of projected tie points between cameras (Figure 5). A SPC may be optimized before further processing. This is done via the gradual selection tool within Photoscan that will automatically detect tie points with the most error for deletion should the user decide to do so. The goal of SPC optimization is to obtain the best camera position estimates across all cameras (Agisoft 2018:20, Douglass et al. 2015:141). This can be identified within the Reference pane on the program interface where each camera image depicts the individual number of tie point projections for that image and its cumulative error. Via gradual selection of tie points with extreme error and their deletion, the error values will drop (Agisoft 2018:74). Generally, an error value of under 1.0 will provide the best results in later processing stages (CHI 2018). It is also at this stage that scale was introduced to the models as defined by the scale bars. Photoscan allows for the automatic detection of points (via the control markers) or the creation of points to measure between. The distance between marker points was entered for at least three scale bars per model with one left undefined as a control for accuracy assessment.

Figure 5. A visual depiction of the photogrammetry process stages: a. sparse point cloud; b. dense point cloud; c. mesh; and d. textured final model.

An optimized SPC is then ready for dense point cloud (DPC) processing. At this stage the MSV algorithm interpolates points with x,y,z-RGB values utilizing the camera angles defined during the alignment step. The DPC processing stage is the costliest in terms of computing power (Douglass et al. 2015:141). Where the SPC is defined by a few thousand tie points, the DPC may generate millions of point values. A DPC, if created properly, may appear as a solid object and can be exported for analysis if so desired. An example of DPC analysis would be the comparison of two or more DPCs with each other to quantify the difference, such as in the case of detecting change of a static subject over time. The data set for this research was processed on a high setting for each scenario.

A DPC may be further processed into a mesh. A mesh is comprised of a number of polygonal faces, that give the model spatial geometry. That is, prior to this stage, the model is

comprised only of points in space and are related to each other but do not have definite geometric shape (Agisoft 2018). Mesh creation may be defined at a certain value for the face count; more faces result in greater resolution, but a larger output file size. Fewer faces may reduce the surface geometry in detrimental ways, roughening otherwise smooth surfaces. For these reasons, models may be decimated within the program to a desire face count. Meshes for this research were processed on high settings and decimated versions were later created for ease of sharing and visualization. Here, a high face count mesh may be saved for archival purposes with a decimated version used for sharing or reporting.

The final step in a standard workflow for 3D model generation is the creation of a texture to overlay the mesh. A texture is derived from the color data from each available camera. This data is stitched together into a single image which can be exported and manipulated within image processing software packages for desire effects: increased contrast, brightening, etc. This is not required, however. A caveat to texture creation is that all extant environmental effects present when capturing the image are present in the texture; if the scene is covered in mottled shadows, the creation of texture in photogrammetric software will not negate these aspects in the final texture (Agisoft 2018). While there are options to limit the impact of these effects on 3D models (such a delighting) these processes may require more specialized software and might be seen as affecting the integrity of the model for the purpose of forensic evaluation as these processes interfere directly with color data collected.

Once these steps are complete, the 3D model is ready for a range of data outputs. Models may be exported as total packages, or as individual components. The purpose of exporting products from this process is to both archive and share data in a compact format. Additionally,

exporting data allows the processed results to be shared with those without access to the specialized software needed to generate 3D models. A major asset of generating a 3D model via CRP is that individual view angles may be shared to better aid in visualization or investigation (Figure 6). Another useful export option is the creation of an orthomosaic generated from the processed model. Generating an orthomosaic image produces a high-quality 2D image with scale preserved throughout the image making it particularly useful for later analysis, measurement, or for the creation of line drawings in computer aided design (CAD) software. Orthomosaics may be positioned in any orientation, allowing for views unachievable when collecting data such as planar overviews of the entirety of a scene (Figure 7). Lastly, Photoscan allows for a report to be generated on each processed model defining in exacting detail the processes utilized during model generation. A report for each model was generated and is available in Appendix I.

Figure 6. Different view angles of Model 1, screenshots and orthomosaicss: a. sideview screenshot. b. orthomosaic sideview. c. oblique screenshot. d. oblique orthomosaic.

Figure 7. Orthomosaic image generated in post-processing of Model 1. This image, though a 2D representation of the excavation, preserves all relationships of scale and can be used for measurement. This view was not possible during data collection and orthomosaic thus represent one of the most useful outputs of a CRP project: the ability to share views of scenes otherwise not possible.

Defining Accuracy

Defining accuracy for CRP projects is still largely a function of comparing 3D generated results to real-world measurements as well as establishing the inherent error within the generated

model based on the scale the user has imposed on the model (Caroti et al. 2014, De Reu et al. 2014, Doneus et al. 2014, Douglass et al. 2015:145, Rieke-Zapp et al. 2009). As such, multiple methods of describing accuracy of the results will be discussed. Models will be described as highly accurate if there exists a, "high level of agreement between the two sets of measurements" (Douglass et al. 2015:145).

Three methods were used to define the accuracy of the generated models: a total error value given by the Photoscan software, a test of a control value on the scale bars used within the model (CHI 2018), and measurements of humeri (maximum length) and femora (bicondylar length) within the model as compared to the actual material. An advantage of CRP data capture is that measurements may be taken and re-evaluated after leaving the scene; where 2D images may provide contextual and some measurement data, a 3D model's view angle may be manipulated to allow for better analysis at any point after data collection at the scene (Figure 8). Photoscan provides a total error metric in the form of a root mean square error value (RMSE) which is the error inherent in the model based on the information parameters the user has entered. Generally, a value below 1.0 (with whatever metric of measurement is desired) is considered to represent highly accurate results. While there are several ways to define accuracy of individual components within the final models, this method provided a broad overview of accuracy or inherent errors and represents a viable method for doing so (Agisoft 2018; Bolognesi 2014).

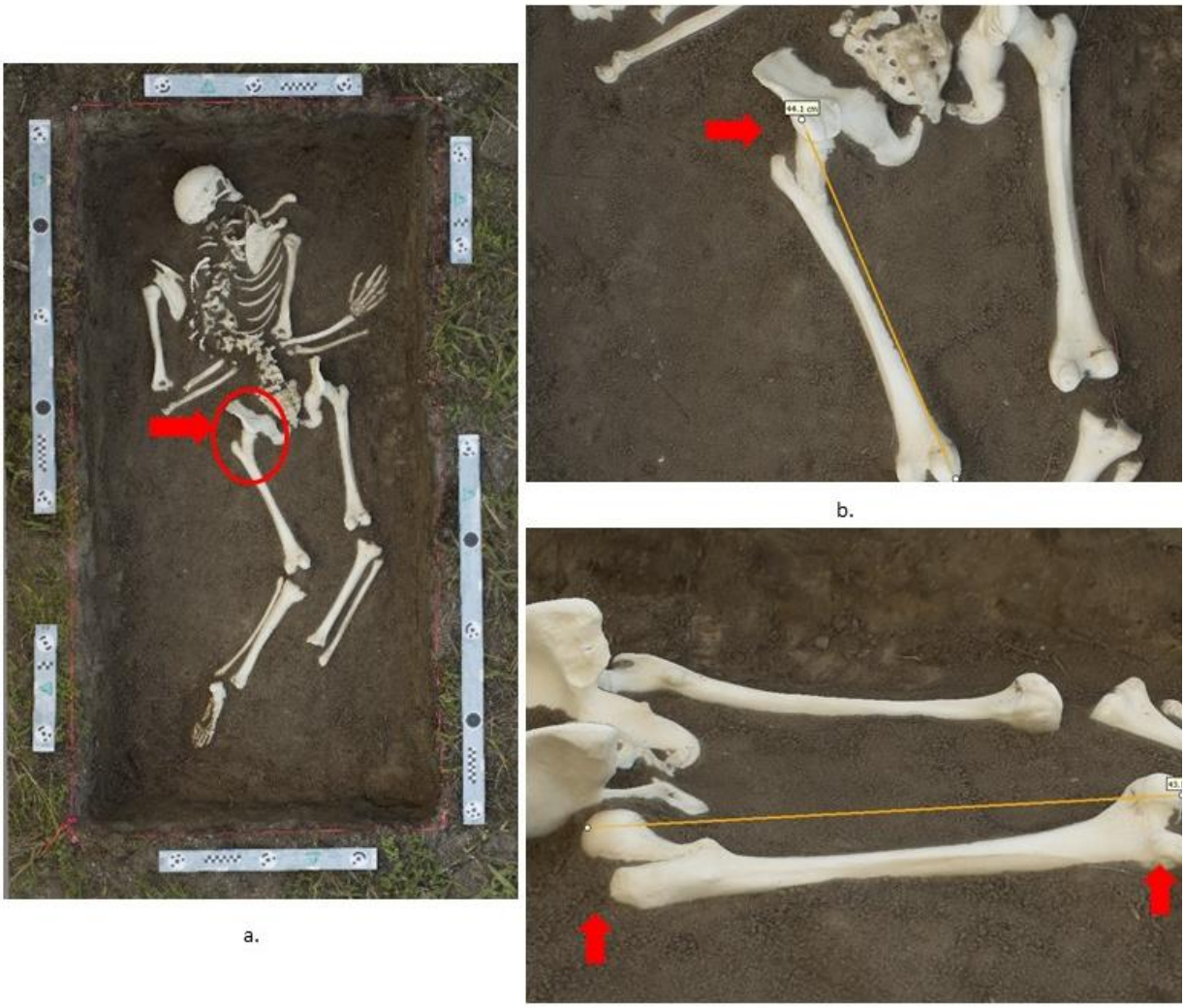

Figure 8. Measuring Model 1 Left Femur. a. In the overview angle, the head of the femur is obscured by the posterior aspect of the illium.b. In a 2D image, this would disallow a bicondylar length measurement to be taken. c. However, a 3D model generated utilizing the CRP process described here can be manipulated to allow for better visualization.

Results

Model 1

This data set collected 84 digital images of a mock excavation with the digital camera held in the hand for the entirety of each circuit at varying heights. Scale bars were placed around the edge of the excavation unit and all images were captured in 7 minutes using the methods described above. Images were processed in Agisoft Photoscan Professional on high settings resulting in a final output model with a RMSE value of 0.0984029 (Figure 9).

Figure 9. Model 1 Results.

Model 1 appears to overall represent the actual faux osteological material with a high degree of accuracy. Stripped of the texture, the final model does an adequate job of representing bone morphology and context. The model represents the actual mock scenario with effective contrast between the sub-surface soil and the faux skeletal material such that individual components are easily identifiable by shape and morphological landmarks. All spatial information is correct including depth.

However, there are various artifacts in the final geometry that are not present in the actual material. Fine details of smaller objects are not entirely accurate and some features are melded together, or missing. Thin, linear objects are similarly impacted with segmentation or data loss occurring. Additionally, the texture portions that represent the osteological material depict a slight blur and bleeding of color data. Scale is largely accurate with a maximum error of 8mm as described in Table 3.

Table 3. Error totals for Data Collection 1.

	Right Femur	**Left Femur**	**Right Humerus**	**Left Humerus**	**Control Scale**
Actual Measurement	428mm	430mm	299mm	293mm	500mm
3D Model Measurement	433mm	431mm	305mm	301mm	501
Error	5mm	1mm	6mm	8mm	1mm

Model 2

This data set collected 86 images of the mock excavation with the digital camera held by hand. Scale bars were placed within the excavation unit with one scale bar placed vertically against the excavation wall. The images were collected in 6 minutes using the methods described

above and then processed on high settings at each processing step. The final model has a RMSE value of 0.100281 (Figure 10).

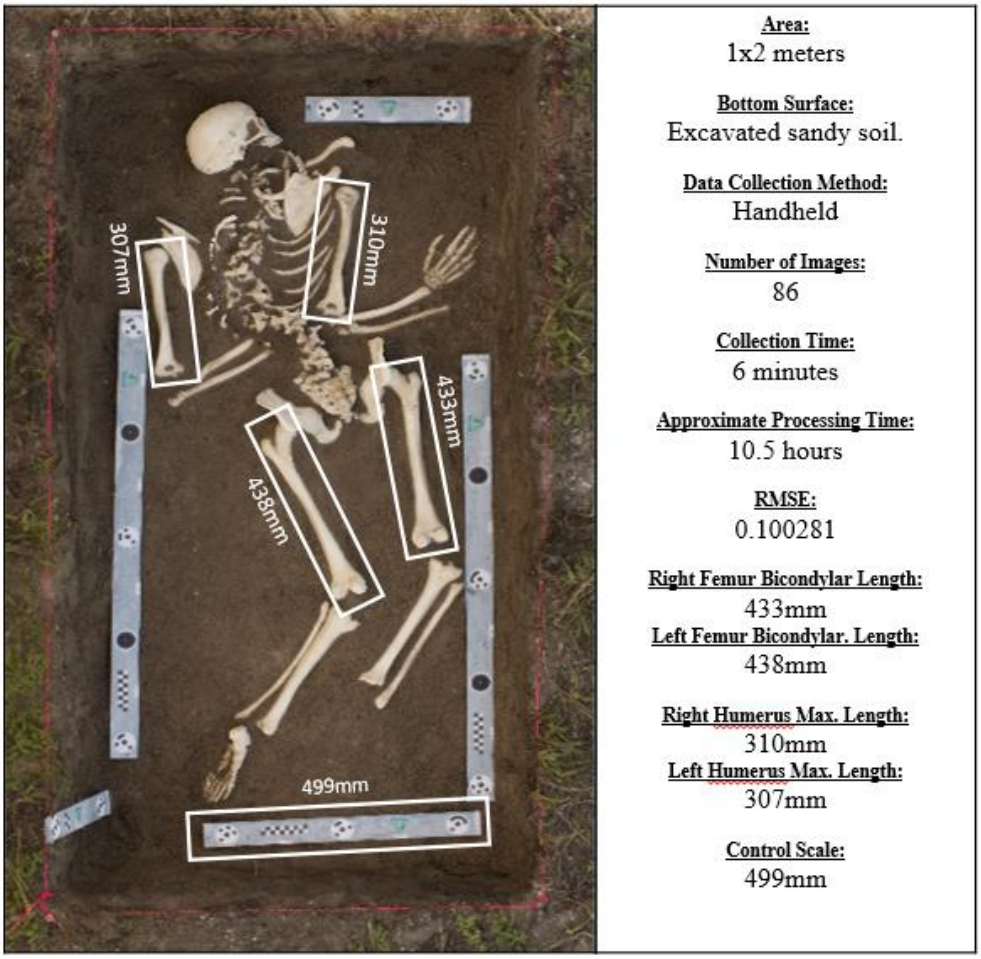

Figure 10. Model 2 Results.

Model 2 is an overall highly accurate representation of the actual mock excavation scene. All contextual data is preserved and is spatially accurate to within a few mm of error. Individual skeletal components are readily identifiable by shape and morphological landmarks and are contrasted well with the soil sub-surface.

However, similar issues with artifacts in the model geometry persist in this model as they did in the first model. While larger objects model well, smaller objects and thin, long objects

tend to lose data or meld together. As in the previous model, the texture data depicts a blur on the plastic material. Scale is largely accurate with a maximum error of 14mm as shown in Table 4.

Table 4. Error totals for Data Collection 2.

	Right Femur	**Left Femur**	**Right Humerus**	**Left Humerus**	**Control Scale**
Actual Measurement	428mm	430mm	299mm	293mm	500mm
3D Model Measurement	433mm	438mm	310mm	307mm	499mm
Error	5mm	8mm	11mm	14mm	1mm

Model 3

This data set collected 92 images of the same mock excavation as the prior examples with the camera mounted on a tripod and a with remote shutter release used. Scale bars were placed around the edge of the test unit. The images were collected in 10 minutes and processed on high settings. The final model has a RMSE value of 0.135521 (Figure 11).

Figure 11. Model 3 Results.

Model 3 represents the overall mock excavation scenario with a high degree of accuracy. Larger, and most smaller, skeletal components depict their actual counterparts with clear similarity. Spatial context is preserved throughout, including an accurate representation of depth and a definite contrast between skeletal material and the soil sub-surface.

Again, the same issues persist in this model as do those in the previous two. Issues with the geometry of smaller and thinner objects are problematic with data loss and melding occurring in many areas. The blur described in the above models is likewise present here. Scale is largely accurate, however, with a maximum error of 8mm as seen in Table 5.

Table 5. Error totals for Data Collection 3.

	Right Femur	**Left Femur**	**Right Humerus**	**Left Humerus**	**Control Scale**
Actual Measurement	428mm	430mm	299mm	293mm	500mm
3D Model Measurement	433mm	437mm	305mm	301mm	500mm
Error	5mm	7mm	6mm	8mm	0mm

Model 4

This data set collected 73 images of the mock excavation with the camera mounted on a tripod and utilizing a remote shutter release. Scale bars were placed within the excavation unit with one scale bar placed vertically against the side of the excavation unit wall. The final model has a RMSE value of 0.144426 (Figure 12).

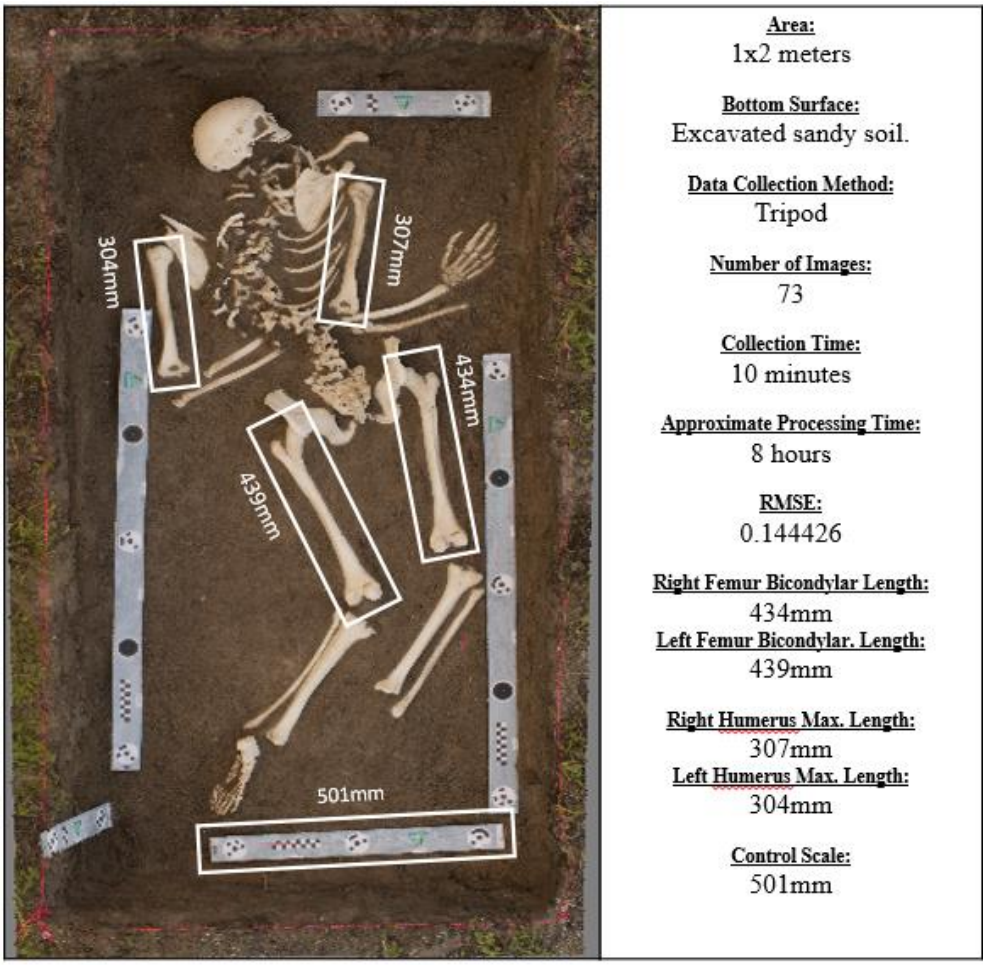

Figure 12. Model 4 Results.

Model 4 provides a highly accurate overview of the faux osteological material and does especially well preserving the geometry of the larger components and many of the smaller. Spatial data is accurate to within a few millimeters. The subject is contrasted well with the soil sub-surface and many morphological landmarks are apparent on the faux skeletal material.

Again, the same issues with artifact geometry in the smaller components persists. Scale remains mostly accurate with a maximum error of 11mm as shown in Table 6.

Table 6. Error totals for Data Collection 4.

	Right Femur	Left Femur	Right Humerus	Left Humerus	Control Scale
Actual Measurement	428mm	430mm	299mm	293mm	500mm
3D Model Measurement	434mm	439mm	307mm	304mm	501mm
Error	6mm	9mm	8mm	11mm	1mm

Discussion

The ability to create 3D models of outdoor forensic scenes is a new scene documentation method that adds to the capabilities of the forensic archaeologist and may provide a faster, more accurate method of preserving scene context than traditional hand-mapping methods currently used. The need to provide accurate, contextual information of forensic scene data is of paramount importance and current protocols, especially those applied to outdoor scenes, are in need of more rigorous approaches towards achieving this goal (Dirkmaat 2012). The use of CRP, among other 3D modeling techniques, is gaining interest among forensic practitioners (Ebert et al. 2011, Fourie 2010, Holowko 2016, Urbanova 2017). Currently, the field is in the formative stage of defining the purpose and limitations of these techniques. While the creation of 3D models has become easier than ever before, the goal now is to define the accuracy of those models such that they can be utilized in a scientific manner. Additionally, considerations should be made for adopting CRP into standard field documentation, as is beginning to be more commonplace within archaeological practice.

The use of CRP as a method of site and artifact documentation is becoming more standard in archaeological practice (Doneus et al. 2011, Douglass et al. 2015, Forte 2014,

Sapirstein and Murray 2017). This is due to the relative low coast of engaging in CRP documentation and the highly accurate results that are capable of being produced via these methods (Galeazzi 2016, Mathews 2018, Opitz and Limp 2015, Sapirstein 2016). The work of forensic archaeology corresponds to the methodology practiced at archaeological sites and, here, specifically corresponds to the work of bioarchaeological documentation utilizing CRP (Fort 2014). As additional research regarding proper protocols and best practices within archaeology is further augmented the standardization of CRP protocols will likely follow. This integration of CRP to standard protocols should also take place within the larger methodological framework of forensic archaeology.

The application of CRP technology is not yet ready to entirely supplant current, standard documentation methods, such as hand mapping, but it may be considered as a useful, cost-effective addition to these methods. Most notably, there is little extra that needs to be added to the kit of a forensic archaeologist who wishes to collect the data for possible photogrammetric processing later; forensic archaeologists already regularly use DSLRs with variable zoom lenses and scale bars are already required for scene mapping (Connor 2007:32, Dupras et al. 2012:7, Robinson 2012). Field data collection takes a matter of minutes (here, a maximum of 10 minutes) and so does not add undue burden to the scene documentation process. Data collected in the methods described above may simply be archived should a 3D model be required of the scene at a later date. Perhaps most importantly, data collection does not need to be conducted by a forensic archaeologist, as other law enforcement individuals who regularly document scenes may be trained to collect image data properly, thus freeing the forensic archaeologist to focus on other issues at a scene or gain a better understanding of the context at a later time.

One drawback is the cost of specialized software, hardware, and the time needed to render data, though this is by no means entirely prohibitive. Depending on the number of images utilized and the capability of the computing hardware available, models may take several hours to fully process. Here, the focus was on a single, discrete burial and so the number of images could be constrained to focus on excessive quality over quantity. However, a more complex scenario would naturally require more imagery and thus more computing power which would equal more processing time. Indeed, it would not be difficult to quickly reach the limits of most commercially purchased desktop computers via photogrammetric processing for large scenes that required more than several hundred images.

The models created as part of this research were highly accurate and exhibited similar discrepancies across each data set. In short, the models are not perfectly accurate representations of the subjects modeled here. They were, however, in many ways better at preserving unmediated contextual data than traditional hand mapping techniques. While CRP techniques allow for great accuracy (BLM 2008, Bolognesi 2014), skeletal material in variable situations offers greater complexity than a structure or archaeological test unit, for example. The issues with these models may be defined as having to do with accuracy of the geometric structure of the subject via the introduction of noise artifacts into the final model due to image capture issues, environmental constraints, or processing issues.

Scale is imposed on the model by the user and depends entirely on the accuracy of the measurement tools utilized in the field, the quality of the image data collected, and the capabilities of the user. As such, there are many ways to affect measurement data in a CRP project. In fact, this is a common issue whenever documenting a scene or site, whether digitally

or manually. The issues in scale here likely do not arise from the highly accurate CHI scale bars; detection of marker points is automated by the program and so allays user error (CHI 2018, Douglass et al. 2015). More than likely error in scale here was introduced at some point of measurement either before modeling or after; that is between measurement of the physical and digital material. One other culprit may be that not enough data was provided in the form of imagery and camera angles to give proper geometry to the components measured. Where complexity was simpler, as in the scale bars, accuracy was more precise. As such, one takeaway is that with complexity of subject material we may assume the greater chance for error. Despite this, the maximum amount of error measured was 14mm and the minimum was 0mm. While this leaves room for improvement, it nonetheless points to CRP as a valuable and viable field documentation technique.

Artifacts introduced to the final model geometry and elements poorly or incompletely modeled represent another issue for utilizing CRP in field documentation techniques. Three main issues with geometry and texture arose from this research: the melding together of individual components, the inaccurate or incomplete modeling of thin components, and a pixelated blur on the white faux skeletal material in the final texture (Figure 13).

Figure 13. Three main issues in final models: (from left to right) a. melding of discrete components (Model 4), b. incomplete data (Model 1), and c. pixel blur (Model 2).

Individual, yet closely associated components may be modeled as one item if not enough image data is provided for the program to correctly delineate the two individual pieces. In fact, a general drawback of photogrammetry software is the tendency for data to be interpolated when it is hard to gain enough tie point data. In this case, the many of the vertebrae were depicted as being melded together when they were in fact individual pieces. One way to potentially counter this is to provide extra imagery data for highly complex, closely situated components at a scene.

Photogrammetric software likewise tends to have difficulty accurately modeling thin, long subject matter. This can be doubly so when the long, thin component has as a back drop a mass of additional complexity as was the case here. The exposed, standing ribs of the faux skeletal material were documented above the mass of vertebrae below. This created an issue

where data was lost and the ribs did not correctly model. This will remain a difficult issue within CRP and a sole possible solution is to again collect extra imagery data of these components for processing.

Lastly, the homogenous, bright, and somewhat reflective material of the faux osteological material created blur in the final texture. This remains a caveat of photogrammetric documentation; reflective surfaces simply do not provide good material for CRP projects and should be avoided in lieu of other, better documentation methods (Agisoft 2018, Douglass et al. 2015). However, as the goal of this research was focused on documenting actual bone which is more varied in texture, color, and tends to not be reflective when encountered in forensic situations, this simply serves to prove the point regarding a taboo against using CRP for material such as this. To determine that the faux material was the result of the geometry or model issues, a mini, corollary test was conducted comparing faux teaching material with actual human osteological material (Figure 14). The relatively low-quality plastic teaching material was placed next to a higher grade, but still plastic, teaching example, and these were placed next to human bone. The final model shows that human bone is by far more accurately depicted due to the varied surface detail, coloration, and lack of reflectivity.

Figure 14. Bone comparison between two plastic teaching examples (left and middle) and human bone (right). The human bone models with much more visual accuracy than the plastic, reflective examples immediately next to it.

Suggested Protocols for On-Site CRP Documentation of Forensic Excavations

As discussed here, CRP should be considered as a standard part of protocol for the forensic archaeologist when documenting the excavation of skeletal remains. Several considerations should be takin into account prior to engaging in a CRP project at a scene, during data capture, and during post-processing. Below, I will provide a general overview of best practices for utilizing CRP during an excavation of skeletal remains in a forensic context. It is important to note that, given the variable nature of outdoor scenes, the following can only be a

set of guidelines to ensure best results and that care should be taken to account for those factors which may introduce error into the final model (Figure 15).

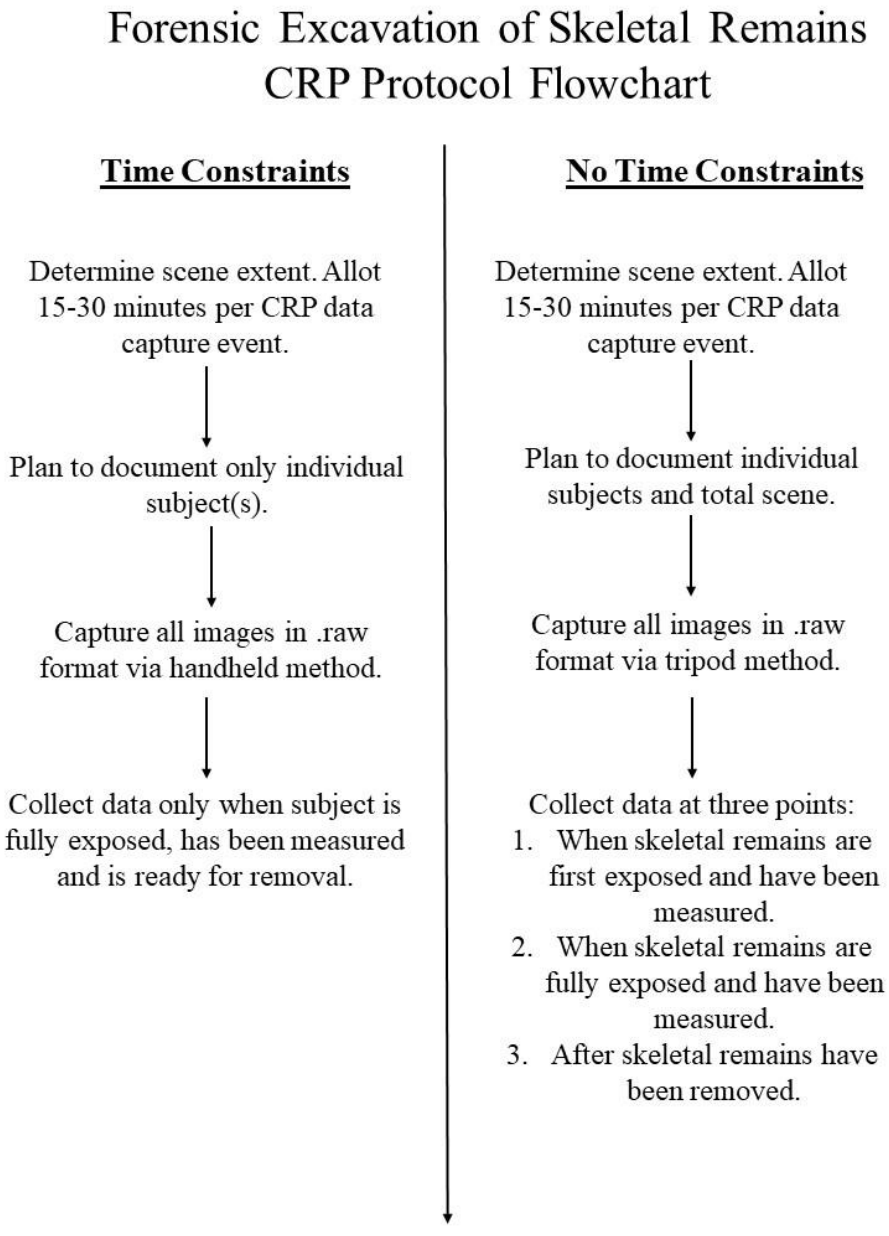

Figure 15. A general protocol for CRP data collection at forensic excavations with and without time constraints.

Prior to arrival at a scene it is worthwhile to know the general extent of the scene and the number of subjects that may require data capture. Here, the forensic archaeologist must decide if the goal is to attempt to capture the entirety of the scene or discrete components. If, for example, a scene was comprised of multiple burials that were to be excavated, would the goal be to individually document each burial or to attempt to capture the entire scene? It is recommended that the priority should be to document individual subjects and to only attempt to document the entirety of a scene if time permits. Additionally, larger scenes comprised of several discrete subjects will require additional data storage. The forensic archaeologist engaging in CRP projects should be prepared to document a scene with at least two camera sd cards (for alternating use), a laptop, and an external hard drive or other data storage device.

Data collection should take place at multiple points during excavation if possible. At each stage, scale bars with control points should be utilized and, if possible, left in place for each subsequent data capture event. The first data set should be captured when skeletal components are first exposed and after the first measurements are taken. The second data set should be captured when the subject is fully exposed, has been measured, and is ready to be removed from the context of the burial. The final data set should be captured after removal of the subject and should focus on capturing the cleaned subsurface of the excavation unit. This may aid in documenting decomposition staining or other evidentiary assets not readily apparent. If time does not allow for each of these data sets to be captured, the primary focus should be on capturing the subject after being fully exposed and after measurements have been taken.

For each data capture set images should be collected at 10-15 degree intervals, or with 80% overlap, 360 degrees around the entirety of the subject to be modeled. This should be

completed a minimum of three circuits, starting as low as possible, perpendicular to the subject if able. Each successive circuit should then increase to a height that still maintains an 80% overlap of the z-value of the previous set. Three circuits are a minimum and, if time permits, additional circuits should be captured with increased percentages of overlap (i.e. >80%) if possible.

All image collection should utilize the digital camera's .raw image format in order to collect the most light data of the subject. Once a focal length has been chosen for a CRP project the lens should not move for the entirety of the data capture process; a strip of tape on the lens casing may be used to ensure that the lens does not move. For variable zoom lenses, the autofocus and auto stabilization features should be switched to off. If using a prime lens there is no need to make these adjustments. For outdoor scenes with variable environmental conditions it is recommended that the camera be set to aperture priority to account for changes in light. While the research here shows little difference in the accuracy of the final models between handheld and tripod data capture methods, it is suggested that a tripod should be used when possible to ensure standardization for circuit photography. However, capturing images via the handheld method is a viable option when without access to a tripod.

If adding CRP documentation into scene protocols an allotment of 15-30 minutes per subject, per data set should be given. This will include the preparation (placing of scale bars/markers and setting of the tripod/camera settings) and the data capture (number of circuits around the subject). Thus, if an excavation has three data sets collected (at initial exposure, at full exposure, and after removal) then the additional time added to scene documentation will be roughly an additional hour and a half. This, of course, will then be multiplied by the number of subjects to be modeled.

All data sets should be separated into individual files prior to pre-processing in Adobe Camera Raw. It is suggested that a file naming protocol be utilized across all projects (Figure 16). File names may have any name subject value desired, but should also include the name of camera model utilized for data capture. This is to quickly identify a data set should there be multiple cameras used at a scene and to assess the relative value of the data therein. Images should be pre-processed into both .dng and .jpg formats; the .dng file will serve as the archive file type and the .jpg will be used to process the model. After this, images are ready to be processed via the methods described above.

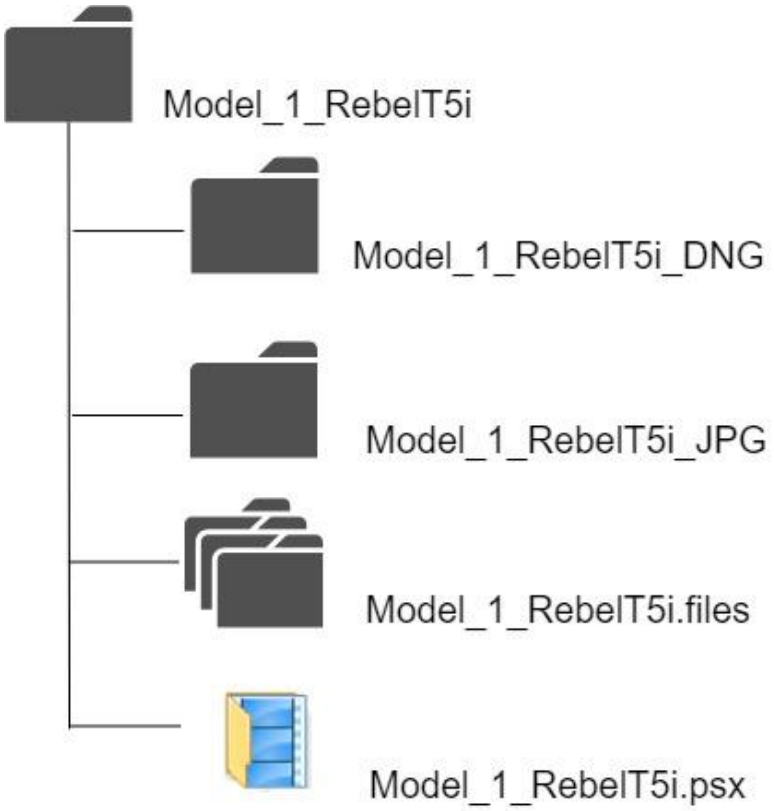

Figure 16. A proposed file structure for properly organizing CRP projects. The root folder file name provides a description, number, and information about the camera used in the field. One sub-folder collects .dng files and another folder collects .jpg files. The files associated with the Agisoft Photoscan project (the .psx and .files in tandem) should be kept in the root folder as well.

Conclusion

Four iterations of data collection were conducted on a mock forensic excavation scene to determine best practices and test the ability of CRP as a method for documentation at an outdoor forensic excavation of skeletonized remains. Most importantly, this research demonstrates that CRP is a useful method for outdoor forensic scene documentation and can readily be applied and implemented into current scene documentation protocols. As with all survey techniques there are drawbacks. Currently, major drawbacks include the cost of computing hardware, time, and the few limitations of photogrammetry software packages to model complex scenes. These drawbacks can be diminished, however, by following best practices outlined above in data collection, data optimization, and attention to issues with accuracy.

While CRP has been utilized more regularly in bioarchaeological investigations its use in forensic scene documentation is in its nascent stage. The exigencies of a forensic scene (time, weather, access to the scene, etc.) thus add a wider selection of variables to contend with. The goal for future endeavors will be to define how we might diminish the impacts of these variables as we develop more standardized documentation techniques.

Future research should focus on testing the limitations of CRP utilization for forensic scenes both indoors and outdoors. A major focus of this future research should be to define acceptable rates of error for scene documentation and how best to utilize the possible data outputs. More specifically to this research, future data collection should utilize actual human osteological material as well as actual forensic scenes. The purpose is two-fold: 1. actual scene documentation is the goal; mock scenarios are useful control tests but will quickly lose their

purpose and 2. we cannot understand the limitations of this technology until we apply it to the varied, complex scenes encountered in real forensic scene documentation.

It is not unrealistic to imagine that as CRP software capabilities increase and as the cost of hardware decreases we will see this technology become a standard part of the forensic archaeologist's toolkit. Already, CRP offers the capability to produce high-quality, context-rich imagery to document scenes faster than traditional hand-mapping and with additional controls against user-generated error. Given the advancement of this technology it is feasible that this process will soon supersede hand-mapping as the preferred method of preserving site context. The goal now is to set the groundwork for its inclusion in the field and to define and promulgate best practices such that accuracy and scientific replicability of scene data is of paramount importance.

CHAPTER THREE: THE APPLICATION OF CLOSE-RANGE PHOTOGRAMMETRY FOR OUTDOOR FORENSIC SCENES WITH SKELETAL SURFACE SCATTER

Introduction

Collecting essential contextual information at a forensic scene is of paramount importance (Dupras et al. 2012; Bass 2005; Blau et al. 2009) Law enforcement officials and forensic anthropologists most often preserve contextual data through hand mapping and digital images. This can be a time-consuming process dependent on the complexity of the scene, especially given extenuating circumstances such as scene access, time since death, scavenging, weather, etc. Outdoor forensic scenes that contain skeletal remains can be among the more difficult scenarios to accurately document where skeletal components may be widely scattered across an area surface. Traditional hand mapping techniques in such situations may only prove as worthwhile as the capabilities of the individual creating the map; indeed, the individual documenting the scene may not be a trained forensic archaeologist and as such the contextual information at the scene is recorded through the mediated efforts of someone unfamiliar with proper forensic scene documentation (Byers 2011: 76). Alternatively, trained individuals documenting a scene may lapse into inattentional blindness (Simons and Chabris 1999) resulting in the potential loss of crucial evidence. Digital images, while useful modes of documentation are nonetheless limited in the scope of how they can portray information and, as with mapping, are only as good as the individual collecting them.

One option to better document outdoor forensic scenes is the use of close-range photogrammetry (CRP). At its most basic, photogrammetry is the derivation of real-world

measurement data from 2D images. Current software packages allow for digital photogrammetry to utilize hundreds or thousands of 2D images in concert to generate highly accurate 3D models of real-world scenes (Douglass 2015, Opitz and Limp 2015). Here, real-world measurement and color data are recreated in 3D space as a geometrically defined model and may have real world coordinate systems applied it. This process utilizes standard DSLR cameras, already present during any scene documentation, and specialized software. Data capture for a CRP project is quick (compared to hand-drawn maps), affecting standard scene documentation protocols only slightly, and images may be collected and archived for later processing if needed (Douglass 2015, Sapirstein and Murray 2017). Additionally, best practices for CRP data capture can be taught to those collecting evidence at a scene, whether a forensic archaeologist or not, and thus aid in preserving 3D contextual information for later analysis.

There is a need for more rigorous documentation protocols for outdoor forensic scenes (Dirkmaat 1997, 2012). The application of CRP offers one way to improve scene documentation at a relatively low coast and with minimal impact on extant protocols. While this technology is not necessarily new, it has not been widely applied to forensic scenes to any great extent thus far (Sansoni et al. 2009:541). Within the wider realm of anthropological research CRP is more often applied to the documentation of structural resources, general cultural resources, archaeological sites, artifacts, and bioarchaeological excavations (Forte 2014, Doneus et al. 2011, Howland et al. 2014, Ioannides et al. 2014, Berggren et al. 2015). While the current research looks to the uses of CRP in these cases (especially to bioarchaeology), the exigencies of forensic scene documentation are such that there is not an exact correlation in usage. As such, efforts must be made to test the capabilities of CRP documentation at outdoor forensic scenes in a variety of

settings, beginning with the most common regionally and working towards finer detail. In Florida, one of the most common terrestrial ecosystems are oak hardwoods and pine flatwoods. These are typified by low, flat areas with poorly drained, sandy soil and may contain significant areas of underbrush (IFAS 2018). Oak hardwoods and pine flatwoods represent potentially highly complex forensic scenes to document due to the distance human remains might be spread when deposited on the ground surface by scavengers as well as the ability of underbrush to obscure skeletal elements. The purpose of this research is to determine the capability of providing law enforcement professionals and forensic archaeologists with a supplemental scene documentation method for scattered skeletonized remains on the ground surface in complex outdoor environmental conditions .More specifically, this chapter will contrast the utility of CRP's use for forensic excavations in the preceding chapter with the more difficult prospect of collecting data in larger, more complex situations, especially those where variability and scene complexity are the predominate features: small and wide scatters of human skeletal remains. While the capabilities of CRP are not yet at the stage that they will entirely supersede pencil and paper documentation, or outshine laser scanning, this method is nonetheless fast approaching the point where it may do so. At this stage, foundational research is needed to build upon and better understand the potential utility of CRP in forensic scene documentation, especially in the documentation of complex, outdoor areas.

To demonstrate and test the utility of CRP for 3D outdoor crime scene modeling this paper will use two staged representative scenarios and discuss the outcomes of the applied methodology for each. These two mock scenes are a close scatter of human skeletal remains and a wide scatter of human skeletal remains within a pine flatwoods/oak hammock environment and

using faux osteological material. Field data collection will be discussed as will the advantages and disadvantages of CRP. An overview of the post-processing requirements and the possible data outputs will be explored as well. An assessment of accuracy will be examined using control points within the scenes and via measurements within the 3D model. Finally, suggestions for future avenues of investigations will be considered.

Background

Why Crime Scene Photography Matters

Photography has been in use to document crime scenes since the latter half of the 19th century (Milliet et al. 2014, Robinson 2012), with the earliest example dating to 1867 (Robinson 2010:8). Crime scene documentation, however, was a relatively late comer to the technology, which took stride near the middle of the 19th century (Robinson 2012). Early daguerreotypes, calotypes, and later ferrotypes, especially of portraits, represent the first major commercial uses of photography. Equally important was its use as a documentary device, as in the Civil War images captured by Mathew Brady and reproduced in periodicals throughout the country (Robinson 2012:7). During this time two advances in photography, pertinent to the subject matter of this paper, were developed: aerial photography and stereo photography. Both would come to have major impacts in the realm of archaeology. By the beginning of the 20th century, U.S. courts deemed certain types of photographs as admissible evidence and by the middle of the 20th century the FBI had units dedicated to the use of photography to document criminal cases. More recently, technological innovations have changed the way photographs are taken, most significantly in the shift away from film to digital imaging. However, while photographic

technology has changed significantly, little in the way that a crime scene is documented using photographs has changed, though certainly advances in digital photography software have made an impact in the technical capabilities of a crime scene photographer (Robinson 2010:3-17).

The purpose of crime scene photographs is three-fold (Table 7): 1) to document, 2) to provide potential leads, and 3) to substantiate testimony (Robinson 2010:594). It creates a fair and accurate record of the scene such that it may be included in court proceedings (Weiss 2009: 25-49). Additionally, crime scene photography assists in depicting the overall configuration of the scene and the associated evidence; its serves to allow for analysis and comparison beyond initial investigations at the time and at the scene (Milliet 2014:471). Images also help to protect and preserve evidence in otherwise changing scenarios; weather, time constraints, aspects of the evidence (susceptible to rapid deterioration), all can affect the capabilities of law enforcement professionals to properly conduct an investigation. Crime scene photos are evidentiary in nature, a departure from archaeological photography, where the purpose is more descriptive. Regardless, both archaeological and forensic photography must document artifacts or evidence in situ. This can prove difficult if forensic archaeologists or anthropologists are not a part of the in-field evidence collection process. Though law enforcement agencies have protocols in place for photo documentation of crime scenes, it is not improbable that important points of information might not be documented simply due to ignorance of their importance. Further, situations of inattentional blindness may inhibit data collection at a forensic scene. Given the demands of site data collection, and under certain pressures, inattentional blindness, or the failure to recognize obvious details even when trained to do so, may mean that evidence is improperly documented or not documented at all (Simons and Chabris 1999). The use of CRP offers a solution to these

scenarios. Though it may be worthwhile to note that this is an initial step forward; its use is not currently poised to make pencil and paper techniques completely obsolete. As Opitz (2015:75) notes, the interpretive sketch still has value and encourages engaged observation of the data during abstractive work. Rather, the development and utilization of CRP field methods for forensic scenes will require proof-of-concept studies such as the present one, and further analysis and refinement of techniques. With time, it may become a regular aspect of crime scene investigation, a skill transferred to non-specialists who must simply follow predetermined data collection methods.

Table 7. The Purpose of Crime Scene Photographs. Adapted from Robinson 2010:594.

Purpose of Crime Scene Photographs	
Document	One of the basic documentation techniques, in addition to sketches and diagrams. Three basic categories: overall, midrange, and close-up.
Provide Leads	Can be used to share information with those not at the scene or to ascertain additional clues. Can review for additional clues not recognized during scene analysis.
Substantiate	Can assist witnesses to clarify or remember aspects of a forensic investigation. Also, serves to provide proof to determine correct information during contradictory statements.

Close Range Photogrammetry

Wolf (1983:1) defines photogrammetry, "as the art, science, and technology of obtaining reliable information about physical objects and the environment through processes of recording, measuring, and interpreting photographic images and patterns of recorded radiant electromagnetic energy and other phenomena." In regard to photogrammetry, the "electromagnetic energy" is visible light. While this is a traditional definition of the science of photogrammetry, it is more widely associated today with digital photogrammetry, computer vision technology, and SfM/MSV algorithms (Doneus et al. 2011). The goal of digital photogrammetry is to create a mathematically derived 3D visualization of a real-world item or scene. This is achieved by taking a series of overlapping photos around or over an item or scene. The use of SfM allows for automated, large bundle analyses of photo sets where tie points are identified among and between the picture set. These tie points are used to triangulate distances to the camera. In this way, virtual geometry is recreated (Doneus et al. 2011; Mathews 2008; Agisoft 2018). The term CRP applies to data collections where the camera and the item are within 300 meters of one and other (Mathews 2008:11).

There are currently several commercial and open source SfM software packages available, however all generally process data in a similar manner (Doneus et al. 2011:82, Sapirstein and Murray 2017: 337). At each processing stage a series of decisions must be made by the user, most pertaining to the relative resolution of the final image (Douglass et al. 2015). These decisions are based on output needs and hardware capabilities. A series of digital photographs are processed and tie points created among the images, the sparse point cloud (SPC). Next, a dense point cloud (DPC) is created based on the estimations of camera distances.

After these are generated, a mesh is created from the DPC. This mesh is a polygonal network upon which a texture stitched from the accumulated images can be set (Doneus et al. 2011, Douglass et al. 2015, Agisoft 2018).

Several outputs are possible and many software options exist to produce those outputs. These include the export of DPCs to be compared to one and other to quantify differences, orthorectified images (orthomosaics), 2D planimetric, tiled models, digital elevation models (DEMs), and of course 3D models (Agisoft 2018, Doneus et al. 2011, Douglass et al. 2015). Outputs are increasingly easy to utilize across software platforms as well. Most CRP outputs can be integrated into computer vision and graphics software packages, computer aided design (CAD), and geographic information systems (GIS). Thus, CRP processing offers a wide array of options to both display and query processed data.

Use of Close-Range Photogrammetry in Archaeology

In recent years the field of archaeology has embraced a suite of technologies that offer faster, cheaper, more accurate documentation and analysis of sites and artifacts (Douglass et al. 2015, Forte 2014, Howland et al. 2014, Opitz et al. 2015, Opitz and Limp 2015, Prins 2016, Wallace 2017). This suite of new technologies may be referred to by the term high-density survey and measurement (HDSM) as defined by Optiz and Limp (2015). This suite of technologies, CRP among them, are currently enjoying unprecedented impacts on the field; most notably, the utilization of HDSM techniques allows for researchers to, "…decouple measurement from interpretation…leading to a fundamental alteration of the abstractive process in archaeology (Optiz and Limp 2015: 359)." This is no small feat and has profound implications germane to the topic of the research discussed here, namely in regard to the needed improvement

of scientific rigor in the field of forensic archaeology (Dirkmaat 2012). An additional benefit of utilizing HDSM technologies for site or scene documentation is the ability to limit the potential for errors to be introduced into data sets via inattentional blindness (Simons and Chabris 1999). This more important in situations where stressful external variables are at play during the data collection process, as may be the case during a forensic recovery under time constraints, weather events, or difficulty in access to a scene.

The use of CRP as a data collection option on archaeological sites is particularly popular due to its relatively low cost and ease of use (Douglass 2015, Forte 2014, Sapirstein and Murray 2017). Photogrammetry has been put to use modeling excavations (De Reu et al. 2014, Doneus et al. 2011, Douglass et al. 2015), entire sites (Forte 2014, Galeazzi 2016, Howland and Falko 2014), structures (Caroti 2015, Ioannides et al. 2014, Opitz 2015), and is even already being implemented in bioarchaeological excavations (Forte 2014). One additional benefit of utilizing CRP on archaeological sites, not often recognized in the pertinent literature, is the controlled environment that many sites offer. This is in contrast to the sites that forensic archaeologists often encounter, where terrain and time may not allow for the creation of an optimal data collection situation for CRP.

Materials and Methods

Research Site

Research was conducted at a site near the University of Central Florida on private property that was offered for this project's data collection (Figure 17). The site was chosen as it offered a oak hammock and pine flatwood environment. Oak hammock and pine flatwood

environments in Florida are one of the most common terrestrial ecosystems, behind areas defined by wetlands (Volk et al. 2017:74). As such, these environments represent a common type of location that forensics scenes may be found in. Specific vegetation is determined by location in the state, (north/central or south) but generally is comprised of various types of tall pine species, intermittent hardwood stands, and understory shrubs (IFAS 2018). Outdoor forensic scenarios comprised of skeletonized remains in such an area provide many challenges based on the surrounding environment: open flatwood areas with minimal understory means that scavenged remains may be widely scattered throughout a scene and that if understory vegetation is present, the skeletal components may be more easily hidden from view. Additionally, the ground surface of the research site, as in any flatwood or hardwood stand, was covered with an array of leaf-litter, adding to the complexity of the environment for data capture purposes.

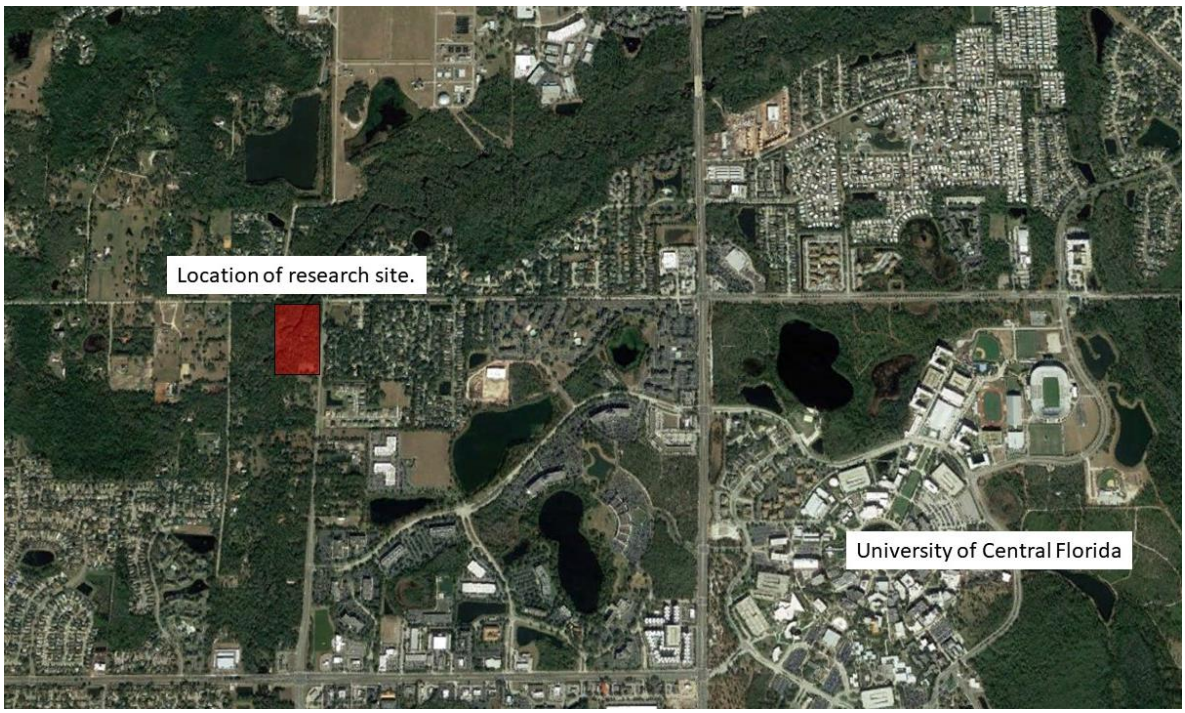

Figure 17. Location of research site in relation to University of Central Florida Campus in Central Florida. The research site was typified by pine flatwoods and oak hammocks (Source: Google Earth Pro).

Faux Skeletal Material

A plastic teaching skeleton was used for each of the scenarios discussed here. The material, while overall exact in terms of morphological features, was nonetheless not a perfect representation of actual human bone. The material was a homogenous, reflective white color and features are not as precise as those on actual osteological material. Prior to generating the scenarios, measurements were taken of the femora at the bicondylar length (Buikstra and Ubelaker 1994:81) and the humeri at the total length (ibid. 82). These were used to later test the accuracy of the completed model.

Small Scatter Scenario

This scenario represented a small scatter of skeletonized human remains minimally disturbed by taphonomic impacts outside of decomposition. Major osteological elements were largely positioned within correct anatomical proximity to each other with smaller elements of the left leg dispersed to mimic minimal scavenging. The faux skeletal material was placed next to a hardwood stand on a surface of sandy soil with considerable leaf litter. The scene, as modeled covered approximately 3 x 5.5m (Figure 18).

The remains utilized in this scatter consist of a nearly complete skeleton including the cranium, mandible, all long bones, 23 ribs, 24 vertebrae, three tarsals, for metatarsals, as well as the shoulder girdle and pelvic girdle. See Appendix II for a complete skeletal inventory.

Two data sets were captured for this scenario, each testing the same variables: camera images taken handheld versus mounted on a tripod and scale bar placement. Scale bars were place around the greater extent of the small scatter with some smaller osteological elements

outside of this perimeter to assess the capability of modeling evidentiary components that may have been neglected, unseen, or forgotten about during data capture.

Prior to arrangement of the faux skeletal material on the ground surface all elements were measured utilizing standard protocol (Buikstra and Ubelaker 1994). Additionally, this area was denuded of as much vegetation within the immediate vicinity of the scene to allow for better documentation.

Three data set circuits of the subject area were completed twice, once handheld and once with a tripod, to collect images with at least 80% overlap. Each circuit rose vertically and with increased angle towards the scene; that is, the initial circuit was captured at waist height, then at chest, then at head with the angle compensating downward to retain the scene as fully within the frame of the camera as possible (Agisoft 2018:8-11).

Figure 18. The small scatter scenario showing the complex ground surface, scale bar placement, denuded subject area, and the author collecting images with the digital camera mounted on a tripod. The denuded area is outlined and individual elements purposefully left outside of the scale bar perimeter are noted with arrows.

Wide Scatter Scenario

The wide scatter scenario represented an expansive scatter of human osteological remains due to extensive scavenging as well as other taphonomic impacts (Figure 20). This scenario was located on the side of a dirt road next to an oak hardwood stand with significant underbrush on the research site. The scene location graded down towards a creek and the faux osteological remains were spread to mimic scavenging with a downhill trend. The faux skeletal material was placed atop the sandy, leaf-littered ground surface. For this scenario, no denuding or other scene preparation was carried out after placement of the skeletal components and the scale bars. The scene covered approximately 3.5 x 7m (Figure 19).

The faux skeletal remains used for this mock scene consisted of a partial skeleton consisting mainly of the cranium and several long bones along with a partial shoulder girdle and a partial pelvic girdle. Additionally, several vertebrae were scattered throughout the scene. See Appendix II for a complete skeletal inventory.

Three data set capture circuits were collected for the wide scatter scenario, as described above, to test the variables of scale bar placement, distance of individual faux osteological components from the scale bars, and the number of images required to achieve highly accurate results.

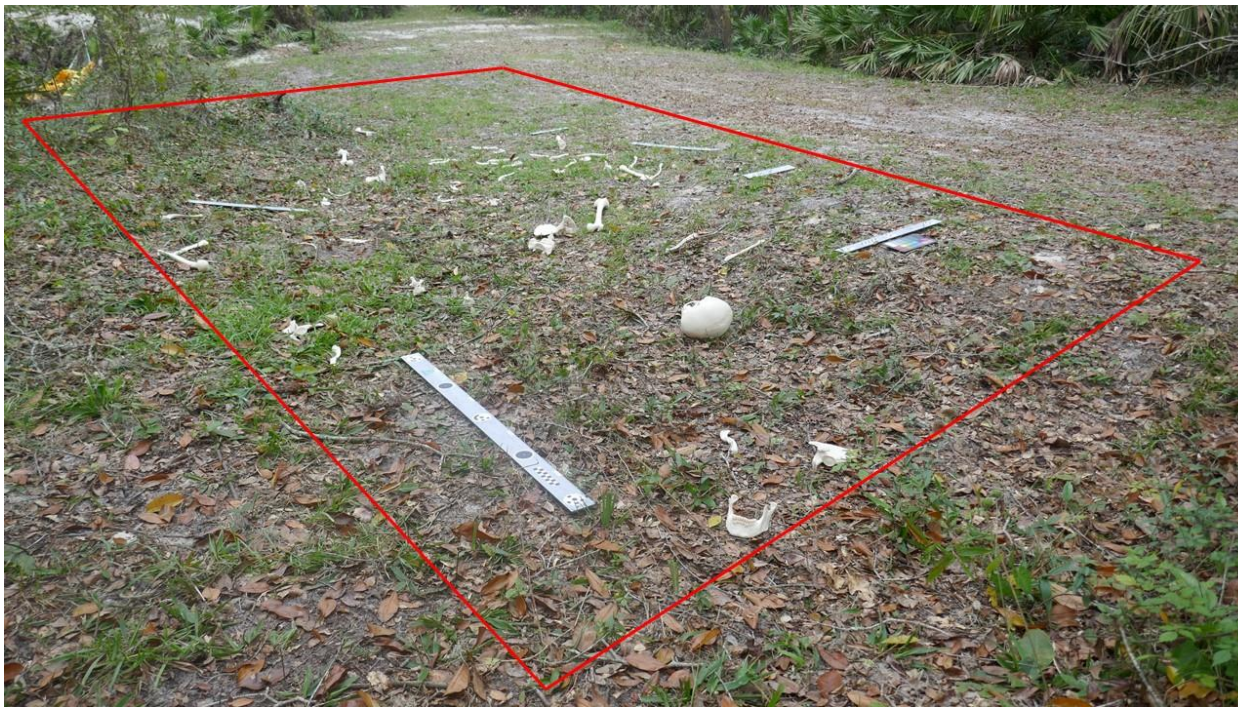

Figure 19. Overview of the wide scatter scenario. This scenario represents scattering due to extensive scavenging and osteological elements rolling downhill. Scale bars were placed more widely around the scene, differing from the perimeter created for the small scatter, and no vegetation was removed prior to data capture.

Hardware and Software

All data were collected using a Canon EOS Rebel T5i camera with a variable zoom (18-55mm) kit lens. The digital camera was set to capture .raw imagery and all images were captured on the aperture priority setting to account for variations in outdoor light. One data collection set utilized a standard tripod while all others were shot by hand. Ground control markers and scale were managed via the use of specialized scale bars manufactured by Cultural Heritage Imaging (CHI 2018). Control markers on the bars are automatically recognized by the photogrammetry software and so add a layer of automation to post-processing (Agisoft 2018).

All data sets were processed using Agisoft Photoscan Professional with settings on high for processing stages (Agisoft 2018). Prior to loading into Photoscan, images were pre-processed

using Adobe Camera Raw to correct for white balance, lens calibrations, and color distortion. Each image set was archived in .dng format and processed into .jpg format for use in Photoscan.

Each data set for the small scatter scenario was processed to both a final 3D model and as a scene overview orthomosaic. Additionally, processing reports were generated for each model (Appendix I).

Testing Accuracy

A total of five models were generated as the result of this research. Accuracy was assessed for each via three measurements per final model. These include a root mean square error (RMSE) metric, generated by Photoscan after processing stages are complete. The RMSE is the aggregate error inherent in a model and represents the accuracy given the user's input parameters (Agisoft 2018). It is not necessarily a measure of precision regarding the actual subject matter. To determine the accuracy of the model to the real-world subject matter two measurements from the subject material are compared to measurements from the finished 3D model. While multiple scale bars are used in each model, only three are given defined distance measurements with at least one left undefined as a control. That measurement is then compared, physical to virtual. Lastly, the digital femora and humeri, measured prior to data collection, are compared to the actual measurements and an error is given. While no one metric can define the overall accuracy of a model generated by CRP for these scenarios, the aggregate units of error will serve to determine relative accuracy (Douglass et al. 2015:145). Additionally, while accurate measurement is of course important, equally important regarding this research is the capability of CRP to preserve scene wide contextual data in a 3D format so that it may be digitally preserved and reinvestigated at later dates. As such, as long as accuracy issues are noted, the value of a

CRP data capture is in its ability to convey information as a total package, not necessarily as an infallibly precise simulacrum of the site itself.

Results

Small Scatter 1

This data set collected 129 digital images of a mock forensic scatter with the digital camera held in the hand for the entirety of each circuit at three distinct heights. Scale bars were placed around the edge of scene in a semi-perimeter and all images were captured in 8 minutes using the methods described above. Images were processed in Agisoft Photoscan Professional on high settings resulting in a final output model with a RMSE value of 0.147723 (Figure 20).

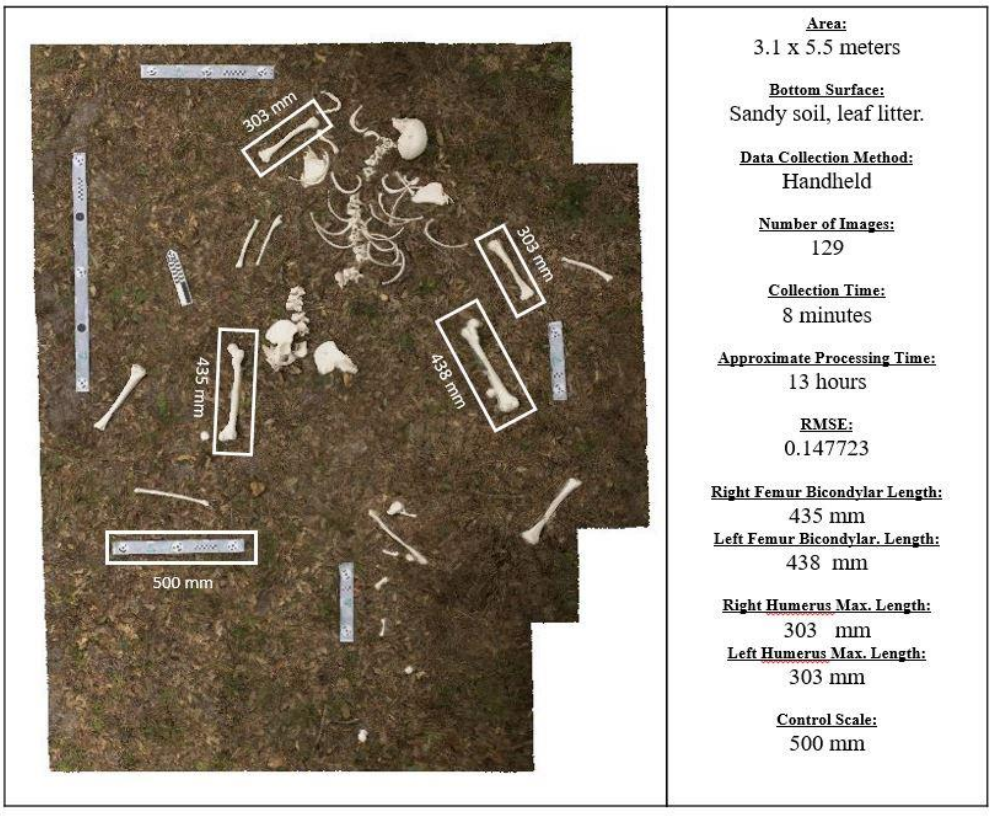

Figure 20. Small Scatter 1 results.

The final 3D model of small scatter 1 appears to overall represent the actual faux osteological material with a high degree of accuracy regarding the contextual location of each skeletal component to each other. Additionally, the morphological shape of the faux skeletal material is overall represented in the model geometry.

There are, however, some issue with the final model geometry. Several issues are similar to those present in the final models of the excavation examples discussed in the previous chapter (see Figures 10-13): combination of discrete features, poor resolution, and blur around the faux osteological material are present in portions of the final model. Issues with model geometry tend to occur in areas away from the scale bar perimeter, outside of which data were collected, and nearer to the oak hardwood stand (Figure 21). Despite these issues, the model is largely accurate in x,y,z dimensions with a maximum error of 10mm (Table 8).

Figure 21. Detail of issues in Small Scatter 1. Note the diminished resolution/geometry in the faux elements from left to right. Arrow 1 highlights the largely accurate radius modeled for this scenario, especially when compared to its counterpart, highlighted by arrow 2. Arrow 3 highlights an error-prone tibia, one of the elements furthest away from scale bars and closest to the underbrush which made maneuverability to capture images difficult.

Table 8. Error totals for Small Scatter 1.

	Right Femur	Left Femur	Right Humerus	Left Humerus	Control Scale
Actual Measurement	428mm	430mm	299mm	293mm	500mm
3D Model Measurement	435mm	438mm	303mm	303mm	500mm
Error	7mm	8mm	4mm	10mm	0mm

Small Scatter 2

This data set collected 146 digital images of a mock forensic scatter with the digital camera mounted on a tripod for the entirety of each circuit at three distinct heights. Scale bars were placed around the edge of scene in a semi-perimeter and all images were captured in 17 minutes using the methods described above. Images were processed in Agisoft Photoscan Professional with high settings resulting in a final output model with a RMSE value of 0.0790753 (Figure 22).

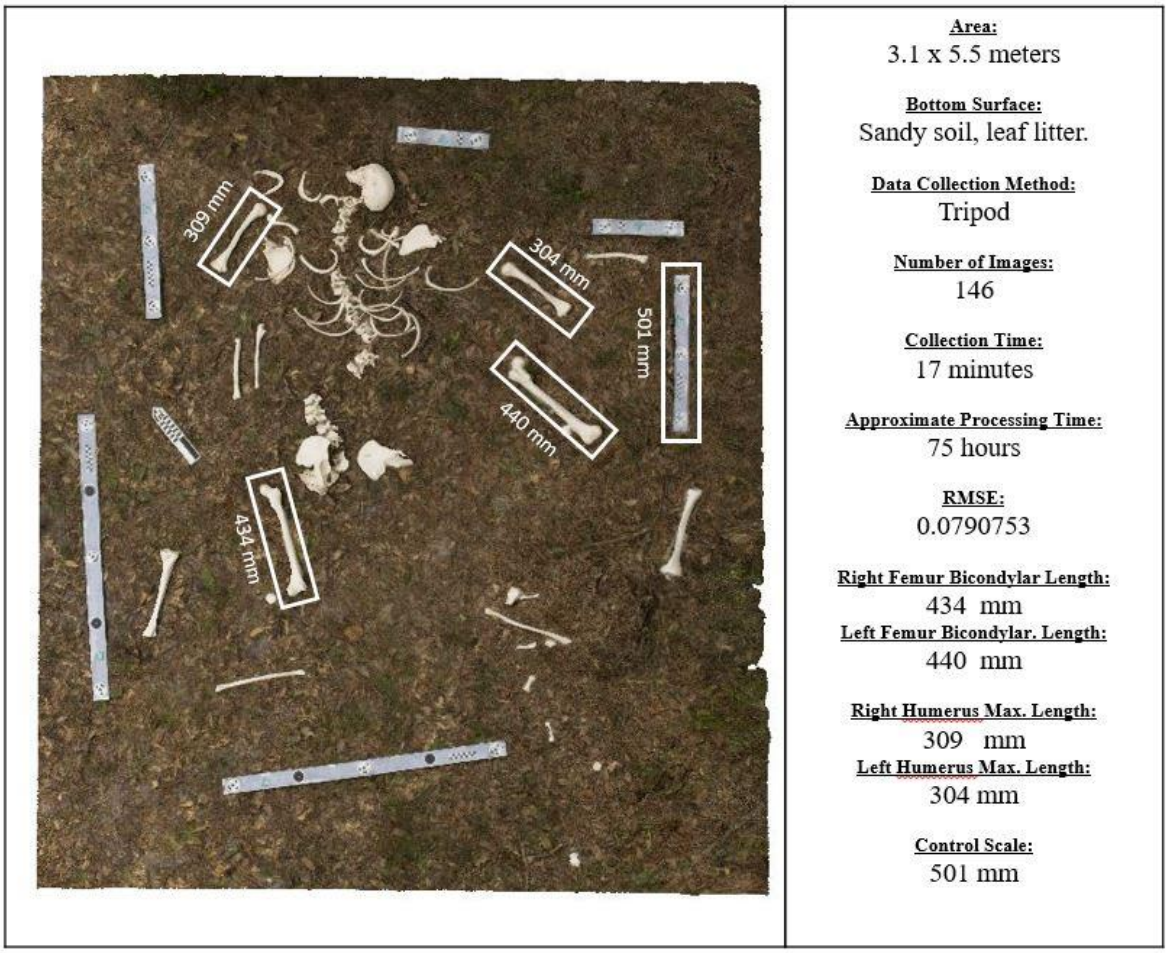

Figure 22. Small Scatter 2 results.

The 3D model of small scatter 2 appears to overall represent the actual faux osteological material with a high degree of accuracy regarding the contextual location of each skeletal component to each other. The shape and morphology of the faux skeletal material is present in the model and easily discernable.

The issues in final model geometry mentioned above persist in this model as well, though are less prevalent. Again, faux skeletal components further from the perimeter, towards the center, exhibit more error in their geometry. These include discrete component melding and a

blurring (Figure 23). However, even with these issues the model is largely accurate in x,y,z dimensions with a maximum error of 11mm (Table 9).

Figure 23. Detail of issues in Small Scatter 2. In image a. the encircled area shows the melding effect on the mass of vertebrae and ribs. Image b. depicts the tendency for elements further away from the scale bar to exhibit more (slightly, here) error in the model geometry in the form of blurring.

Table 9. Error totals for Small Scatter 2.

	Right Femur	Left Femur	Right Humerus	Left Humerus	Control Scale
Actual Measurement	428mm	430mm	299mm	293mm	500mm
3D Model Measurement	434mm	440mm	309mm	304mm	501mm
Error	6mm	10mm	10mm	11mm	1mm

Wide Scatter 1

This data set collected 123 digital images of a mock forensic wide scatter with the digital camera held in the hand for the entirety of each circuit at three distinct heights. Additionally, images were captured while walking through the scene. Scale bars were placed around the edge of scene in a loose perimeter and all images were captured in 13 minutes using the methods described above. Images were processed in Agisoft Photoscan Professional with high settings resulting in a final output model with a RMSE value of 0.0779446 (Figure 24).

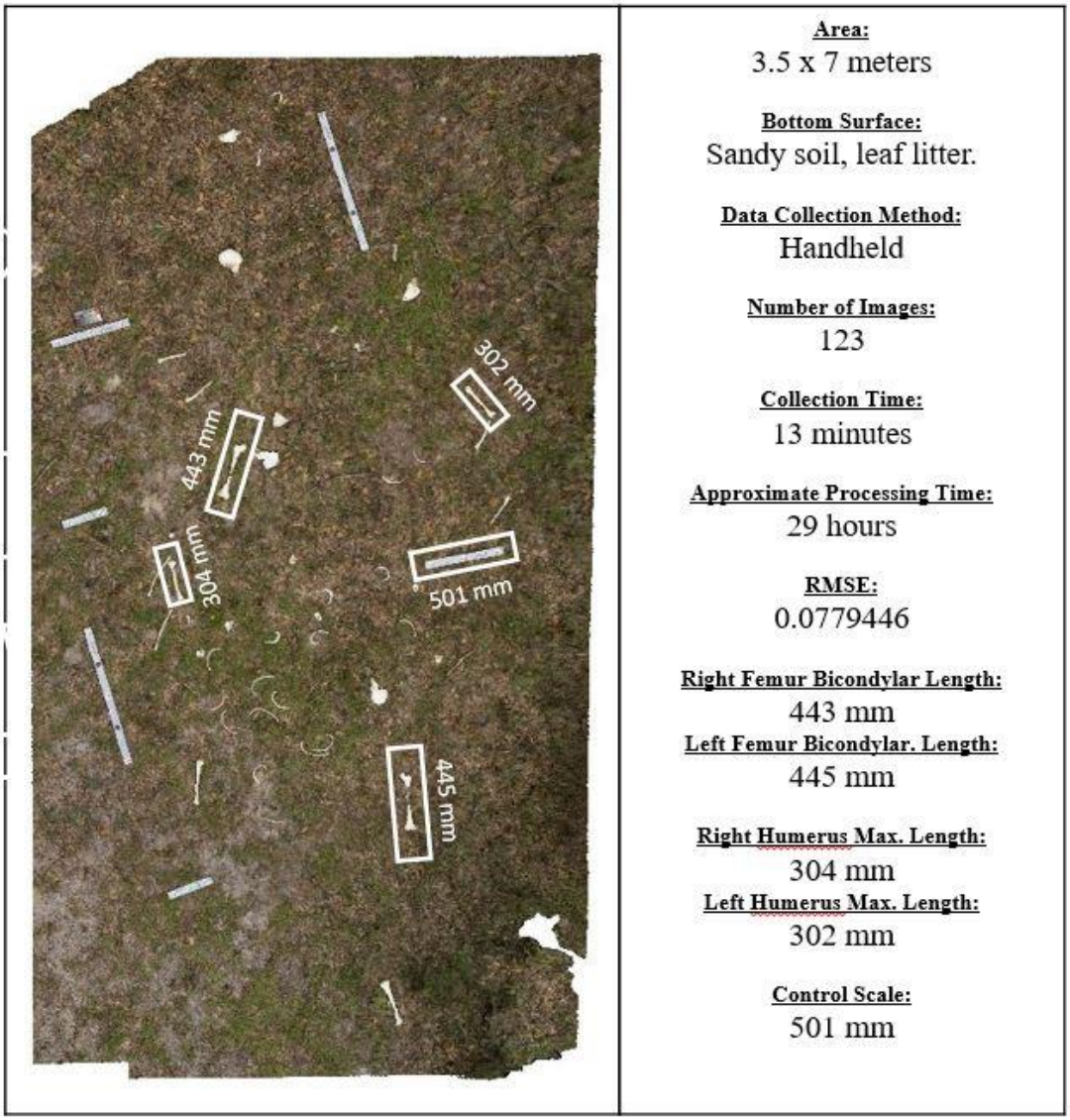

Figure 24. Wide Scatter 1 Results.

The 3D model of wide scatter 1 overall represents the contextual location of individual elements in relation to one and other. Generally, individual morphological characteristics of the skeletal material is apparent. Overall, there is a high degree of accuracy for the final model output. The model represents generally good accuracy of x and y coordinate values, though appears to have issues with z values

Issues in final model geometry include blur, melding, and the absence of data in some portions of the model geometry, particularly on portions of linear bone (e.g. ribs) and some long bone (e.g. femora). Skeletal elements nearer to scale bars appear to have less inherent error though the overall complexity of the ground surface appears to affect many individual elements within the model (Figure 25). The maximum error is 15mm (Table 10).

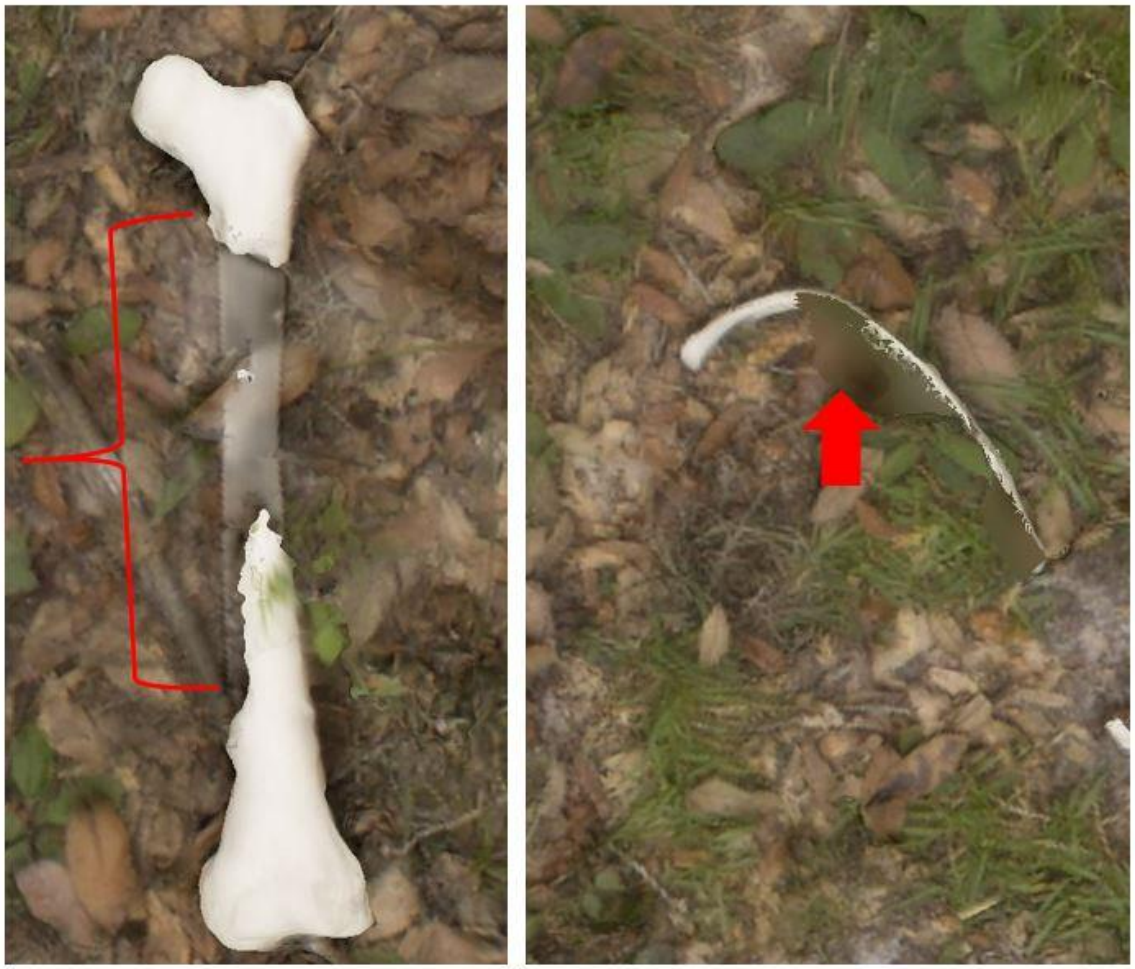

a. b.

Figure 25. Closeup of issues with discrete elements in Wide Scatter 1 model. Image a. shows incomplete data on the shaft of the left femur. While some data was used in generating the model (note the opaque section) not enough data was present to fully model the femur. In Image b. a similar situation has occurred on the body of the rib, where image blurring and loss of information are seen.

Table 10. Error totals for Wide Scatter 1.

	Right Femur	Left Femur	Right Humerus	Left Humerus	Control Scale
Actual Measurement	428mm	430mm	299mm	293mm	500mm
3D Model Measurement	443mm	445mm	304mm	302mm	501mm
Error	15mm	15mm	5mm	9mm	1mm

Wide Scatter 2

This data set collected 198 digital images of a mock forensic wide scatter with the digital camera held in the hand for the entirety of each circuit at three distinct heights. Additionally, images were captured while walking through the scene. Scale bars were placed around the edge of the scene in a loose perimeter and all images were captured in 13 minutes using the methods described above. Images were processed in Agisoft Photoscan Professional with high settings resulting in a final output model with a RMSE value of 0.0555378 (Figure 26).

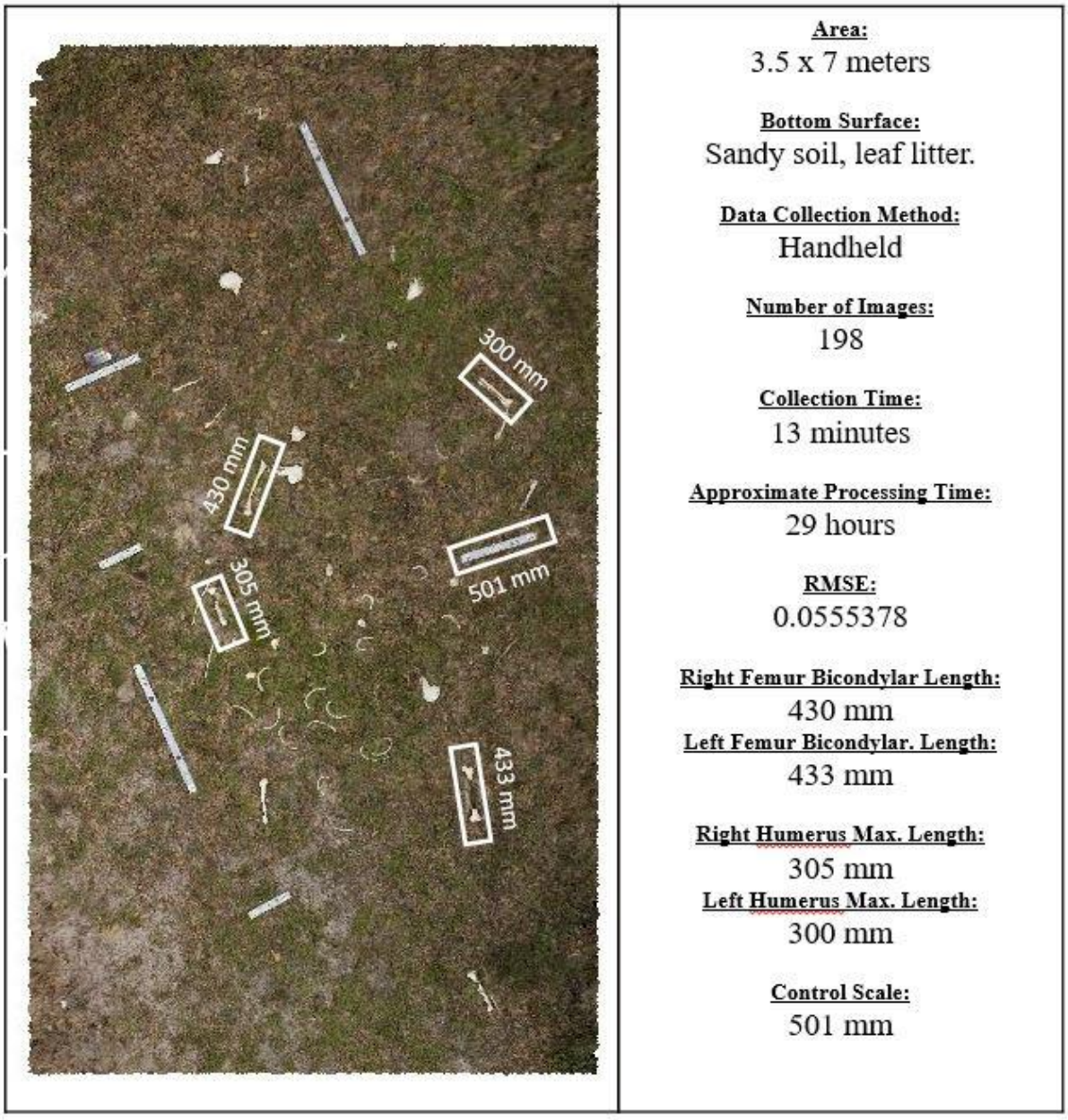

Figure 26. Wide Scatter 2 Results.

The wide scatter 2 model is overall contextually accurate and most individual skeletal elements are apparent. Spatially, x and y values are largely accurate with issues in overall z values.

The final model for wide scatter 2 exhibits additional issues in model geometry when compared to wide scatter 1. Issues of discrete element melding and blur are more prevalent across

the model, even in elements near the scale bar positions. Additionally, some portions of individual faux skeletal material failed to accurately model, especially on long, thin portions of the material (Figure 27). For those elements measured the spatial accuracy of scale was nonetheless high with a maximum error of 13mm (Table 11).

Figure 27. Issues with Wide Scatter 2 modeling are seen in the blurred representation of a humerus and ulna. Both are incomplete, and modeling has juxtaposed the plastic material and the leaf-littered ground below.

Table 11. Error totals for Wide Scatter 2.

	Right Femur	Left Femur	Right Humerus	Left Humerus	Control Scale
Actual Measurement	428mm	430mm	299mm	293mm	500mm
3D Model Measurement	430mm	433mm	305mm	300mm	501mm
Error	2mm	13mm	6mm	7mm	1mm

Wide Scatter 3

This data set collected 298 digital images of a mock forensic wide scatter with the digital camera held in the hand for the entirety of each circuit at three distinct heights. Additionally, images were captured while walking through the scene. Scale bars were placed around the edge of scene in a loose perimeter and all images were captured in 15 minutes using the methods described above. Images were processed in Agisoft Photoscan Professional with high settings resulting in a final output model with a RMSE value of 0.0704679 (Figure 28).

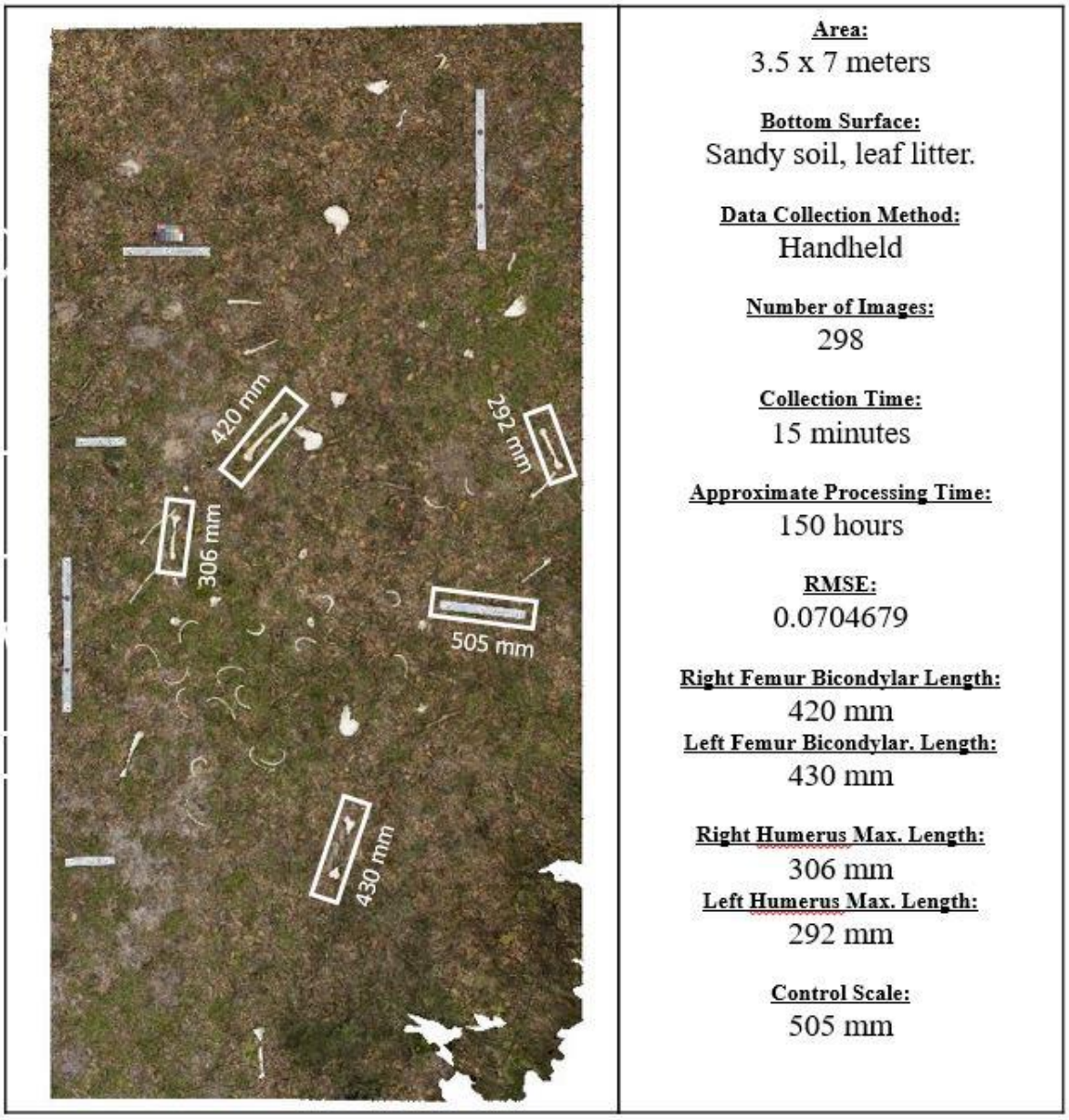

Figure 28. Wide Scatter 3 Results.

The wide scatter 3 model is largely accurate in terms of spatial context of individual elements. The scene is visually represented such that discrete skeletal components are identifiable.

This model, however, exhibits the most apparent error upon visual inspection of the three wide scatter scenarios. Model geometry is persistently and overarchingly affected by melding, blur, and incomplete data. While x and y values are within acceptable levels of accuracy (relative to previous models) z values are impacted as in previous model outputs. Relative location to scale bars does not appear to impact discrete element geometry. Additionally, where error appeared to affect the scale bars in previous models, each scale bar in wide scatter 3 is affected by geometry error (Figure 29). While measurements were taken for this model, all should be considered approximations due to the geometry distortion and inability to accurately, visually define morphological landmarks on bone elements. Given this stipulation, the approximate maximum error value was 8mm (Table 12).

Figure 29. Wide Scatter 3 exhibited the greatest number of issues in final model geometry of both scatter scenarios. Above, arrows point to the long, linear features that did not model completely. Circled, the ribs exhibit blurring and melding with the grass ground surface. The box around the scale bar highlights the overall poor resolution achieved with this model as scale bars in each other iteration are generally some of the best modeled aspects.

Table 12. Error totals for Wide Scatter 3. Note: due to issues in the model, these are closest approximations.

	Right Femur	Left Femur	Right Humerus	Left Humerus	Control Scale
Actual Measurement	428mm	430mm	299mm	293mm	500mm
3D Model Measurement	420mm	430mm	306mm	292mm	505mm
Error	8mm	0mm	7mm	1mm	5mm

Discussion

The application of CRP to outdoor forensic scene documentation offers a cost and time effective method to add to the array of more common scene documentation efforts. Two of these more common scene documentation methods include the collection of a series of 2D images and hand mapping. The purpose of scene documentation is the preservation of contextual data at forensic scenes to provide evidentiary support for law enforcement investigations (Dirkmaat and Adovoasio 1997, Dupras et al. 2012, Dupras and Schultz 2008). As such, any method that adds to the capability of preserving contextual data at a scene is of unique value. The 3D documentation method described here answers the need for more rigorous approaches to outdoor forensic scene documentation specifically (Dirkmaat et al. 2008, Dirkmaat 2012) and to the need to for more rigor in the forensic sciences more generally (NAS 2009).

The CRP method discussed in this research utilizes hardware already in use during scene documentation (digital camera and scale bars) and so does not overly burden the forensic archaeologist or law enforcement official with additional equipment which must be brought to sometimes difficult to reach scenes (Blau and Ubelaker 2009, Connor 2007, Dupras et al. 2012, Hoshower 1998). Additionally, this method does not add a significant amount of time during scene documentation as, once control points and scale bars are in place, the data capture process

takes a matter of minutes; here, the maximum time taken for data capture was 15 minutes (Table 13).

Table 13. Comparison of Scenarios; method, number of images, capture time, and final RMSE.

Model	Method	Number of Images	Capture Time (minutes)	RMSE
Small Scatter 1	Handheld	129	8	0.147723
Small Scatter 2	Tripod	146	17	0.0790753
Wide Scatter 1	Handheld	123	13	0.0779446
Wide Scatter 2	Handheld	198	13	0.0555378
Wide Scatter 3	Handheld	298	15	0.0704679

All models were generated with less than 1mm RMSE value and so represent outputs that accurately model the scene spatially in terms of scale data imposed on the model (Table 13). This does not mean that each model created an absolutely precise representation of the scene, but rather, as is the case in hand-mapping, it is an overall valid representation of the scene and may be used as a point of reference for later investigation.

As such, this research shows that CRP should be considered as a part of standard protocols for forensic scene documentation outdoors. Models are generally highly accurate, do not impose unnecessary time or equipment constraints in the field, and have a variety of outputs, beyond the final 3D model, that may assist the forensic archaeologist in interpretation of scene data.

One valuable output is the ability for CRP software to generate high-quality orthomosaics (Figure 30). Orthomosaics represent the entirety of a scene in a 2D format that preserves scale. As such, they can be utilized to create measurement data. Orthomosaics are derived from the stitching of textures based on camera locations within the model. Exported in .tiff format, the

orthomosaic is capable of being examined in close detail with minimal loss of resolution. The orthomosaic also provides the capability to visualize a site from an overview position (if desired) even when that was not possible during scene documentation. This provides the forensic archaeologist and law enforcement officials with additional views of the scene outside of those able to be experienced physically.

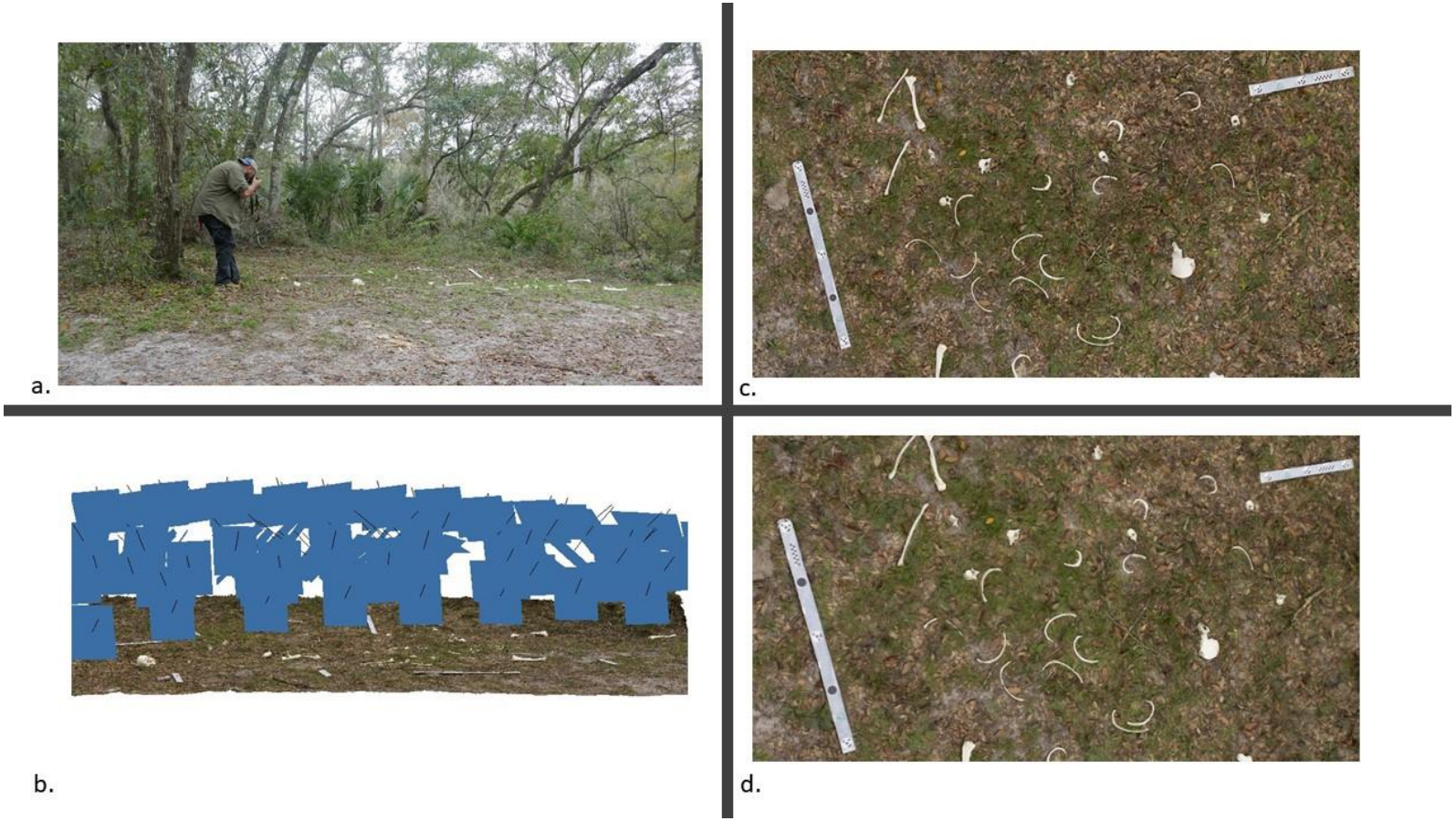

Figure 30. An overview of orthomosaic applications using Wide Scatter 1 as an example: a. no single image was capable of capturing the entirety of the scatter with sufficient resolution, as is seen in the comparison to the scatter and the author capturing images; b. a series of images(represented by the blue rectangles) could only be captured at roughly 6 feet from the ground surface, not high enough to capture the scene in its entirety; c. the orthomosaic is a scaled 2D representation that accurately depicts the final output of the final model and can provide any view of the scene desired; d. the sane representation of the 3D model as in image c.

Discussion of Small Scatter Scenarios

The small scatter scenarios tested the variables of scale bar placement, proximity of faux skeletal elements to the scale bars, and whether data was captured with the digital camera held in the hand or mounted on a tripod. Both models were generated with a high degree of accuracy and served to represent contextual data of the outdoor scene faithfully.

For both models, skeletal components nearer the scale bars tended to model more accurately with fewer artifact issues in the final geometry. Those in areas away from the scale bars or in positions that were difficult to capture images from (e.g. capturing images while maneuvering within the stand of scrub next to the scene, see Figure 19) presented more issues such as blur, melding, and incomplete data. Additionally, regardless of location, long, linear features proved difficult to model (Figure 31). Despite the issue of scale bar proximity, CRP was able to accurately document smaller elements not directly within the scale bar perimeter, showing that this method may serve to assist in preserving smaller, more easily missed pieces of evidence that may be overlooked during hand-mapping or surface collection.

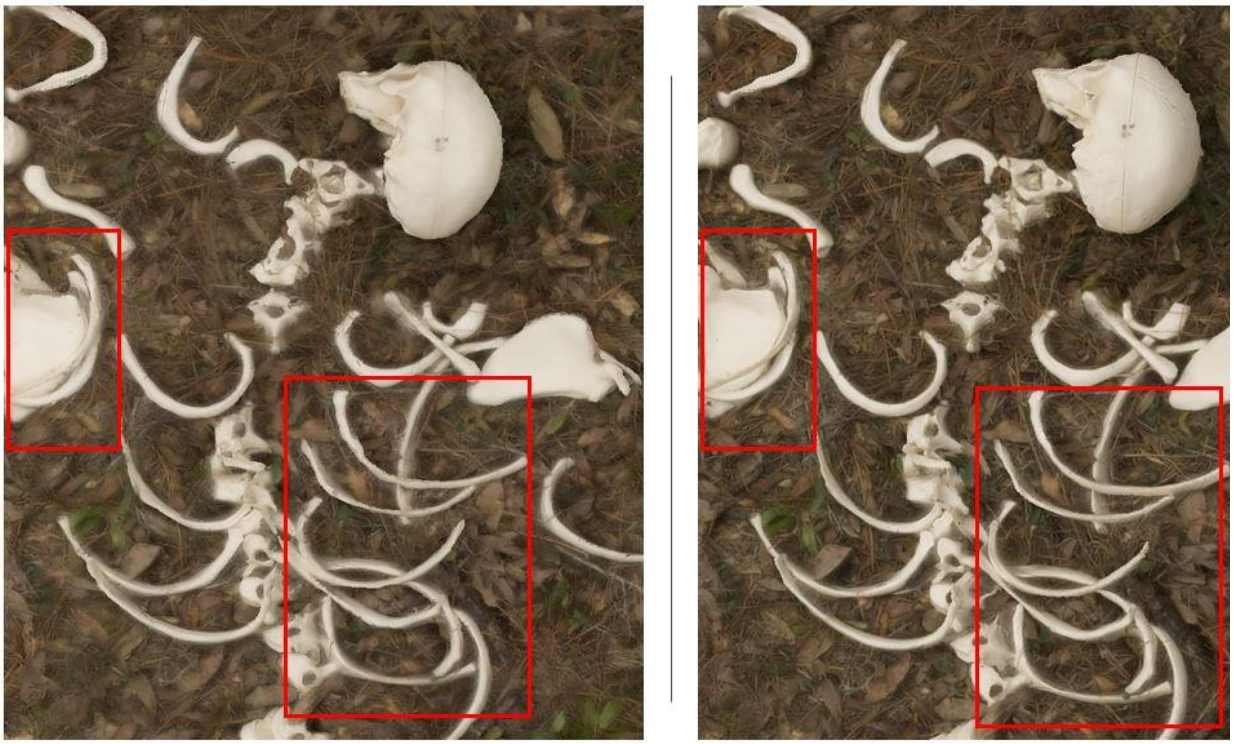

Figure 31. Showing a closeup comparison of Small Scatter 1 and 2. Note the slightly better distinction between individual components within the boxes between Small Scatter 1 (handheld) and Small Scatter 2 (tripod). However, in both images, issues of blurring and melding are apparent.

There appeared to be a negligible difference between collecting images with the camera held in the hand versus mounted on a tripod. Maximum error values were within 1mm for each scene (see Figures 21 and 22), with the second scenario (with tripod), displaying more error. However, as will be discussed further, it may benefit data collection to utilize a tripod for all scenes, time permitting. While the differences can be difficult to discern it does appear that capturing data with the camera mounted on a tripod provides a better series of images for processing and, as a result, slightly better models. While the use of a tripod does add time to data collection it may benefit the final model by reducing camera shake which introduces noise into the final model if not properly accounted for. Additionally, while these image sets utilized the camera's aperture priority setting (thus allowing for automatic control of shutter speed) a tripod

may be needed for those using manual settings or collecting images in low-light (necessitating a slower shutter speed), a variable the current research did not assess.

Discussion of Wide Scatter Scenarios

The wide scatter scenarios tested the variables of scale bar placement, lack of scene denuding, and whether the number of images affected the outcome of the final 3D model using CRP. All three models were contextually accurate though with varying degrees of precision in the final geometry.

Scale bars were placed in a loose perimeter around the extent of the wide scatter scene and so fewer individual osteological elements were nearer to scale bars by default. Generally, those nearer scale bars were more accurate. Those further from scale bars or closer to locations where image capture was difficult (e.g. standing in the scrub next to the scene, Figure 26a) presented more issues in their final geometry than did others. An additional issue here was the lack of scene denuding; the additional vegetation and grass was subject to movement from breezes and the data collector moving through the scene. Proper scene preparation is one control for error though it is apparent that the inclusion of additional control points/scale bars would have benefitted the final model in that it would provide a greater number of tie point data for camera alignment, thus giving more accurate depictions to those elements that were furthest away from both other skeletal elements and scale bars in the Wide Scatter scenarios.

The wide scatter scenario was captured using 123, 198, and 298 digital images. The goal was to test the impact the number of images had on the final model output. Generally, more images make for a better final product and the belief was that wide scatter 3, with the most images, would produce the most accurate model. In fact, wide scatter 3 proved to be the least useful of the three

wide scatter iterations; while contextual scene accuracy was preserved, precision of model geometry was the poorest of all three data sets. Additionally, wide scatter 2, at 198 digital images, proved less precise than did wide scatter 1, with 123 images (Figure 32).

Element	Wide Scatter 1 123 images	Wide Scatter 2 198 images	Wide Scatter 3 298 images
Skull			
Scapula			
Femur			

Figure 32. A comparison of discrete elements between Wide Scatters 1, 2, and 3. Note that despite the increase of images for each data set, the precision of the final model geometry appears to decrease. A number of issues may contribute to this, however the reason for decreased precision may be due to the amplification of errors by the addition of images.

Despite the issues inherent in wide scatter 2 and 3, CRP proved to be a useful method for capturing a difficult scene and provided good visual outputs in the form of a 3D models and orthomosaic overviews. Furthermore, the orthomosaic output from a CRP project, offering plan views of the site, when it is not possible to collect this view with traditional photographic methods, may be one of the more significant contributions of CRP to forensic scene documentation. The ability to create scaled, 2D representations of scenes quickly and accurately, and that can be incorporated into a GIS, in and of itself makes CRP an important tool for standard operating procedure.

Discussion of Issues for Outdoor Forensic Scenes and Close-Range Photogrammetry

A number of variables potentially impacted the final model geometry of each of the scatter scenarios discussed here. One caveat for CRP use is that there is no one standard way to collect or post-process imagery data. Rather, as in archaeological documentation, attention must be paid to the particular variables of the scene. In this case, these particular variables include imagery capture, lighting, movement of objects, the faux osteological material, and complexity of the subject to be modeled. It is apparent why CRP is more easily used in archaeological settings, where many of these variables may be controlled for. However, the forensic archaeologist does not enjoy the same opportunity to prepare a scene for documentation and so must work to minimize the impacts of these variables on the final model outcome.

Capturing imagery with a tripod and, if possible, shutter release remote will work to minimize the potential for blurring to be introduced into images. Capturing imagery using the handheld method is nonetheless valid, but efforts should be made to ensure both the stability of the camera when capturing images and an appropriately fast shutter speed, if possible. Another

benefit of utilizing a tripod is the ability to shoot with lower camera ISO values, which also limits the amount of noise or grain introduced into images (Agisoft 2018:8).

Lighting is a major variable for the forensic archaeologist utilizing CRP in outdoor scenarios (Douglass et al. 2015:140, Sapirstein 2016:142, Sapirstein and Murray 2017:343). Scenes documented during the day (as is the case here) will differ from those documented in low-light or night situations. Scenes documented during the day may have to account for variable light conditions from moment to moment, such as clouds passing in front of the sun or overhead branches moving and thus creating mottled lighting over the scene to be documented. For these reasons, capturing images utilizing the aperture priority setting is one useful default method to use as this maintains a static aperture setting (ensuring quality depth of field imagery) while automatically manipulating the shutter speed to account for lighting variations (Agisoft 2018:8). Ideally, a scene can be captured while in steady, even lighting, such as with a tarp or tent providing shade. However, for larger scatters, such as the wide scatter scenarios, this is unlikely to occur.

The movement of objects is anathema to the CRP process and by itself introduces error into a final model. Objects that are moving or are moved during the data capture process create error in that tie points cannot be accurately ascribed, making camera calibration increasingly difficult in relation to the amount of movement (Agisoft 2018). In the scatter scenarios discussed above, as may be possible in common outdoor forensic scenarios, wind moved leaf scatter during the data capture process. Additionally, in moving through the scene to collect image data, the author created moved objects with each step, thus introducing error unwittingly into the final model. Unfortunately, barring the capability to control environmental factors, the issue of elements at a scene moving during data capture may be a constant issue to be aware of. While the small scatters could be documented without stepping into the scene, the wide scatter was impossible to

document without doing so. One alternative would have been to implement a camera pole to collect imagery data over the scene without the need to step inside. This would also serve the purpose of collecting additional look angles for imagery and would potentially impact the quality of accuracy for the better.

One issue inherent to each of the scenarios discussed above was the reflectivity of the faux skeletal material used in these mock scenarios. The homogenous white, plastic skeletal components did not accurately represent the look of actual, weathered bone nor did they convey the intricate morphological structure of real osteological material. Reflective surfaces should be avoided in general for CRP projects as they disallow the software to assess tie points during camera calibration (Agisoft 2018). Given the overall reflective nature of the faux skeletal material it may be suggested that this introduced a significant amount of error into the final model geometry. As such, this only bolsters the statement that CRP is a valid tool for outdoor forensic scene documentation given actual osteological material. To test this supposition real osteological material was placed next to plastic teaching material and modeled. The results show that given the equality of size, spacing, and lighting, actual osteological material generates superior model geometry (see Figure 15).

Perhaps one of the most important impacts on error for the scatter models was the incredible complexity introduced via the complicated, leaf scatter on the ground surface. While one can focus processing efforts on the desired subject within the software, little can be done about the surrounding features of a scene in an outdoor scenario. Again, where the archaeological site can impose control on the scene (via careful excavation and site cleanup prior to a CRP project) the forensic archaeologist may not be afforded the same opportunity. In the scatter scenarios, the photogrammetry software had to not only model the faux skeletal elements, but also each leaf,

blade of grass, and dirt clump on the ground surface. This may account for the long processing times for several of the models and may also account for some of the error introduced into the final model geometry. In the case of wide scatter 3 the number of additional images did not appear to provide greater accuracy in the final model and may well have hindered it due to the excess of information/error introduced by the added number of images. In addition, the wide scatter scenario was not denuded prior to documentation, as a forensic scene be prior to documentation (Dupras et al. 2012:21-23). Given the amount of error registered in the Wide Scatter scenarios, scene clearing should continue to be a standard operating procedure for CRP scene documentation. For outdoor scene documentation there is little that can be done except that it is imperative to define the scene and to focus imagery data accordingly. As is seen in the issues of wide scatter 3, the quality of images likely outweighs the quantity of images.

Conclusion

The present research demonstrates that CRP is a useful addition to the forensic archaeologist's documentation tools and should be considered for inclusion in standard protocols for outdoor scene documentation. Overall, CRP allowed for highly accurate 3D models and orthomosaics to be generated of the two representative outdoor forensic scenes. Skeletal elements nearer to scale bars tended to model more accurately suggesting that it is useful to have enough scale bars and ground control markers to encompass a forensic scene. Unlike the controlled environment of archaeological sites, or the forensic excavations discussed in Chapter 2, outdoor scatter scenarios present a set of challenges that are unique and need to be considered at all times. Care should be taken to collect images of high quality for post-processing and this may best be achieved by utilizing a tripod and collecting image data with the camera set to aperture priority. This has the added benefit of mitigating the effects changing light has on the data capture process,

which is another challenge the forensic archaeologist utilizing CRP must contend with. While the complexity of ground surfaces may be beyond control at an outdoor scene the impact on post-processing may be lessened by defining the scene, collecting high quality imagery, and utilizing additional scale bars and ground control markers. As was shown, a major source of error for the research discussed here was the utilization of plastic teaching skeletons as the subject material; these reflective surfaces do not model as well as actual human bone, as shown, and thus adds to the argument that CRP is a valid and useful tool for scene documentation.

Future areas of research should focus on testing the capability of CRP to document outdoor forensic scatters in a variety of other environmental settings in order to determine the relative utility and shortcomings of this method for scene documentation. While the scenarios discussed here depict a common Florida landscape, the lessons learned are widely applicable as the issues encountered are general and not specific just to Florida's oak hardwood and pine flatwood forests. Future research should continue to refine the issues encountered in the field that generate error in final model geometry and develop methods to mitigate that error. Additionally, future research should only utilize actual osteological material as faux material has been shown here to introduce too much error. One useful line of research will be to explore the use of CRP to document scenes in low-light or nighttime settings; this should be done only with equipment that may readily available to a forensic archaeologist at an outdoor scene. Regardless of the setting, future research should also seek to refine the best practices for data capture with an aim to demonstrate the quickest, most accurate method in each scenario.

CHAPTER FOUR: DISCUSSION AND CONCLUSION

The ability to create 3D models of outdoor forensic scenes is a new scene documentation method that adds to the capabilities of the forensic archaeologist. The need to provide accurate, contextual information of forensic scene data is of paramount importance and current protocols, especially those applied to outdoor scenes, are in need of more rigorous approaches towards achieving this goal (Dirkmaat 2012). The use of CRP, among other 3D modeling techniques, is gaining interest among forensic practitioners (Ebert et al. 2011, Fourie 2010, Holowko 2016, Urbanova 2017). Currently, the field is in the formative stage of defining the purpose and limitations of these techniques. While the creation of 3D models has become easier than ever before, the goal now is to define the accuracy of those models such that they can be utilized in a scientific manner. Additionally, considerations should be made for adopting CRP into standard field documentation, as is beginning to be more commonplace within archaeological practice.

The use of CRP as a method of site and artifact documentation is becoming more standard in archaeological practice (Doneus et al. 2011, Douglass et al. 2015, Forte 2014, Sapirstein and Murray 2017). This is due to the relative low cost of engaging in CRP documentation and the highly accurate results that are capable of being produced via these methods (Galeazzi 2016, Mathews 2018, Opitz and Limp 2015, Sapirstein 2016). The work of forensic archaeology corresponds to the methodology practiced at archaeological sites and, here, specifically corresponds to the work of bioarchaeological documentation utilizing CRP (Fort 2014). As additional research regarding proper protocols and best practices within archaeology is further augmented the standardization of CRP protocols will likely follow. This integration of CRP to standard protocols should also take place within the larger methodological framework of forensic archaeology.

The application of CRP technology is not yet ready to supplant current, standard documentation methods, such as hand mapping, but it may be considered as a useful, cost-effective addition to these methods. Most notably, there is little extra that needs to be added to the kit of a forensic archaeologist who wishes to collect the data for possible photogrammetric processing later; forensic archaeologists already regularly use DSLRs with variable zoom lenses and scale bars that are already required for scene mapping (Connor 2007:32, Dupras et al. 2012:7, Robinson 2012). Close-range photogrammetry data collection minimally impacts the overall amount of time required for scene documentation (generally 10 additional minutes) and so does not add undue burden to the scene documentation process. Data collected in the methods described above may simply be archived should a 3D model be required of the scene at a later date. Perhaps most importantly, data collection does not need to be conducted by a forensic archaeologist, as other law enforcement individuals who regularly document scenes may be trained to collect image data properly, thus freeing the forensic archaeologist to focus on other issues at a scene or gain a better understanding of the context at a later time.

One drawback is the cost of specialized software, hardware, and the time needed to render data, though this is by no means entirely prohibitive. Depending on the number of images utilized and the capability of the computing hardware available, models may take several hours to fully process. Here, the focus was on a single, discrete burial and so the number of images could be constrained to focus on excessive quality over quantity. However, a more complex scenario would naturally require more imagery and thus more computing power which would equal more processing time. Indeed, it would not be difficult to quickly reach the limits of most commercially purchased desktop computers via photogrammetric processing for large scenes that required more than several hundred images.

The models created as part of this research were highly accurate and exhibited similar discrepancies across each data set. In short, the models are not perfectly accurate representations of the subjects modeled here. They were, however, in many ways better at preserving unmediated contextual data than traditional hand mapping techniques. While CRP techniques allow for great accuracy (BLM 2008, Bolognesi 2014), skeletal material in variable situations offers greater complexity than a structure or archaeological test unit, for example. The issues with these models may be defined as having to do with accuracy of the geometric structure of the subject via the introduction of noise artifacts into the final model due to image capture issues, environmental constraints, or processing issues.

Future areas of research should focus on testing the capability of CRP to document outdoor forensic scatters in a variety of other environmental settings in order to determine the relative utility and shortcomings of this method for scene documentation. While the scenarios discussed here depict a common Florida landscape, the lessons learned are widely applicable as the issues encountered are general and not specific just to Florida's oak hardwood and pine flatwood forests. Future research should continue to refine the issues encountered in the field that generate error in final model geometry and develop methods to mitigate that error. Additionally, future research should only utilize actual osteological material as faux material has been shown here to introduce too much error. One useful line of research will be to explore the use of CRP to document scenes in low-light or nighttime settings; this should be done only with equipment that may readily available to a forensic archaeologist at an outdoor scene. Regardless of the setting, future research should also seek to refine the best practices for data capture with an aim to demonstrate the quickest, most accurate method in each scenario.

APPENDIX A: PROCESSING REPORTS

Excavation 1

Processing Report
03 June 2018

Survey Data

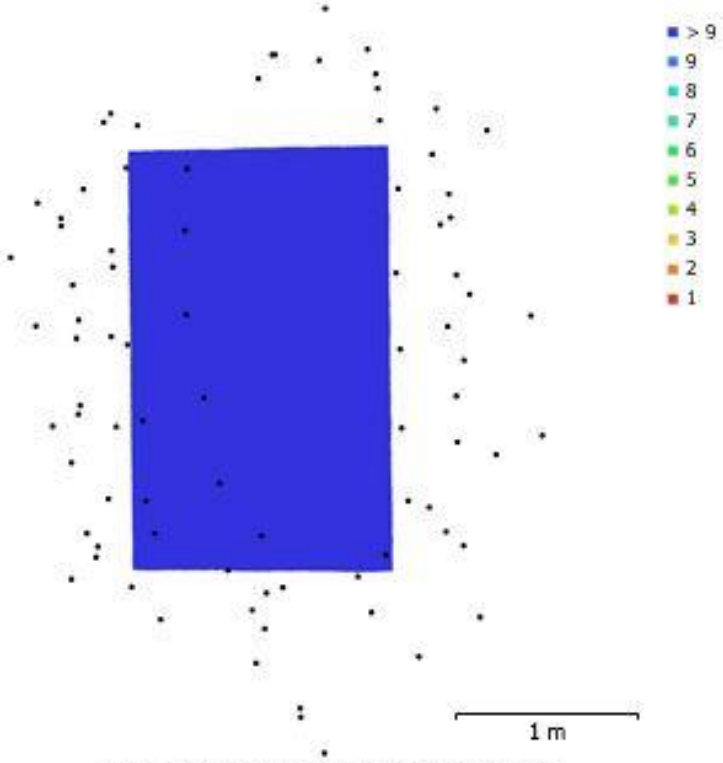

Fig. 1. Camera locations and image overlap.

Number of images:	84	Camera stations:	84
Flying altitude:	1.75 m	Tie points:	78,122
Ground resolution:	0.404 mm/pix	Projections:	200,215
Coverage area:	3.32 m²	Reprojection error:	0.259 pix

Camera Model	Resolution	Focal Length	Pixel Size	Precalibrated
Canon EOS REBEL T5 (18 mm)	5184 x 3456	18 mm	4.4 x 4.4 µm	No

Table 1. Cameras.

Camera Calibration

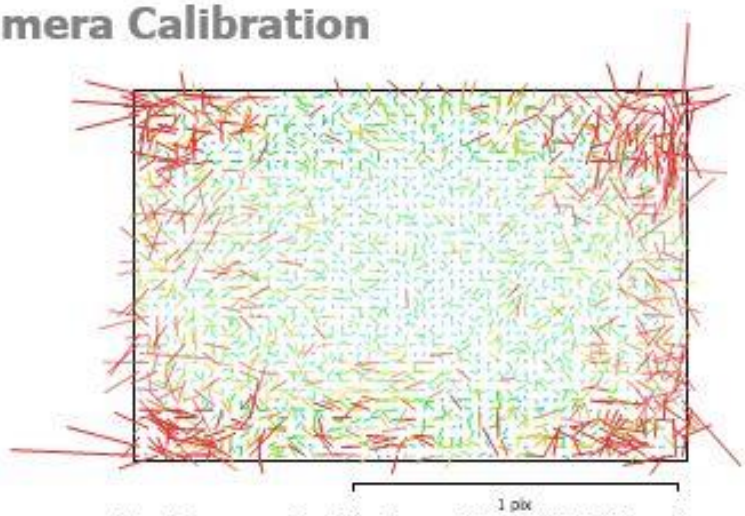

Fig. 2. Image residuals for Canon EOS REBEL T5 (18 mm).

Canon EOS REBEL T5 (18 mm)

84 images

Type	Resolution	Focal Length	Pixel Size
Frame	**5184 x 3456**	**18 mm**	**4.4 x 4.4 µm**

	Value	Error	F	Cx	Cy	B1	B2	K1	K2	K3	K4	P1	P2	P3	P4
F	**4324.84**	0.071	1.00	0.09	-0.24	0.03	0.02	-0.28	0.26	-0.23	0.21	0.01	-0.08	0.01	-0.02
Cx	**-28.569**	0.062		1.00	-0.01	0.06	0.36	-0.01	0.01	-0.01	0.01	0.66	0.04	-0.07	0.11
Cy	**35.6617**	0.057			1.00	-0.34	0.08	0.00	-0.02	0.02	-0.02	0.13	0.56	-0.19	0.19
B1	**-0.625026**	0.013				1.00	-0.02	0.01	-0.00	0.00	0.00	0.01	-0.13	0.03	-0.03
B2	**0.857248**	0.012					1.00	0.01	-0.01	0.01	-0.01	0.13	-0.02	0.04	-0.01
K1	**-0.181329**	0.00012						1.00	-0.97	0.92	-0.86	0.00	0.02	-0.03	0.03
K2	**0.221363**	0.00096							1.00	-0.98	0.95	-0.01	-0.04	0.04	-0.04
K3	**-0.170724**	0.0029								1.00	-0.99	0.01	0.04	-0.04	0.04
K4	**0.137792**	0.003									1.00	-0.01	-0.03	0.04	-0.04
P1	**0.000857082**	4.5e-06										1.00	0.59	-0.68	0.64
P2	**0.0014077**	5.8e-06											1.00	-0.84	0.77
P3	**-0.0913699**	0.021												1.00	-0.97
P4	**0.0693496**	0.042													1.00

Table 2. Calibration coefficients and correlation matrix.

Scale Bars

Label	Distance (m)	Error (m)
target 23_target 24	0.250083	-1.65409e-05
target 31_target 32	0.250069	-1.37677e-06
target 28_target 30	0.500309	9.27869e-06
Total		**1.09786e-05**

Table 3. Control scale bars.

Digital Elevation Model

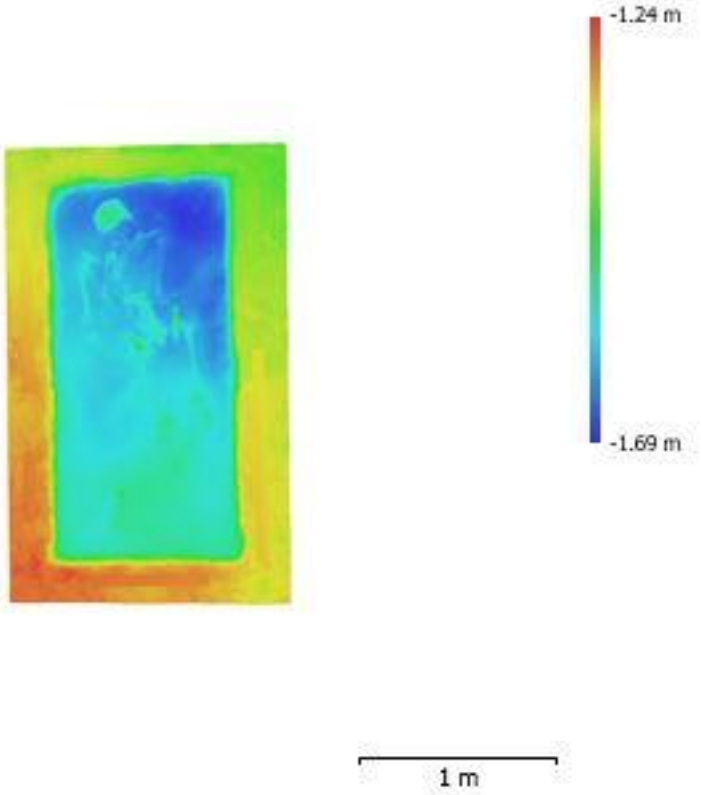

Fig. 3. Reconstructed digital elevation model.

Resolution:	unknown
Point density:	unknown

Processing Parameters

General	
Cameras	84
Aligned cameras	84
Markers	16
Scale bars	3
Coordinate system	Local Coordinates (m)
Rotation angles	Yaw, Pitch, Roll
Point Cloud	
Points	78,122 of 310,471
RMS reprojection error	0.0984029 (0.258507 pix)
Max reprojection error	0.262311 (1.12889 pix)
Mean key point size	2.56385 pix
Point colors	3 bands, uint8
Key points	No
Average tie point multiplicity	3.17636
Alignment parameters	
Accuracy	High
Generic preselection	Yes
Key point limit	60,000
Tie point limit	0
Adaptive camera model fitting	No
Matching time	24 minutes 17 seconds
Alignment time	1 minutes 19 seconds
Optimization parameters	
Parameters	f, b1, b2, cx, cy, k1-k4, p1-p4
Optimization time	1 seconds
Dense Point Cloud	
Points	22,411,458
Point colors	3 bands, uint8
Reconstruction parameters	
Quality	High
Depth filtering	Aggressive
Depth maps generation time	9 hours 0 minutes
Dense cloud generation time	3 hours 18 minutes
Model	
Faces	1,591,044
Vertices	797,756
Vertex colors	3 bands, uint8
Texture	8,192 x 8,192, 4 bands, uint8
Reconstruction parameters	
Surface type	Arbitrary
Source data	Dense
Interpolation	Enabled
Quality	High
Depth filtering	Aggressive
Face count	4,482,291
Processing time	23 minutes 24 seconds
Texturing parameters	
Blending mode	Mosaic
Texture size	8,192 x 8,192
Enable color correction	No
Enable hole filling	Yes
UV mapping time	6 minutes 20 seconds
Blending time	5 minutes 53 seconds

Orthomosaic

Size	4,807 x 2,958
Coordinate system	Local Coordinates (m)
Colors	3 bands, uint8
Reconstruction parameters	
Blending mode	Mosaic
Surface	Mesh
Enable hole filling	Yes
Processing time	4 minutes 24 seconds
Software	
Version	1.4.2 build 6205
Platform	Windows 64

Excavation 2

Processing Report
03 June 2018

Survey Data

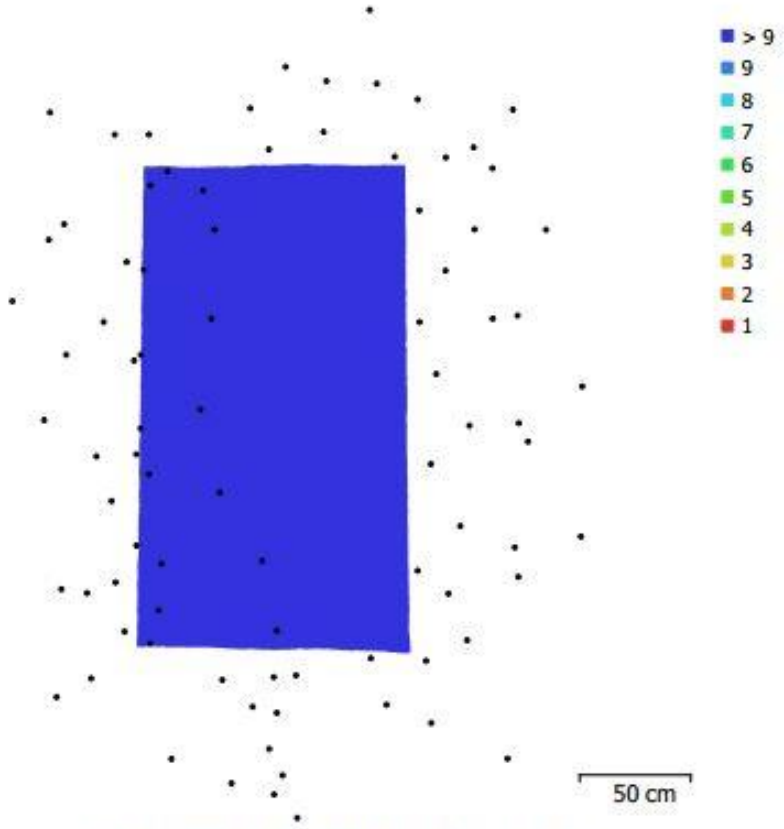

Fig. 1. Camera locations and image overlap.

Number of images:	86	Camera stations:	86
Flying altitude:	1.6 m	Tie points:	81,413
Ground resolution:	0.371 mm/pix	Projections:	193,260
Coverage area:	2.6 m²	Reprojection error:	0.324 pix

Camera Model	Resolution	Focal Length	Pixel Size	Precalibrated
Canon EOS REBEL T5 (18 mm)	5184 x 3456	18 mm	4.4 x 4.4 µm	No

Table 1. Cameras.

Camera Calibration

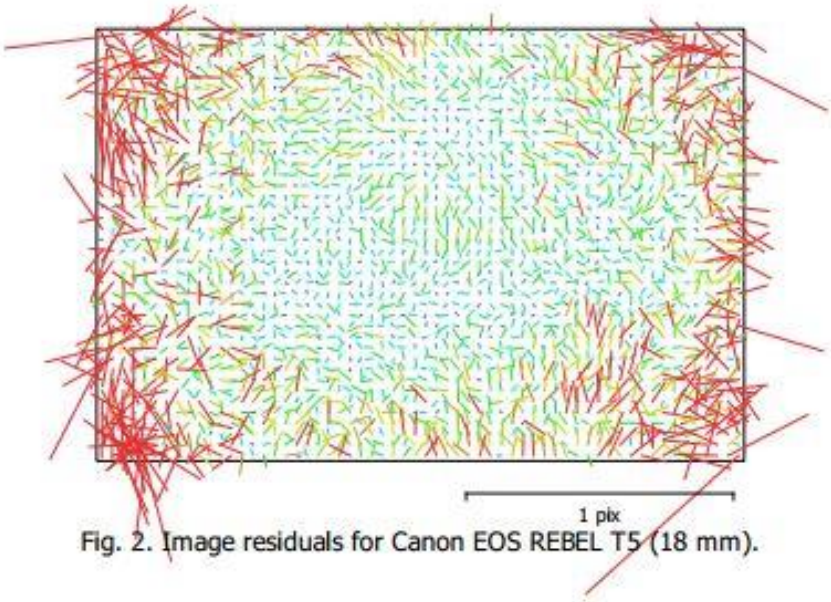

Fig. 2. Image residuals for Canon EOS REBEL T5 (18 mm).

Canon EOS REBEL T5 (18 mm)

86 images

Type	Resolution	Focal Length	Pixel Size
Frame	**5184 x 3456**	**18 mm**	**4.4 x 4.4 µm**

	Value	Error	F	Cx	Cy	B1	B2	K1	K2	K3	K4	P1	P2	P3	P4
F	**4311.9**	1.1	1.00	0.08	-0.17	0.01	-0.02	-0.26	0.24	-0.20	0.18	0.02	-0.05	-0.00	0.01
Cx	**-23.7316**	0.72		1.00	0.00	0.09	0.28	-0.00	0.00	0.01	-0.01	0.59	0.06	-0.11	0.13
Cy	**35.5056**	0.65			1.00	-0.27	0.07	-0.01	-0.01	0.01	-0.01	0.16	0.51	-0.19	0.15
B1	**0.697731**	0.16				1.00	0.01	-0.00	0.00	-0.00	0.00	0.03	-0.09	0.01	-0.01
B2	**0.905381**	0.14					1.00	0.02	-0.01	0.01	-0.01	0.12	-0.01	0.02	-0.02
K1	**-0.180077**	0.0016						1.00	-0.97	0.91	-0.85	0.01	0.01	-0.03	0.04
K2	**0.199778**	0.013							1.00	-0.98	0.95	-0.03	-0.04	0.06	-0.07
K3	**-0.104014**	0.041								1.00	-0.99	0.05	0.05	-0.08	0.09
K4	**0.0694334**	0.044									1.00	-0.06	-0.06	0.09	-0.11
P1	**0.000887339**	5.7e-05										1.00	0.71	-0.79	0.72
P2	**0.00120718**	6.7e-05											1.00	-0.87	0.79
P3	**0.695633**	0.4												1.00	-0.97
P4	**-1.34137**	0.77													1.00

Table 2. Calibration coefficients and correlation matrix.

Scale Bars

Label	Distance (m)	Error (m)
target 23_target 24	0.249799	-0.000301042
target 31_target 32	0.249924	-0.00014636
target 17_target 19	1.00065	0.000108775
Total		**0.000203207**

Table 3. Control scale bars.

Digital Elevation Model

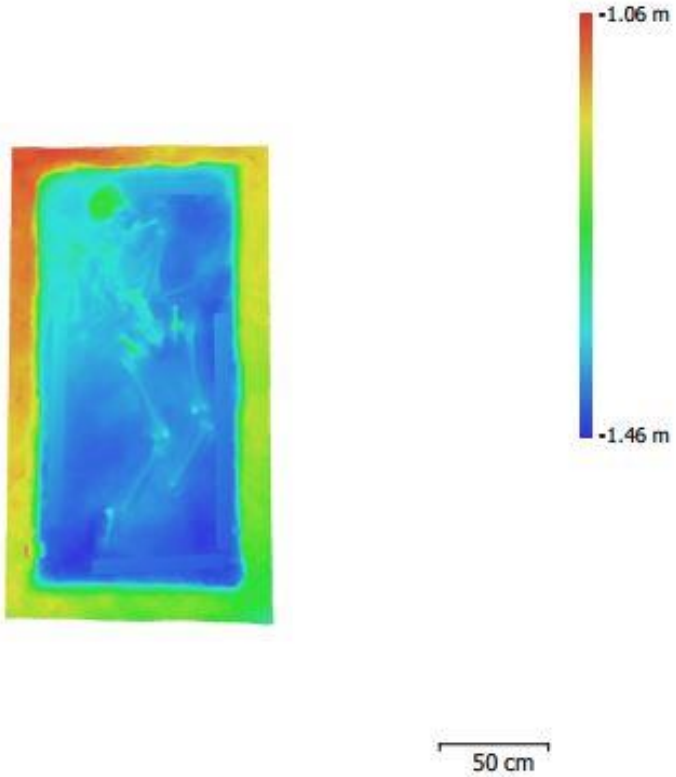

Fig. 3. Reconstructed digital elevation model.

Resolution:	unknown
Point density:	unknown

Processing Parameters

General	
Cameras	86
Aligned cameras	86
Markers	13
Scale bars	3
Coordinate system	Local Coordinates (m)
Rotation angles	Yaw, Pitch, Roll
Point Cloud	
Points	81,413 of 299,643
RMS reprojection error	0.100281 (0.323617 pix)
Max reprojection error	0.215024 (1.50536 pix)
Mean key point size	3.08065 pix
Point colors	3 bands, uint8
Key points	No
Average tie point multiplicity	3.25584
Alignment parameters	
Accuracy	High
Generic preselection	Yes
Key point limit	60,000
Tie point limit	0
Adaptive camera model fitting	No
Matching time	28 minutes 57 seconds
Alignment time	53 seconds
Optimization parameters	
Parameters	f, b1, b2, cx, cy, k1-k4, p1-p4
Optimization time	3 seconds
Dense Point Cloud	
Points	22,210,502
Point colors	3 bands, uint8
Reconstruction parameters	
Quality	High
Depth filtering	Aggressive
Depth maps generation time	8 hours 16 minutes
Dense cloud generation time	2 hours 9 minutes
Model	
Faces	1,404,428
Vertices	704,214
Vertex colors	3 bands, uint8
Texture	8,192 x 8,192, 4 bands, uint8
Reconstruction parameters	
Surface type	Arbitrary
Source data	Dense
Interpolation	Enabled
Quality	High
Depth filtering	Aggressive
Face count	4,442,100
Processing time	20 minutes 1 seconds
Texturing parameters	
Blending mode	Mosaic
Texture size	8,192 x 8,192
Enable color correction	No
Enable hole filling	Yes
UV mapping time	5 minutes 52 seconds
Blending time	5 minutes 57 seconds
Orthomosaic	

Size	8,224 x 9,865
Coordinate system	Local Coordinates (m)
Colors	3 bands, uint8
Reconstruction parameters	
Blending mode	Mosaic
Surface	Mesh
Enable color correction	No
Enable hole filling	Yes
Processing time	5 minutes 6 seconds
Software	
Version	1.4.2 build 6205
Platform	Windows 64

Excavation 3

Processing Report
03 June 2018

Survey Data

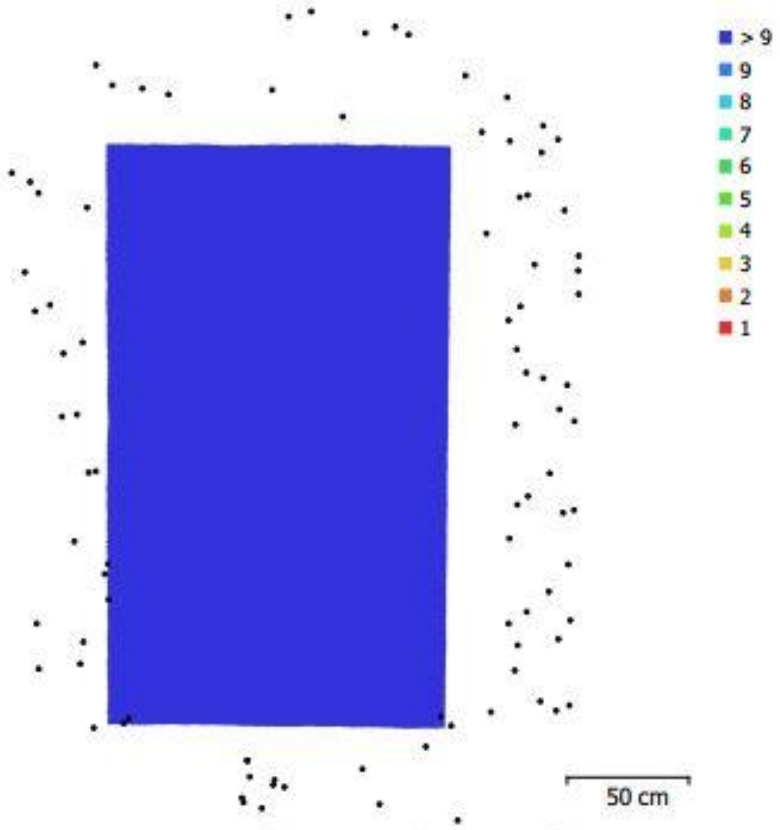

Fig. 1. Camera locations and image overlap.

Number of images:	92	Camera stations:	92
Flying altitude:	1.56 m	Tie points:	137,883
Ground resolution:	0.362 mm/pix	Projections:	457,834
Coverage area:	3.34 m²	Reprojection error:	0.366 pix

Camera Model	Resolution	Focal Length	Pixel Size	Precalibrated
Canon EOS REBEL T5 (18 mm)	5184 x 3456	18 mm	4.4 x 4.4 µm	No

Table 1. Cameras.

Camera Calibration

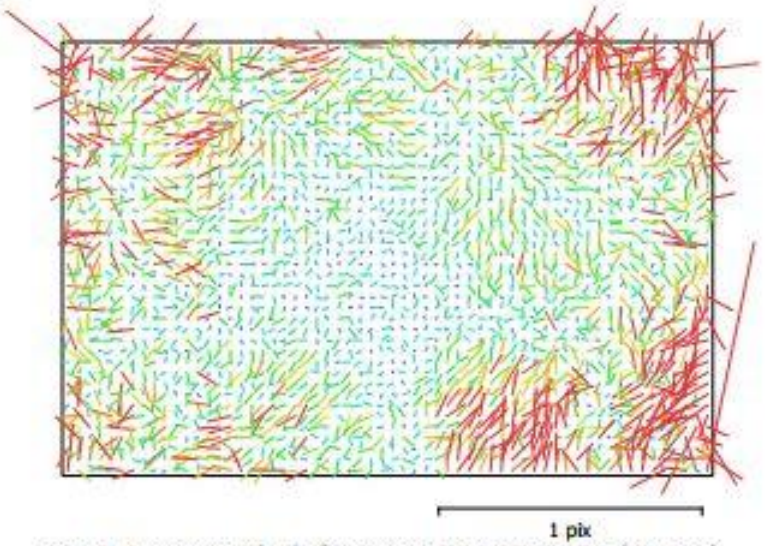

Fig. 2. Image residuals for Canon EOS REBEL T5 (18 mm).

Canon EOS REBEL T5 (18 mm)

92 images

Type	Resolution	Focal Length	Pixel Size
Frame	**5184 x 3456**	**18 mm**	**4.4 x 4.4 µm**

	Value	Error	F	Cx	Cy	B1	B2	K1	K2	K3	K4	P1	P2	P3	P4
F	4307.82	0.065	1.00	0.03	-0.20	-0.00	0.00	-0.18	0.19	-0.16	0.15	0.01	0.01	-0.03	0.02
Cx	-50.5975	0.04		1.00	-0.02	0.10	0.33	0.02	-0.00	-0.00	0.01	0.82	-0.01	-0.03	0.05
Cy	37.7852	0.038			1.00	-0.27	0.03	-0.02	0.01	-0.01	0.01	0.06	0.51	-0.16	0.17
B1	-1.33859	0.0099				1.00	0.02	0.02	-0.02	0.01	-0.01	0.09	-0.09	-0.00	-0.01
B2	-0.337776	0.0092					1.00	-0.00	0.00	-0.01	0.01	0.20	-0.02	0.03	-0.01
K1	-0.180888	8.4e-05						1.00	-0.97	0.91	-0.86	-0.00	-0.04	0.03	-0.03
K2	0.203797	0.00068							1.00	-0.98	0.95	0.02	0.03	-0.04	0.04
K3	-0.118625	0.0021								1.00	-0.99	-0.02	-0.04	0.04	-0.05
K4	0.0884567	0.0021									1.00	0.03	0.04	-0.06	0.06
P1	0.000497123	2.7e-06										1.00	0.34	-0.41	0.38
P2	0.00185643	4.6e-06											1.00	-0.85	0.77
P3	-0.656235	0.014												1.00	-0.97
P4	0.670614	0.028													1.00

Table 2. Calibration coefficients and correlation matrix.

Scale Bars

Label	Distance (m)	Error (m)
target 31_target 32	0.250121	5.05262e-05
target 23_target 24	0.24997	-0.00013011
target 20_target 22	0.50011	3.95852e-05
Total		**8.37624e-05**

Table 3. Control scale bars.

Digital Elevation Model

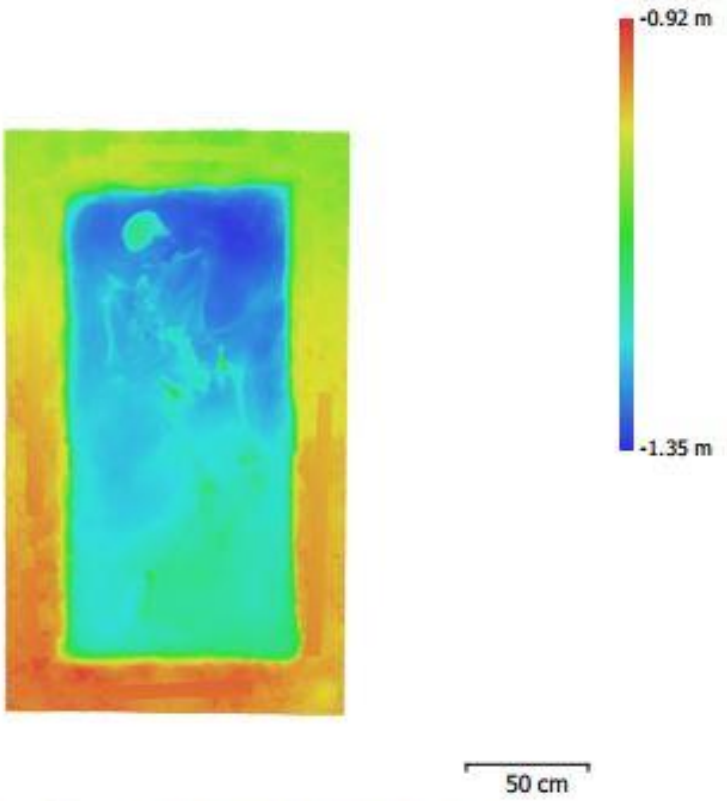

Fig. 3. Reconstructed digital elevation model.

Resolution:	unknown
Point density:	unknown

Processing Parameters

General	
Cameras	92
Aligned cameras	92
Markers	16
Scale bars	3
Coordinate system	Local Coordinates (m)
Rotation angles	Yaw, Pitch, Roll
Point Cloud	
Points	137,883 of 489,982
RMS reprojection error	0.135521 (0.366036 pix)
Max reprojection error	0.432382 (1.53813 pix)
Mean key point size	2.66048 pix
Point colors	3 bands, uint8
Key points	No
Average tie point multiplicity	3.86269
Alignment parameters	
Accuracy	High
Generic preselection	Yes
Key point limit	60,000
Tie point limit	0
Adaptive camera model fitting	No
Matching time	25 minutes 38 seconds
Alignment time	3 minutes 41 seconds
Optimization parameters	
Parameters	f, b1, b2, cx, cy, k1-k4, p1-p4
Optimization time	4 seconds
Dense Point Cloud	
Points	27,780,081
Point colors	3 bands, uint8
Reconstruction parameters	
Quality	High
Depth filtering	Aggressive
Depth maps generation time	11 hours 31 minutes
Dense cloud generation time	2 hours 5 minutes
Model	
Faces	1,606,191
Vertices	805,259
Vertex colors	3 bands, uint8
Texture	8,192 x 8,192, 4 bands, uint8
Reconstruction parameters	
Surface type	Arbitrary
Source data	Dense
Interpolation	Enabled
Quality	High
Depth filtering	Aggressive
Face count	5,556,015
Processing time	26 minutes 13 seconds
Texturing parameters	
Blending mode	Mosaic
Texture size	8,192 x 8,192
Enable color correction	No
Enable hole filling	Yes
UV mapping time	9 minutes 10 seconds
Blending time	6 minutes 5 seconds
Orthomosaic	

Size	10,445 x 10,540
Coordinate system	Local Coordinates (m)
Colors	3 bands, uint8
Reconstruction parameters	
Blending mode	Mosaic
Surface	Mesh
Enable color correction	No
Enable hole filling	Yes
Processing time	6 minutes 12 seconds
Software	
Version	1.4.2 build 6205
Platform	Windows 64

Excavation 4

Processing Report
03 June 2018

Survey Data

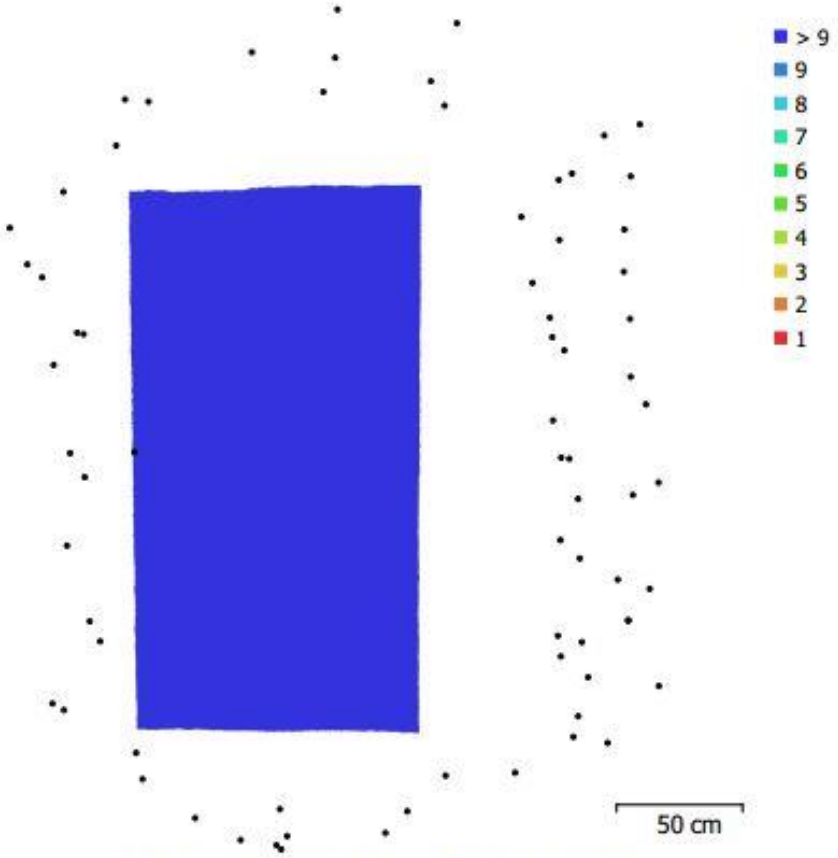

Fig. 1. Camera locations and image overlap.

Number of images:	73	Camera stations:	73
Flying altitude:	1.77 m	Tie points:	280,425
Ground resolution:	0.409 mm/pix	Projections:	926,113
Coverage area:	2.44 m²	Reprojection error:	0.681 pix

Camera Model	Resolution	Focal Length	Pixel Size	Precalibrated
Canon EOS REBEL T5 (18 mm)	5184 x 3456	18 mm	4.4 x 4.4 µm	No

Table 1. Cameras.

Camera Calibration

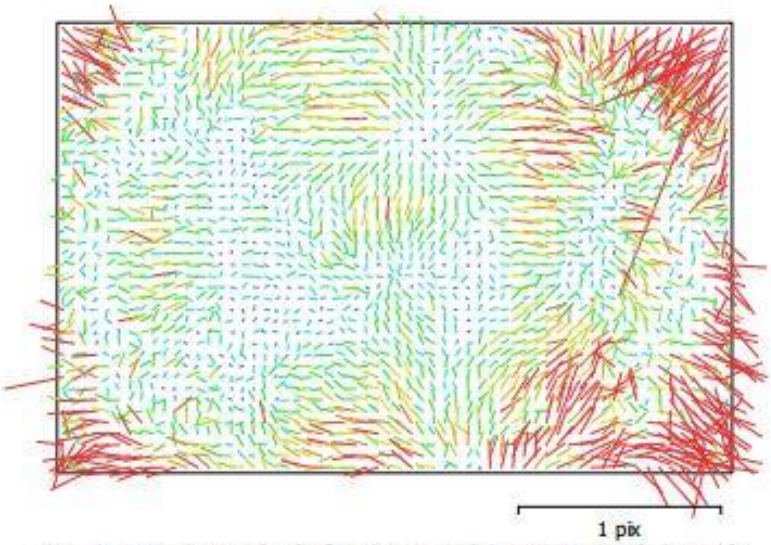

Fig. 2. Image residuals for Canon EOS REBEL T5 (18 mm).

Canon EOS REBEL T5 (18 mm)

73 images

Type	Resolution	Focal Length	Pixel Size
Frame	**5184 x 3456**	**18 mm**	**4.4 x 4.4 µm**

	Value	Error	F	Cx	Cy	K1	K2	K3	P1	P2
F	**4328.12**	0.059	1.00	-0.09	-0.12	-0.11	0.17	-0.10	0.09	-0.10
Cx	**-44.9837**	0.029		1.00	-0.01	0.00	-0.00	-0.01	0.86	-0.05
Cy	**38.4528**	0.028			1.00	-0.04	0.01	-0.02	-0.04	0.80
K1	**-0.175738**	3.5e-05				1.00	-0.95	0.89	0.03	-0.05
K2	**0.177003**	0.00017					1.00	-0.98	0.00	0.01
K3	**-0.0310114**	0.00023						1.00	-0.00	-0.02
P1	**0.000394466**	1.7e-06							1.00	-0.06
P2	**0.00140257**	1.5e-06								1.00

Table 2. Calibration coefficients and correlation matrix.

Scale Bars

Label	Distance (m)	Error (m)
point 1_point 2	0.250014	-8.62002e-05
point 3_point 4	0.250157	8.6629e-05
Total		**8.64149e-05**

Table 3. Control scale bars.

Digital Elevation Model

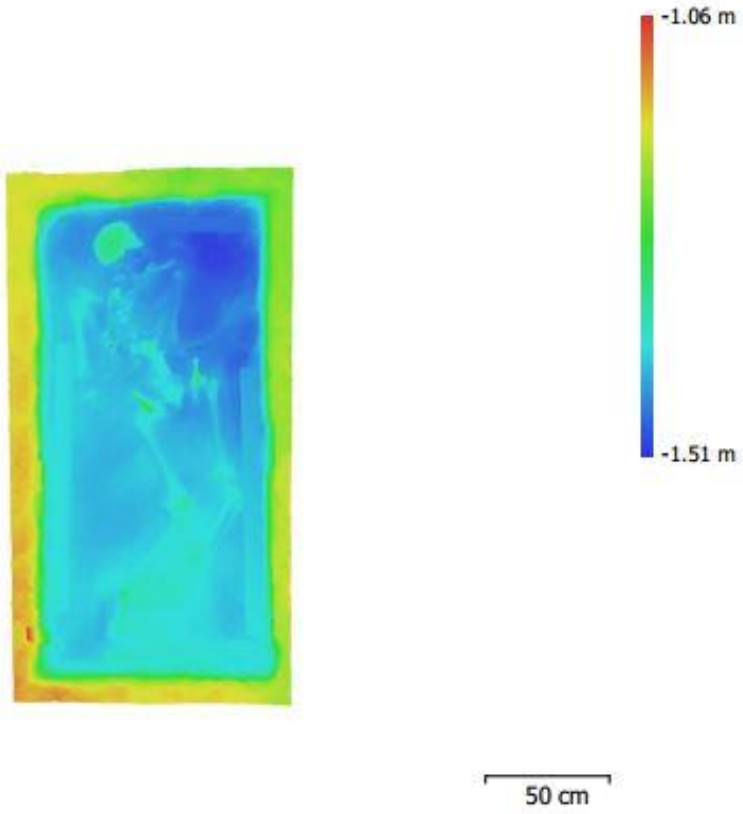

Fig. 3. Reconstructed digital elevation model.

Resolution:	unknown
Point density:	unknown

Processing Parameters

General	
Cameras	73
Aligned cameras	73
Markers	4
Scale bars	2
Coordinate system	Local Coordinates (m)
Rotation angles	Yaw, Pitch, Roll
Point Cloud	
Points	280,425 of 320,659
RMS reprojection error	0.144426 (0.681262 pix)
Max reprojection error	0.512333 (35.918 pix)
Mean key point size	3.82374 pix
Point colors	3 bands, uint8
Key points	No
Average tie point multiplicity	3.5939
Alignment parameters	
Accuracy	High
Generic preselection	Yes
Key point limit	60,000
Tie point limit	0
Adaptive camera model fitting	No
Matching time	17 minutes 26 seconds
Alignment time	1 minutes 50 seconds
Optimization parameters	
Parameters	f, cx, cy, k1-k3, p1, p2
Optimization time	7 seconds
Dense Point Cloud	
Points	27,311,661
Point colors	3 bands, uint8
Reconstruction parameters	
Quality	High
Depth filtering	Aggressive
Depth maps generation time	4 hours 40 minutes
Dense cloud generation time	3 hours 54 minutes
Model	
Faces	1,017,555
Vertices	510,467
Vertex colors	3 bands, uint8
Texture	8,192 x 8,192, 4 bands, uint8
Reconstruction parameters	
Surface type	Arbitrary
Source data	Dense
Interpolation	Enabled
Quality	High
Depth filtering	Aggressive
Face count	5,462,328
Processing time	25 minutes 16 seconds
Texturing parameters	
Blending mode	Mosaic
Texture size	8,192 x 8,192
Enable color correction	Yes
Enable hole filling	Yes
UV mapping time	10 minutes 51 seconds
Blending time	11 minutes 54 seconds
Orthomosaic	

Size	3,218 x 5,995
Coordinate system	Local Coordinates (m)
Colors	3 bands, uint8
Reconstruction parameters	
Blending mode	Mosaic
Surface	Mesh
Enable color correction	No
Enable hole filling	Yes
Processing time	3 minutes 16 seconds
Software	
Version	1.4.2 build 6205
Platform	Windows 64

Small Scatter 1

Processing Report
03 June 2018

Survey Data

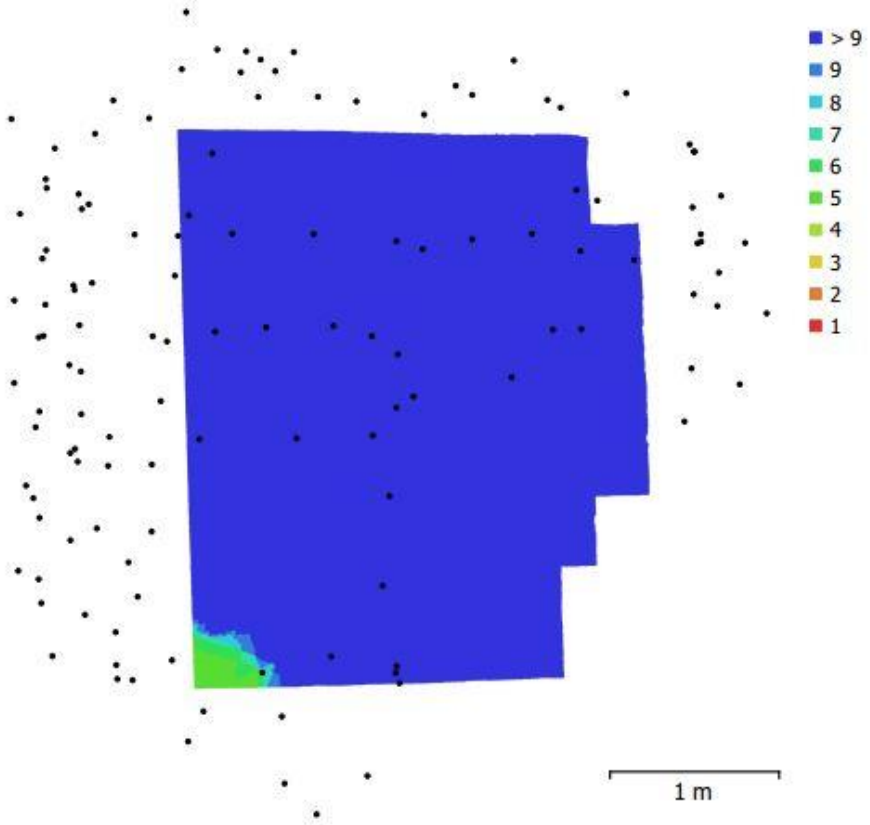

Fig. 1. Camera locations and image overlap.

Number of images:	129	Camera stations:	129
Flying altitude:	1.8 m	Tie points:	80,646
Ground resolution:	0.333 mm/pix	Projections:	222,201
Coverage area:	8.16 m²	Reprojection error:	0.627 pix

Camera Model	Resolution	Focal Length	Pixel Size	Precalibrated
Canon EOS REBEL T5 (23 mm)	5184 x 3456	23 mm	4.4 x 4.4 µm	No

Table 1. Cameras.

Camera Calibration

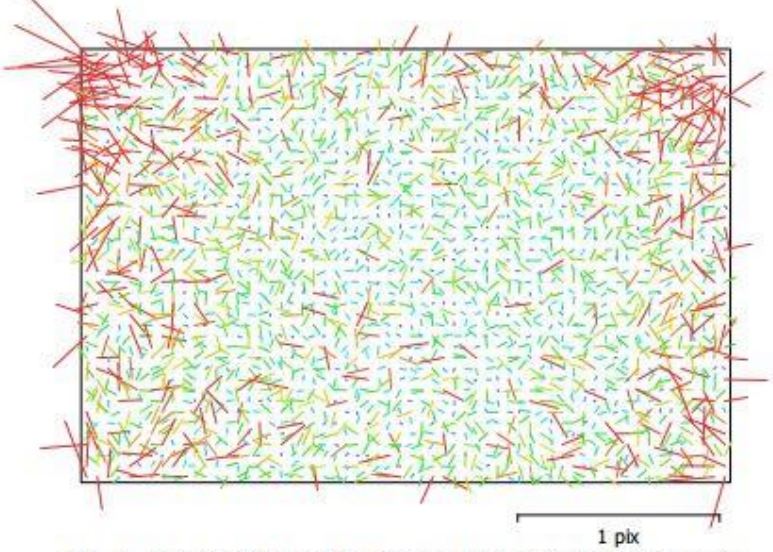

Fig. 2. Image residuals for Canon EOS REBEL T5 (23 mm).

Canon EOS REBEL T5 (23 mm)

129 images

Type	Resolution	Focal Length	Pixel Size
Frame	**5184 x 3456**	**23 mm**	**4.4 x 4.4 µm**

	Value	Error	F	Cx	Cy	K1	K2	K3	P1	P2
F	**5402.05**	0.27	1.00	-0.12	-0.16	-0.07	0.13	-0.10	-0.06	-0.07
Cx	**-29.21**	0.18		1.00	0.01	-0.02	0.01	-0.00	0.88	-0.04
Cy	**47.8899**	0.17			1.00	-0.03	-0.01	0.01	-0.04	0.83
K1	**-0.13192**	0.00019				1.00	-0.96	0.90	-0.02	-0.02
K2	**0.173205**	0.0014					1.00	-0.98	0.01	-0.01
K3	**-0.0330062**	0.0029						1.00	-0.00	0.01
P1	**0.000719381**	9.1e-06							1.00	-0.07
P2	**0.00194493**	8.7e-06								1.00

Table 2. Calibration coefficients and correlation matrix.

Scale Bars

Label	Distance (m)	Error (m)
target 17_target 19	1.00062	8.26293e-05
target 28_target 30	0.500393	9.30031e-05
target 23_target 24	0.249577	-0.000522709
Total		**0.000310216**

Table 3. Control scale bars.

Digital Elevation Model

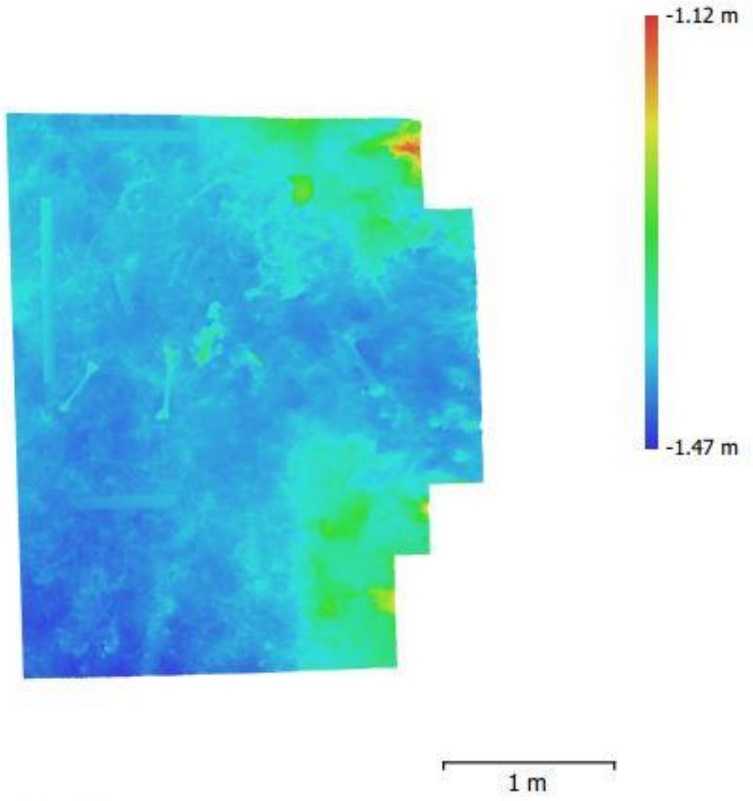

Fig. 3. Reconstructed digital elevation model.

Resolution:	unknown
Point density:	unknown

Processing Parameters

General	
Cameras	129
Aligned cameras	129
Markers	13
Scale bars	3
Coordinate system	Local Coordinates (m)
Rotation angles	Yaw, Pitch, Roll
Point Cloud	
Points	80,646 of 292,342
RMS reprojection error	0.147723 (0.627072 pix)
Max reprojection error	0.475088 (3.51893 pix)
Mean key point size	4.08055 pix
Point colors	3 bands, uint8
Key points	No
Average tie point multiplicity	2.83917
Alignment parameters	
Accuracy	High
Generic preselection	No
Key point limit	60,000
Tie point limit	0
Adaptive camera model fitting	No
Matching time	1 hours 19 minutes
Alignment time	9 minutes 51 seconds
Optimization parameters	
Parameters	f, cx, cy, k1-k3, p1, p2
Optimization time	7 seconds
Dense Point Cloud	
Points	33,371,110
Point colors	3 bands, uint8
Reconstruction parameters	
Quality	High
Depth filtering	Aggressive
Depth maps generation time	4 hours 38 minutes
Dense cloud generation time	13 hours 51 minutes
Model	
Faces	3,573,347
Vertices	1,790,581
Vertex colors	3 bands, uint8
Texture	8,192 x 8,192, 4 bands, uint8
Reconstruction parameters	
Surface type	Arbitrary
Source data	Dense
Interpolation	Enabled
Quality	High
Depth filtering	Aggressive
Face count	6,674,218
Processing time	31 minutes 27 seconds
Texturing parameters	
Blending mode	Mosaic
Texture size	8,192 x 8,192
Enable color correction	No
Enable hole filling	Yes
UV mapping time	18 minutes 4 seconds
Blending time	3 minutes 11 seconds
Orthomosaic	

Size	8,165 x 9,730
Coordinate system	Local Coordinates (m)
Colors	3 bands, uint8
Reconstruction parameters	
Blending mode	Mosaic
Surface	Mesh
Enable hole filling	Yes
Processing time	11 minutes 12 seconds
Software	
Version	1.4.2 build 6205
Platform	Windows 64

Small Scatter 2

Processing Report
03 June 2018

Survey Data

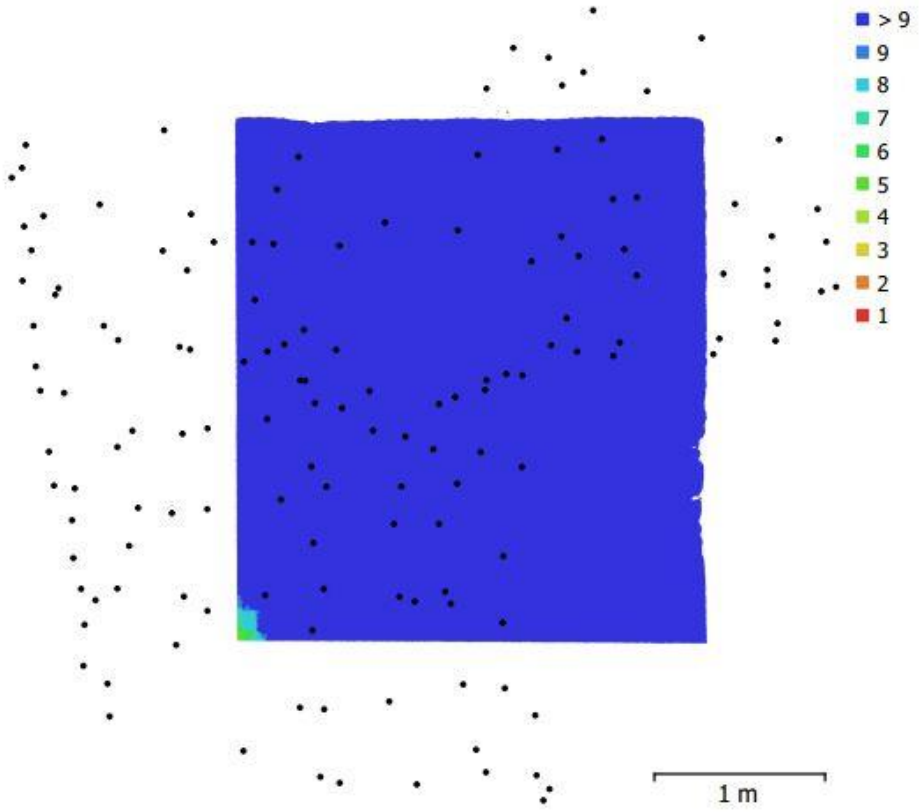

Fig. 1. Camera locations and image overlap.

Number of images:	146	Camera stations:	145
Flying altitude:	1.82 m	Tie points:	89,796
Ground resolution:	0.336 mm/pix	Projections:	208,463
Coverage area:	8.38 m²	Reprojection error:	0.309 pix

Camera Model	Resolution	Focal Length	Pixel Size	Precalibrated
Canon EOS REBEL T5 (23 mm)	5184 x 3456	23 mm	4.4 x 4.4 µm	No

Table 1. Cameras.

Camera Calibration

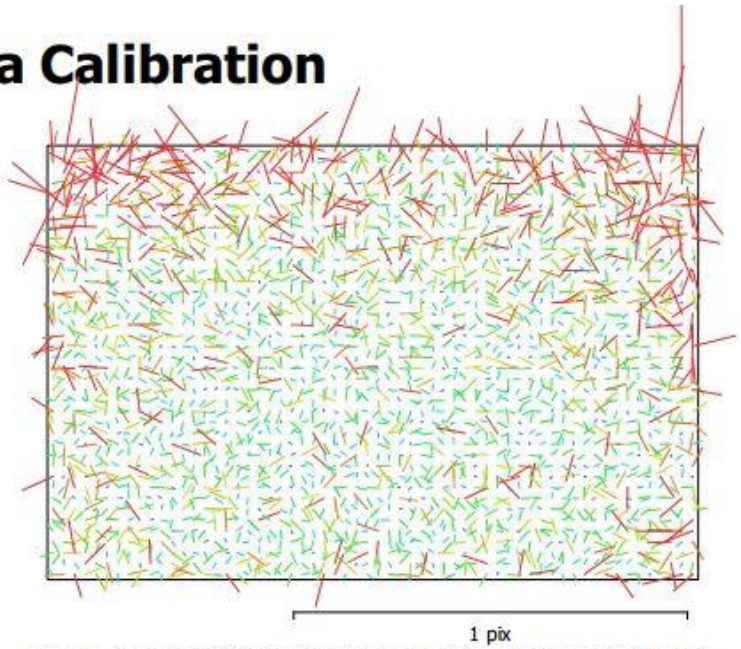

Fig. 2. Image residuals for Canon EOS REBEL T5 (23 mm).

Canon EOS REBEL T5 (23 mm)

146 images

Type	Resolution	Focal Length	Pixel Size
Frame	**5184 x 3456**	**23 mm**	**4.4 x 4.4 µm**

	Value	Error	F	Cx	Cy	B1	B2	K1	K2	K3	K4	P1	P2	P3	P4
F	**5415.39**	0.32	1.00	0.03	-0.43	-0.29	-0.04	-0.08	0.12	-0.10	0.09	0.03	0.03	-0.06	0.03
Cx	**-50.6608**	0.18		1.00	0.01	0.01	0.44	-0.02	0.02	-0.02	0.03	0.89	-0.01	0.02	-0.01
Cy	**36.9575**	0.14			1.00	-0.13	0.09	-0.04	-0.02	0.03	-0.03	0.04	0.47	-0.10	0.09
B1	**0.649641**	0.071				1.00	-0.08	0.03	-0.02	0.01	-0.00	-0.02	0.04	-0.08	0.07
B2	**-2.02467**	0.087					1.00	0.03	-0.02	0.02	-0.01	0.17	-0.07	0.07	-0.04
K1	**-0.136679**	0.00027						1.00	-0.96	0.91	-0.85	-0.05	-0.11	0.10	-0.09
K2	**0.203386**	0.003							1.00	-0.98	0.95	0.04	0.06	-0.08	0.08
K3	**-0.129803**	0.014								1.00	-0.99	-0.03	-0.03	0.05	-0.04
K4	**0.119064**	0.021									1.00	0.03	0.00	-0.01	0.01
P1	**0.000175633**	7e-06										1.00	0.13	-0.15	0.13
P2	**0.00183446**	1.4e-05											1.00	-0.82	0.73
P3	**0.228452**	0.063												1.00	-0.97
P4	**0.184191**	0.16													1.00

Table 2. Calibration coefficients and correlation matrix.

Scale Bars

Label	Distance (m)	Error (m)
target 31_target 32	0.250248	0.000177864
target 23_target 24	0.251188	0.00108795
target 28_target 30	0.499716	-0.00058375
target 17_target 19	1.00051	-2.65329e-05
Total		**0.000623845**

Table 3. Control scale bars.

Digital Elevation Model

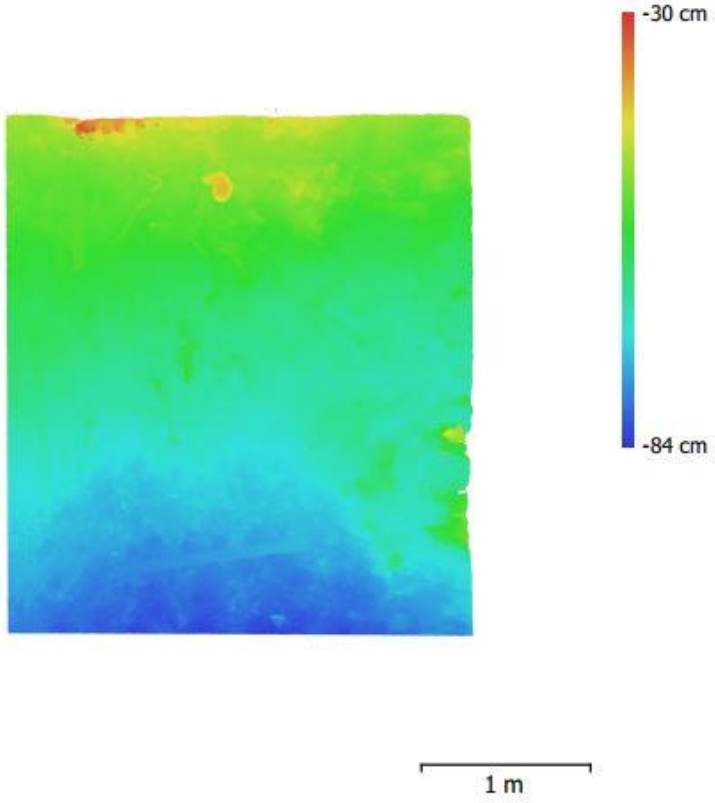

Fig. 3. Reconstructed digital elevation model.

Resolution:	unknown
Point density:	unknown

Processing Parameters

General	
Cameras	146
Aligned cameras	145
Markers	16
Scale bars	4
Coordinate system	Local Coordinates (m)
Rotation angles	Yaw, Pitch, Roll
Point Cloud	
Points	89,796 of 467,186
RMS reprojection error	0.0790753 (0.308753 pix)
Max reprojection error	0.217098 (1.25557 pix)
Mean key point size	3.80418 pix
Point colors	3 bands, uint8
Key points	No
Average tie point multiplicity	2.80357
Alignment parameters	
Accuracy	High
Generic preselection	Yes
Key point limit	60,000
Tie point limit	0
Adaptive camera model fitting	No
Matching time	18 minutes 43 seconds
Alignment time	12 minutes 39 seconds
Optimization parameters	
Parameters	f, b1, b2, cx, cy, k1-k4, p1-p4
Optimization time	7 seconds
Dense Point Cloud	
Points	30,357,242
Point colors	3 bands, uint8
Reconstruction parameters	
Quality	High
Depth filtering	Aggressive
Depth maps generation time	50 minutes 9 seconds
Dense cloud generation time	3 days 2 hours
Model	
Faces	5,130,612
Vertices	2,569,086
Vertex colors	3 bands, uint8
Texture	8,192 x 8,192, 4 bands, uint8
Reconstruction parameters	
Surface type	Arbitrary
Source data	Dense
Interpolation	Enabled
Quality	High
Depth filtering	Aggressive
Face count	6,071,448
Processing time	1 hours 39 minutes
Texturing parameters	
Blending mode	Mosaic
Texture size	8,192 x 8,192
Enable color correction	No
Enable hole filling	Yes
UV mapping time	1 hours 17 minutes
Blending time	23 minutes 1 seconds
Orthomosaic	

Size	8,337 x 9,468
Coordinate system	Local Coordinates (m)
Colors	3 bands, uint8
Reconstruction parameters	
Blending mode	Mosaic
Surface	Mesh
Enable color correction	No
Enable hole filling	Yes
Processing time	27 minutes 16 seconds
Software	
Version	1.4.2 build 6205
Platform	Windows 64

Wide Scatter 1

Processing Report
03 June 2018

Survey Data

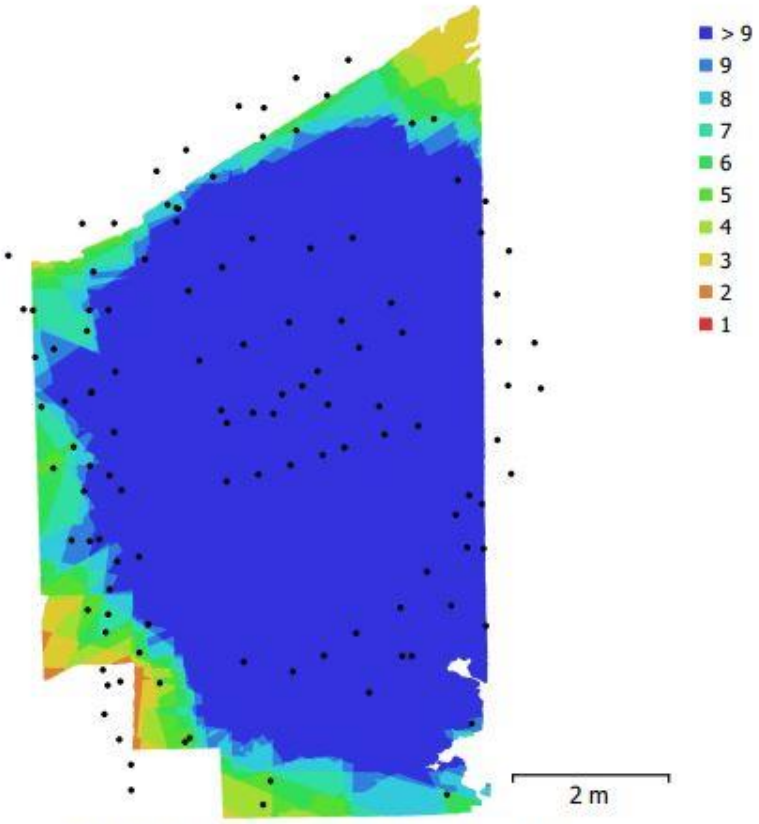

Fig. 1. Camera locations and image overlap.

Number of images:	123	Camera stations:	120
Flying altitude:	2.64 m	Tie points:	64,498
Ground resolution:	0.486 mm/pix	Projections:	146,347
Coverage area:	45.6 m²	Reprojection error:	0.198 pix

Camera Model	Resolution	Focal Length	Pixel Size	Precalibrated
Canon EOS REBEL T5 (23 mm)	5184 x 3456	23 mm	4.4 x 4.4 µm	No

Table 1. Cameras.

Camera Calibration

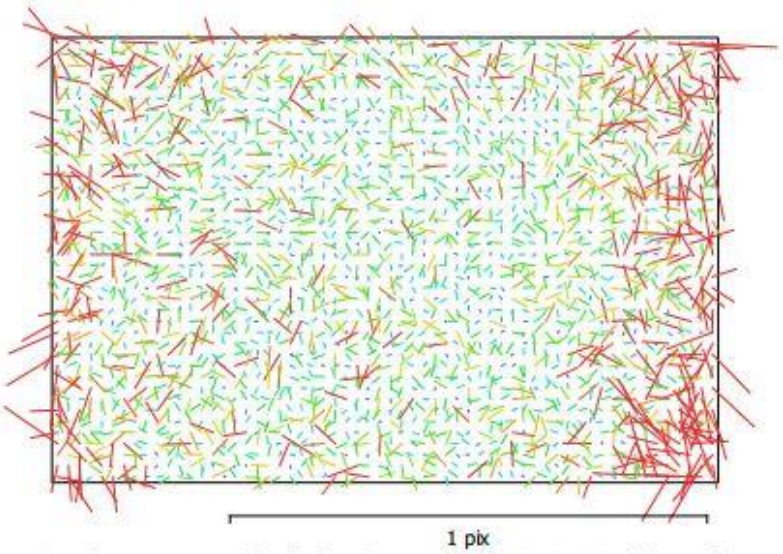

Fig. 2. Image residuals for Canon EOS REBEL T5 (23 mm).

Canon EOS REBEL T5 (23 mm)

123 images

Type	Resolution	Focal Length	Pixel Size
Frame	**5184 x 3456**	**23 mm**	**4.4 x 4.4 µm**

	Value	Error	F	Cx	Cy	K1	K2	K3	P1	P2
B1	**1.34238**									
B2	**1.39219**									
K4	**0.0658069**									
P3	**0.336463**									
P4	**-0.461414**									
F	**5433.67**	0.19	1.00	0.06	-0.07	-0.01	0.11	-0.07	-0.01	-0.05
Cx	**-30.2221**	0.086		1.00	0.04	0.02	-0.02	0.01	0.86	0.09
Cy	**39.4087**	0.074			1.00	-0.04	0.01	-0.01	0.08	0.79
K1	**-0.133406**	0.0001				1.00	-0.95	0.90	0.01	-0.04
K2	**0.191973**	0.0007					1.00	-0.98	-0.02	0.01
K3	**-0.0899878**	0.0015						1.00	0.02	-0.01
P1	**0.000765288**	4.4e-06							1.00	0.11
P2	**0.00184429**	4e-06								1.00

Table 2. Calibration coefficients and correlation matrix.

Scale Bars

Label	Distance (m)	Error (m)
target 31_target 32	0.250164	9.36462e-05
target 23_target 24	0.250089	-1.08179e-05
target 20_target 22	0.500027	-4.30031e-05
Total		**5.98217e-05**

Table 3. Control scale bars.

Digital Elevation Model

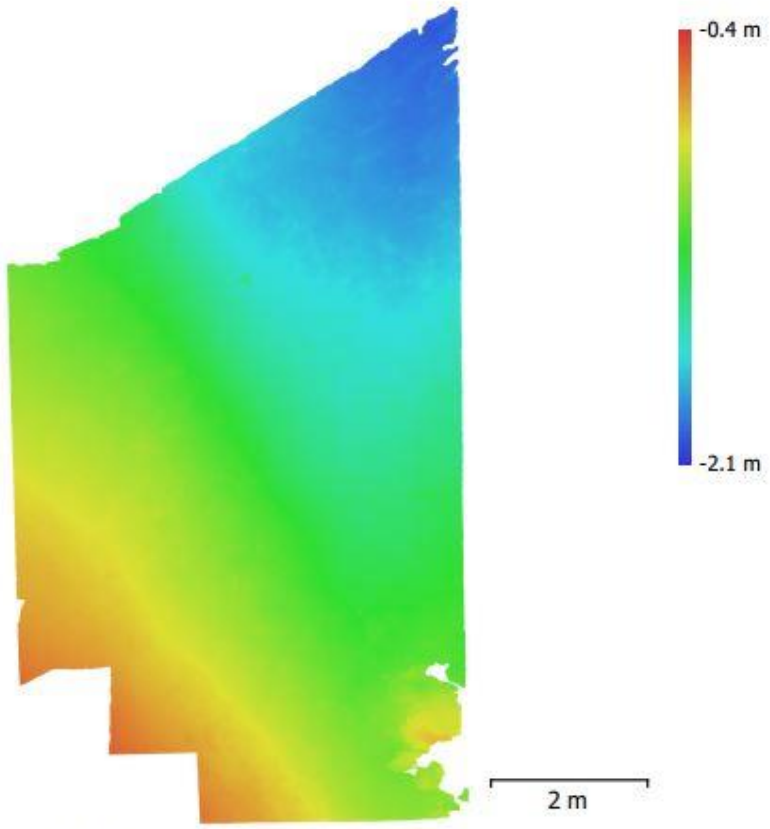

Fig. 3. Reconstructed digital elevation model.

Resolution:	unknown
Point density:	unknown

Processing Parameters

General	
Cameras	123
Aligned cameras	120
Markers	16
Scale bars	3
Coordinate system	Local Coordinates (m)
Rotation angles	Yaw, Pitch, Roll
Point Cloud	
Points	64,498 of 345,719
RMS reprojection error	0.0779446 (0.197505 pix)
Max reprojection error	0.682091 (1.2958 pix)
Mean key point size	2.49384 pix
Point colors	3 bands, uint8
Key points	No
Average tie point multiplicity	2.39841
Alignment parameters	
Accuracy	High
Generic preselection	Yes
Key point limit	60,000
Tie point limit	0
Adaptive camera model fitting	No
Matching time	7 minutes 39 seconds
Alignment time	13 minutes 31 seconds
Optimization parameters	
Parameters	f, b1, b2, cx, cy, k1-k4, p1-p4
Optimization time	10 seconds
Dense Point Cloud	
Points	54,632,356
Point colors	3 bands, uint8
Reconstruction parameters	
Quality	High
Depth filtering	Aggressive
Depth maps generation time	38 minutes 47 seconds
Dense cloud generation time	20 hours 6 minutes
Model	
Faces	9,617,641
Vertices	4,814,963
Vertex colors	3 bands, uint8
Texture	8,192 x 8,192, 4 bands, uint8
Reconstruction parameters	
Surface type	Arbitrary
Source data	Dense
Interpolation	Enabled
Quality	High
Depth filtering	Aggressive
Face count	10,926,466
Processing time	5 hours 38 minutes
Texturing parameters	
Blending mode	Mosaic
Texture size	8,192 x 8,192
Enable color correction	No
Enable hole filling	Yes
UV mapping time	2 hours 1 minutes
Blending time	30 minutes 35 seconds
Orthomosaic	

Size	12,776 x 22,220
Coordinate system	Local Coordinates (m)
Colors	3 bands, uint8
Reconstruction parameters	
Blending mode	Mosaic
Surface	Mesh
Enable color correction	No
Enable hole filling	Yes
Processing time	51 minutes 59 seconds
Software	
Version	1.4.2 build 6205
Platform	Windows 64

Wide Scatter 2

Processing Report
03 June 2018

Survey Data

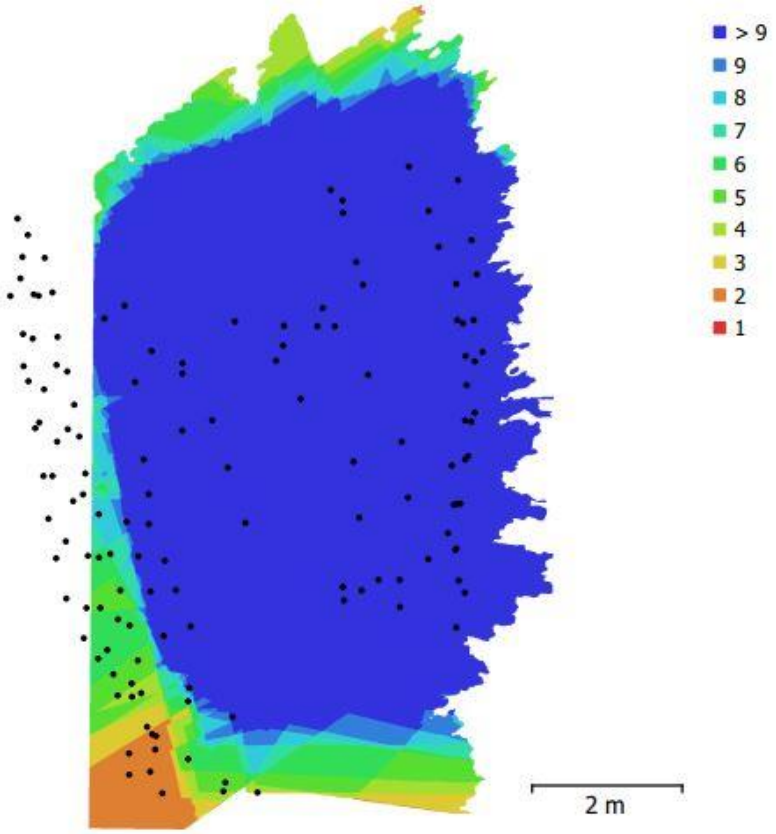

Fig. 1. Camera locations and image overlap.

Number of images:	198	Camera stations:	139
Flying altitude:	2.45 m	Tie points:	283,684
Ground resolution:	0.451 mm/pix	Projections:	619,055
Coverage area:	53.5 m²	Reprojection error:	0.366 pix

Camera Model	Resolution	Focal Length	Pixel Size	Precalibrated
Canon EOS REBEL T5 (23 mm)	5184 x 3456	23 mm	4.4 x 4.4 µm	No

Table 1. Cameras.

Camera Calibration

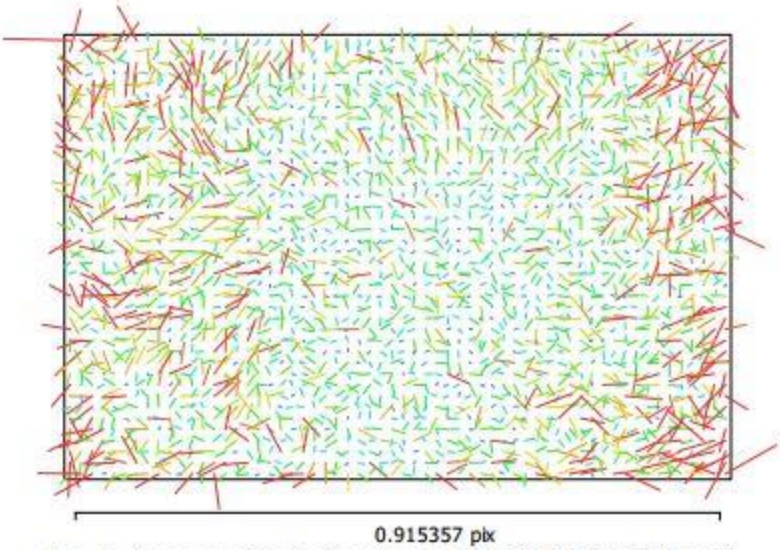

Fig. 2. Image residuals for Canon EOS REBEL T5 (23 mm).

Canon EOS REBEL T5 (23 mm)

198 images

Type	Resolution	Focal Length	Pixel Size
Frame	**5184 x 3456**	**23 mm**	**4.4 x 4.4 µm**

	Value	Error	F	Cx	Cy	B1	B2	K1	K2	K3	K4	P1	P2	P3	P4
F	5416.75	0.097	1.00	-0.04	0.02	-0.11	-0.07	-0.08	0.12	-0.11	0.10	0.00	0.03	-0.05	0.05
Cx	-35.9557	0.056		1.00	0.01	-0.23	0.42	0.04	-0.05	0.04	-0.04	0.78	0.04	-0.05	0.04
Cy	45.8942	0.05			1.00	-0.37	-0.15	-0.02	-0.00	0.01	-0.01	0.03	0.57	-0.31	0.27
B1	-0.261175	0.019				1.00	0.00	0.02	-0.01	0.01	-0.01	0.03	-0.06	0.08	-0.09
B2	2.29775	0.024					1.00	0.02	-0.02	0.02	-0.02	0.13	0.04	-0.03	0.02
K1	-0.134843	0.00011						1.00	-0.97	0.92	-0.86	0.03	-0.05	0.07	-0.07
K2	0.2149	0.0014							1.00	-0.99	0.95	-0.02	0.04	-0.07	0.07
K3	-0.18605	0.0066								1.00	-0.99	0.01	-0.04	0.07	-0.08
K4	0.188408	0.011									1.00	-0.01	0.04	-0.08	0.09
P1	0.000269793	2.5e-06										1.00	0.27	-0.29	0.25
P2	0.00182018	5.4e-06											1.00	-0.89	0.80
P3	0.574485	0.029												1.00	-0.97
P4	-1.03035	0.079													1.00

Table 2. Calibration coefficients and correlation matrix.

Scale Bars

Label	Distance (m)	Error (m)
target 31_target 32	0.250324	0.000254101
target 20_target 22	0.499121	-0.000948577
target 28_target 30	0.501118	0.00081778
Total		**0.000737819**

Table 3. Control scale bars.

Digital Elevation Model

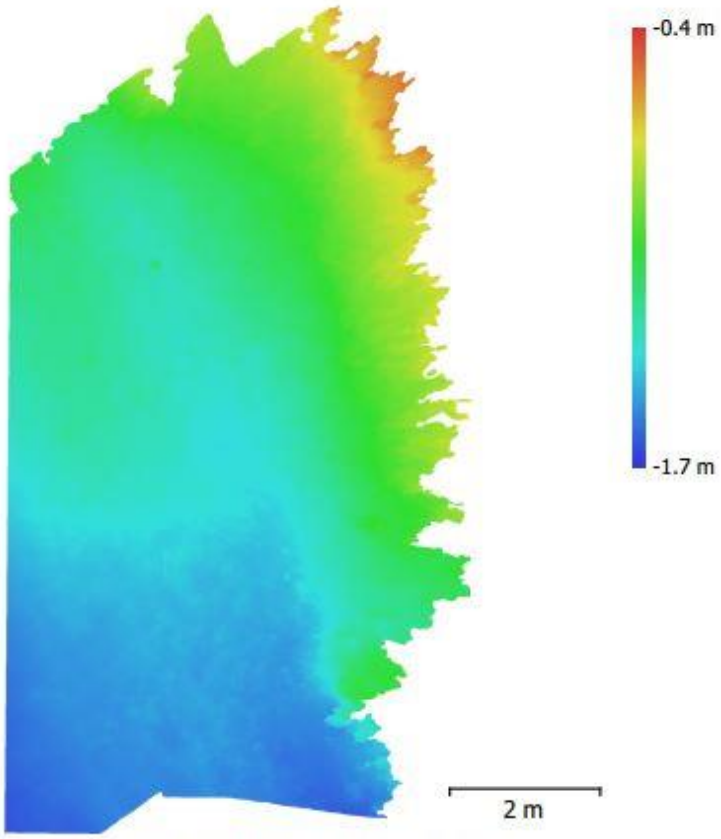

Fig. 3. Reconstructed digital elevation model.

Resolution:	unknown
Point density:	unknown

Processing Parameters

General	
Cameras	198
Aligned cameras	139
Markers	17
Scale bars	3
Coordinate system	Local Coordinates (m)
Rotation angles	Yaw, Pitch, Roll
Point Cloud	
Points	283,684 of 618,547
RMS reprojection error	0.0555378 (0.365996 pix)
Max reprojection error	0.313014 (10.6427 pix)
Mean key point size	5.54676 pix
Point colors	3 bands, uint8
Key points	No
Average tie point multiplicity	2.62459
Alignment parameters	
Accuracy	High
Generic preselection	No
Key point limit	60,000
Tie point limit	0
Adaptive camera model fitting	No
Matching time	4 hours 9 minutes
Alignment time	6 minutes 39 seconds
Optimization parameters	
Parameters	f, b1, b2, cx, cy, k1-k4, p1-p4
Optimization time	5 seconds
Dense Point Cloud	
Points	54,647,491
Point colors	3 bands, uint8
Reconstruction parameters	
Quality	High
Depth filtering	Aggressive
Depth maps generation time	3 hours 36 minutes
Dense cloud generation time	8 hours 28 minutes
Model	
Faces	999,999
Vertices	505,526
Vertex colors	3 bands, uint8
Texture	8,192 x 8,192, 4 bands, uint8
Reconstruction parameters	
Surface type	Arbitrary
Source data	Dense
Interpolation	Enabled
Quality	High
Depth filtering	Aggressive
Face count	10,929,480
Processing time	1 hours 15 minutes
Texturing parameters	
Blending mode	Mosaic
Texture size	8,192 x 8,192
Enable color correction	Yes
Enable hole filling	Yes
UV mapping time	21 minutes 52 seconds
Blending time	17 minutes 32 seconds
Software	

Version	1.4.2 build 6205
Platform	Windows 64

Wide Scatter 3

Processing Report
03 June 2018

Survey Data

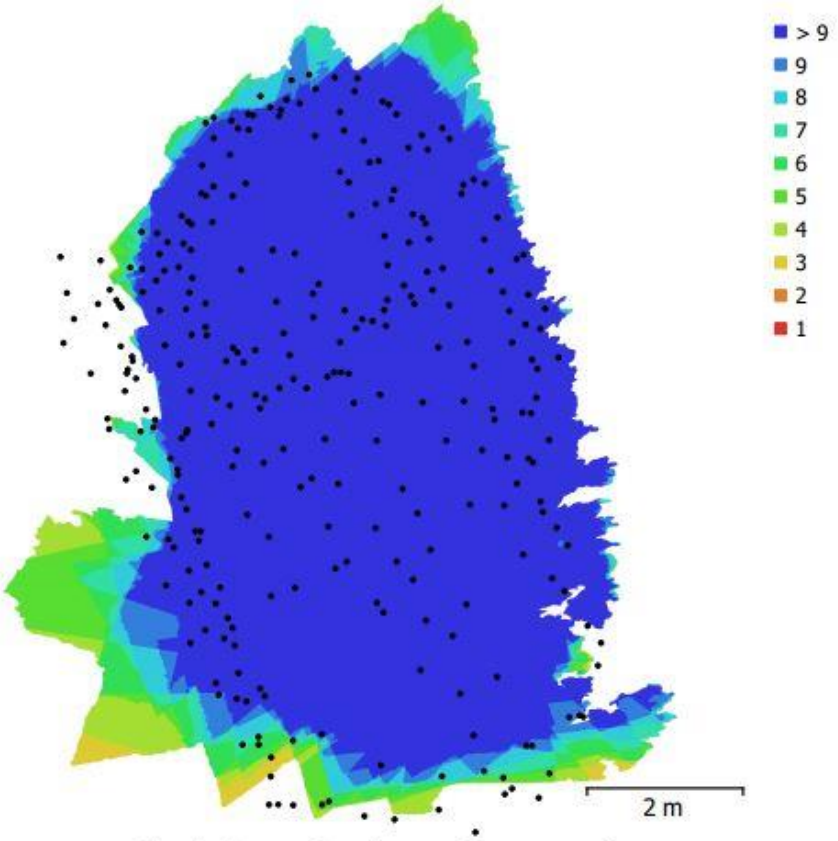

Fig. 1. Camera locations and image overlap.

Number of images:	298	Camera stations:	295
Flying altitude:	1.96 m	Tie points:	304,685
Ground resolution:	0.362 mm/pix	Projections:	706,736
Coverage area:	53.5 m²	Reprojection error:	0.332 pix

Camera Model	Resolution	Focal Length	Pixel Size	Precalibrated
Canon EOS REBEL T5 (23 mm)	5184 x 3456	23 mm	4.4 x 4.4 µm	No

Table 1. Cameras.

Scale Bars

Label	Distance (m)	Error (m)
target 28_target 30	0.500248	-5.19462e-05
target 31_target 32	0.250285	0.000214729
target 20_target 22	0.499997	-7.33838e-05
Total		**0.000134403**

Table 3. Control scale bars.

Digital Elevation Model

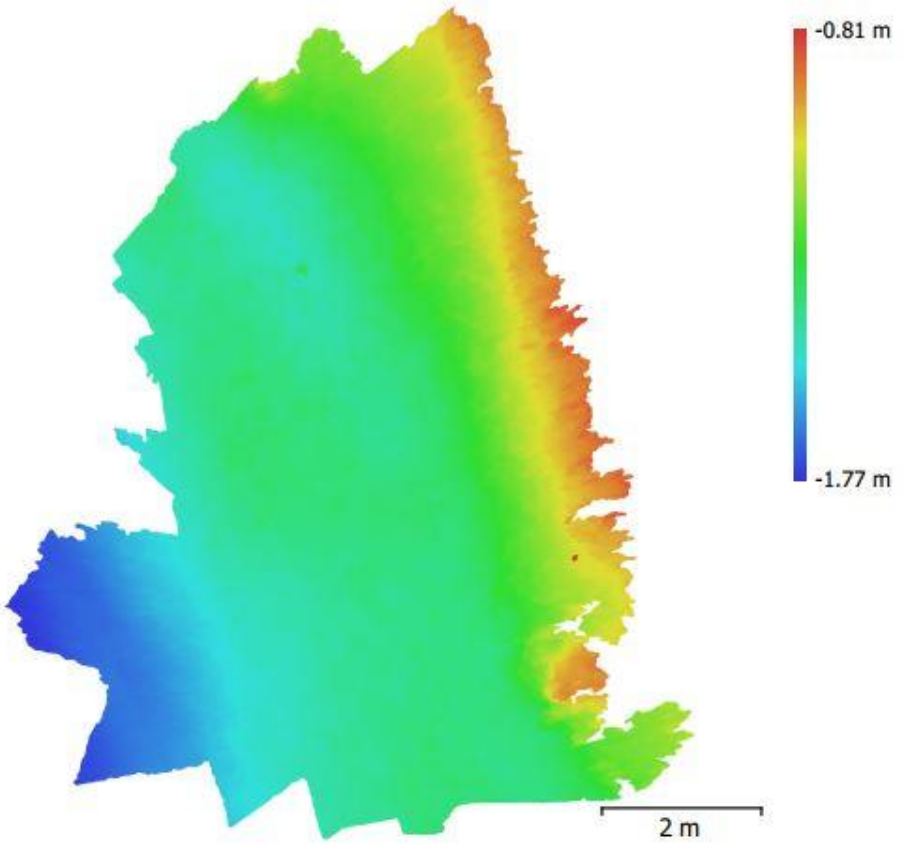

Fig. 3. Reconstructed digital elevation model.

Resolution:	unknown
Point density:	unknown

Processing Parameters

General	
Cameras	298
Aligned cameras	295
Markers	16
Scale bars	3
Coordinate system	Local Coordinates (m)
Rotation angles	Yaw, Pitch, Roll
Point Cloud	
Points	304,685 of 841,661
RMS reprojection error	0.0704679 (0.331605 pix)
Max reprojection error	0.229489 (2.0929 pix)
Mean key point size	4.51456 pix
Point colors	3 bands, uint8
Key points	No
Average tie point multiplicity	2.67914
Alignment parameters	
Accuracy	High
Generic preselection	No
Key point limit	60,000
Tie point limit	0
Adaptive camera model fitting	No
Matching time	6 hours 49 minutes
Alignment time	28 minutes 0 seconds
Optimization parameters	
Parameters	f, b1, b2, cx, cy, k1-k4, p1-p4
Optimization time	22 seconds
Dense Point Cloud	
Points	90,320,445
Point colors	3 bands, uint8
Reconstruction parameters	
Quality	High
Depth filtering	Aggressive
Depth maps generation time	1 hours 41 minutes
Dense cloud generation time	6 days 12 hours
Model	
Faces	18,064,089
Vertices	9,043,478
Vertex colors	3 bands, uint8
Texture	8,192 x 8,192, 4 bands, uint8
Reconstruction parameters	
Surface type	Arbitrary
Source data	Dense
Interpolation	Enabled
Quality	High
Depth filtering	Aggressive
Face count	18,064,089
Processing time	11 hours 12 minutes
Texturing parameters	
Blending mode	Mosaic
Texture size	8,192 x 8,192
Enable color correction	No
Enable hole filling	Yes
UV mapping time	2 hours 7 minutes
Blending time	1 hours 16 minutes
Orthomosaic	

Size	20,807 x 26,571
Coordinate system	Local Coordinates (m)
Colors	3 bands, uint8
Reconstruction parameters	
Blending mode	Mosaic
Surface	Mesh
Enable color correction	No
Enable hole filling	Yes
Processing time	1 hours 49 minutes
Software	
Version	1.4.2 build 6205
Platform	Windows 64

APPENDIX B: SKELETAL INVENTORIES

SKELETAL INVENTORY: Small Scatter Scenarios

Skull

Bone	L	R	M
Parietal	✓	✓	
Temporal	✓	✓	
Zygomatic	✓	✓	
Nasal	✓	✓	
Lacrimal	✓	✓	
Palatine	✓	✓	
Maxilla	✓	✓	
Mandible	✓	✓	
Frontal	✓	✓	
Occipital	✓	✓	
Sphenoid	✓	✓	
Ethmoid	✓	✓	
Vomer	✓	✓	
Bone	**L**	**R**	**M**
Hyoid			✓

Upper Limbs

Bone	L	R	M
Scapula	✓	✓	
Clavicle	✓	✓	
Humerus	✓	✓	
Radius	✓	✓	
Ulna	✓	✓	

Hands

Bone	L	R	M
Scaphoid			
Lunate			
Triquetral			
Pisiform			
Trapezium			
Trapezoid			
Capitate			
Hamate			
Metacarpals			
MC-1			
MC-2			
MC-3			
MC-4			
MC-5			
Phalanx			
Proximal			
Intermediate			
Distal			

Pelvis

Bone	L	R	M
Sacrum S1-S5			✓
Coccyx			
Os Coxa	✓	✓	

Sternum

Bone	L	R	M
Manubrium			✓
Sternal Body			✓
Xiphoid Process			✓

Ribs

Bone	L	R	M
R-1	✓	✓	
R-2	✓	✓	
R-3	✓	✓	
R-4	✓	✓	
R-5	✓	✓	
R-6	✓	✓	
R-7	✓	✓	
R-8	✓	✓	
R-9	✓		
R-10	✓		
R-11	✓		
R-12			

Vertebrae

Bone	L	R	M
Cervical			
C-1			✓
C-2			✓
C-3			✓
C-4			✓
C-5			✓
C-6			✓
C-7			✓
Thoracic			
T-1			✓
T-1			✓
T-2			✓
T-3			✓
T-4			✓
T-5			✓
T-6			✓
T-7			✓
T-8			✓
T-9			✓
T-10			✓
T-11			✓
T-12			✓
Lumbar			
L-1			✓
L-2			✓
L-3			✓
L-4			✓
L-5			✓

Lower Limbs

Bone	L	R	M
Femur	✓	✓	
Patella	✓	✓	
Tibia	✓	✓	
Fibula	✓	✓	

Feet

Bone	L	R	M
Calcaneus	✓		
Talus	✓		
Navicular	✓		
1st Cuneiform			
2nd Cuneiform			
3rd Cuneiform			
Cuboid			
Metatarsals			
MT-1	✓		
MT-2	✓		
MT-3	✓		
MT-4	✓		
MT-5			
Phalanx			
Proximal			
Intermediate			
Distal			

Notes
All elements, plastic teaching material.

SKELETAL INVENTORY: Wide Scatter Scenarios

Skull

Bone	L	R	M
Parietal	✓	✓	
Temporal	✓	✓	
Zygomatic	✓	✓	
Nasal	✓	✓	
Lacrimal	✓	✓	
Palatine	✓	✓	
Maxilla	✓	✓	
Mandible	✓	✓	
Frontal	✓	✓	
Occipital	✓	✓	
Sphenoid	✓	✓	
Ethmoid	✓	✓	
Vomer	✓	✓	
Bone	**L**	**R**	**M**
Hyoid			

Upper Limbs

Bone	L	R	M
Scapula	✓	✓	
Clavicle	✓	✓	
Humerus	✓	✓	
Radius	✓	✓	
Ulna	✓	✓	

Hands

Bone	L	R	M
Scaphoid			
Lunate			
Triquetral			
Pisiform			
Trapezium			
Trapezoid			
Capitate			
Hamate			
Metacarpals			
MC-1			
MC-2			
MC-3			
MC-4			
MC-5			
Phalanx			
Proximal			
Intermediate			
Distal			

Pelvis

Bone	L	R	M
Sacrum S1-S5			✓
Coccyx			
Os Coxa	✓	✓	

Sternum

Bone	L	R	M
Manubrium			✓
Sternal Body			✓
Xiphoid Process			✓

Ribs

Bone	L	R	M
R-1	✓	✓	
R-2	✓	✓	
R-3	✓		
R-4	✓		
R-5	✓	✓	
R-6	✓		
R-7	✓		
R-8	✓		
R-9	✓		
R-10	✓	✓	
R-11	✓	✓	
R-12	✓	✓	

Vertebrae

Bone	L	R	M
Cervical			
C-1			✓
C-2			✓
C-3			✓
C-4			✓
C-5			✓
C-6			
C-7			
Thoracic			
T-1			
T-1			
T-2			
T-3			
T-4			
T-5			
T-6			
T-7			
T-8			
T-9			
T-10			✓
T-11			✓
T-12			✓
Lumbar			
L-1			
L-2			
L-3			
L-4			
L-5			

Lower Limbs

Bone	L	R	M
Femur	✓	✓	
Patella			
Tibia	✓	✓	
Fibula	✓	✓	

Feet

Bone	L	R	M
Calcaneus			
Talus			
Navicular			
1st Cuneiform			
2nd Cuneiform			
3rd Cuneiform			
Cuboid			
Metatarsals			
MT-1			
MT-2			
MT-3			
MT-4			
MT-5			
Phalanx			
Proximal			
Intermediate			
Distal			

Notes
All elements, plastic teaching material.

LIST OF REFERENCES

Anderson, Richard C.
1982 Photogrammetry: The Pros and Cons for Archaeology. *World Archaeology* 14(2):200-205.

Bass, William M.
2005 *Human Osteology: A Laboratory and Field Manual, Fifth Edition*. Missouri Archaeological Society, Springfield, MO.

Berggren, Asa, Nicolo Dell'Unto, Maurizio Forte, Scott Haddow, Ian Hodder, Justine Issavi, Nicola Lercari, Camilla Mazzucato, Allison Mickel, and James S. Taylor
2015 Revisiting Reflexive Archaeology at Catalhoyuk: Integrating Digital and 3D Technologies at the Trowel's Edge. Antiquity 89(344): 433-448.

Blau, Soren and Douglas H. Ubelaker (editors)
2009 *Handbook of Forensic Archaeology and Anthropology*. Left Coast Press, Walnut Creek, California.

Bolognesi, M., A. Furini, V. Russo, A. Pellegrinelli, and P. Russo
2014 Accuracy of cultural heritage 3D models by rpas and terrestrial photogrammetry. ISPRS Technical Commission V Symposium, 23-35 June 2014, Riva Del Garda, Italy.

Buck, Ursula, Silvio Naether, Beat Rass, Christian Jackowski, and Michael J. Thali
2013 Accident or Homicide-Virtual Crime Scene Reconstruction Using 3D Methods. *Forensic Science International* 225: 75-84.

Buikstra, Jane E. and Douglas H. Ubelaker (editors)
1994 *Standards for Data Collection From Human Skeletal Remains*. Arkansas Archeological Survey Research Series No. 44, Fayetville, AR.

Byers, Steven N.
2011 *Introduction to Forensic Anthropology*, Fourth Edition. Prentice Hall, Upper Saddle River, NJ.

Caroti, G. I. Martinez-Espejo Zaragoza, A. Piemonte
2015 Accuracy Assessment in Structure From Motion 3D Reconstruction from UAV-Born Images: The Influence of the Data Processing Methods. The International Archives of the Photogrammetry, Remote Sensing and Spatial Information Sciences, Volume XL-1/W4:103-109.

Committee on Identifying the Needs of the Forensic Sciences Community, National Research Council
2009 Strengthening Forensic Science in the United States: A Path Forward. National Research Council.

Connor, Melissa A.
2007 *Forensic Methods: Excavation for the Archaeologist and Investigator*. Altamira Press, Lanham, MD.

Constantino, D., M.G. Angelini, and F. Mazzone
2016 Integrated Survey Methodology for the Crime Reconstruction. *The Imagine Science Journal* 64(6): 341-351.

De Reu, Jeroen, Philippe De Smedt, Davy Herremans, Marc Van Meirvenne, Pieter Laloo, and Wim De Clercq
2014 On Introducing an Image-Based 3D Reconstruction Method in Archaeological Excavation Practice. *Journal of Archaeological Science* 41:251-262.

Dirkmaat, Dennis C. and James M. Adovasio
1997 The Role of Archaeology in the Recovery and Interpretation of Human Remains from an Outdoor Forensic Setting. In *Forensic Taphonomy: The Postmortem Fate of Human Remains*, W.D. Haglund and M.H. Sorg, editors, pp. 39-64. CRC Press, Boca Raton, FL.

Dirkmaat, Dennis C., Luis L. Cabo, Stephen D. Ousley, and Steven A. Symes
2008 New Perspectives in Forensic Anthropology. *Yearbook of Physical Anthropology* 51:33-52.

Dirkmaat, Dennis C.
2012 Documenting Context at the Outdoor Crime Scene: Why Bother? In *A Companion to Forensic Anthropology*, Dennis C. Dirkmaat, editor, pp. 49-65. Wiley-Blackwell, UK.

Doneus, Michael, Geert J. Verhoeven, Martin Fera, C. Briese, Mathias Kucera, and Wolfgang Neubauer
2011 From Deposit to Point Cloud-A Study of Low-cost Computer Vision Approaches for the Straighforward Documentation of Archaeological Excavations. *Geoinformatics* 6:81-88.

Douglass, Matthew, Sam Lin, and Michael Chodoronek
2015 The Application of 3D Photogrammetry for In-Field Documentation of Archaeological Features. *Advances in Archaeological Practice* 3(2):136-152.

Dupras, Tosha L. and John J. Schultz
2008 The Contribution of Forensic Archaeology to Homicide Investigations. Homicide Studies 12(4): 399-413.

Dupras, Tosha L., John J. Schultz, Sandra M. Wheeler, and Lana J. Williams
2012 *Forensic Recovery of Human Remains: Archaeological Approaches*. CRC Press, Boca Raton, FL.

Ebert, Lars Chr., Michael J. Thali, and Steffen Ross
2011 Getting in Touch-3D Printing in Forensic Imaging. *Forensic Science International* 211: 1-6.

Forte, Maurizio
2014 3D Archaeology: New Perspectives and Challenges-The Example of Çatalhöyük. *Journal of Eastern Mediterranean Archaeology* 2(1): 1-29.

Fourie, Zacharias, Janalt Damstra, Peter O. Gerrits, and Yijin Ren
2010 Evaluation of Anthropometric Accuracy and Reliability Using Different Three-Dimensional Scanning Systems. *Forensic Science International* 207: 127-134.

Galeazzi, Fabrizio
2016 Towards the Definition of Best 3D Practices in Archaeology: Assessing 3D Documentation Techniques for Intra-Site Data Recording. *Journal of Cultural Heritage* 17:159-169.

Green, Susie, Andrew Bevan, and Michael Shapland
2014 A Comparative Assessment of Structure From Motion Methods for Archaeological Research. *Journal of Archaeological Science* 45:173-181.

Hołowko, Elwira, Januszkiewicz Kamil, Bolewicki Paweł, Sitnik Robert, and Michoński Jakub
2016 Application of Multi-Resolution 3D Techniques in Crime Scene Documentation with Bloodstain Pattern Analysis. *Forensic Science International*.

Hoshower, Lisa M.
1998 Forensic Archeology and the Need for Flexible Excavation Strategies: A Case Study. *Journal of Forensic Sciences* 43:53-56.

Howland, Mathew D., Falko Kuester, and Thomas E. Levy
2014 Structure from Motion: Twenty-First Century Field Recording with 3D Technology. *Near Eastern Archaeology* 77(3): 187-191.

Ioannides, Marinos, Nadia Magnenat-Thalmann, Eleanor Fink, Roko Žarnić, Alex-Yianing Yen, and Ewald Quak (editors)
2014 *Progress in Cultural Heritage: Documentation, Preservation, and Protection*. Springer International Publishing, Switzerland.

Kerley, Ellis R.
1978 Recent Developments in Forensic Anthropology. *Yearbook of Physical Anthropology* 21:160-173.

Kettner, Mattias, Peter Schmidt, Stefan Potente, Frank Ramsthaler, and Michael Schrodt
2011 Reverse Engineering-Rapid Prototyping of the Skull in Forensic Trauma Analysis. *Journal of Forensic Science* 54(4): 1015-1017.

Komar, Debra A., Stephanie Davy-Jow, Summer J. Decker
2012 The Use of a 3D Laser Scanner to Document Ephemeral Evidence at Crime Scenes and Postmortem Examinations. *Journal of Forensic Science* 57(1): 188-191.

Kuzminsky, Susan C. and Megan S. Gardiner
2012 Three-Dimensional Laser Scanning: Potential Uses for Museum Conservation and Scientific Research. *Journal of Archaeological Science* 39(8): 2744-2751.

Kuziminsky, Susan C., Omar Reyes Baez, Bernardo Arriaza, Cesar Mendez, Vivien G. Standen, Manuel San Roman, Ivan Munoz, Angel Duran Herrera, and Mark Hubbe
2017 Investigating Cranial Morphological Variation of Early Human Skeletal Remains from Chile: A 3D Geometric Morphometric Approach. American Journal of Physical Anthropology 165:223-237.

Lewis, Krystle, Daniel J. Wescott, Eugene J. Robinson, John Buell, and Michael Josephs
2017 Mapping Surface Scatter of Scavenged Human Remains Using Drone Aerial Photography. *Proceedings of the American Academy of Forensic Sciences* 23: 211.

López, J.A. Benavides, G. Aranda Jiménez, M Sanchez Romero, E. Alarcón García, S. Fernandez Martín, A Lozano Medina, and J.A. Esquivel Guerrero
2016 3D Modelling in Archaeology: The Application of Structure from Motion Methods to the Study of the Megalithic Necropolis of Panoria (Granada, Spain). *Journal of Archaeological Science*, Reports 10: 495-506.

Lovis, W.A.
1992 Forensic Archaeology as Mortuary Anthropology. *Social Sciences and Medicine* 34(2): 113-117.

Mathews, Neffra A.
2008 *Aerial and Close-Range Photogrammetric Technology: Providing Resource Documentation, Interpretation, and Preservation*. U.S. Department of the Interior, Bureau of Land Management, Denver, CO.

Milliet, Quentin, Olivier Delémont, and Pierre Margot
2014 A Forensic Science Perspective on the Role of Images in Crime Investigation and Reconstruction. *Science and Justice* 54:470-480.

Morgan, Colleen and Holly Wright
2018 Pencils and Pixels: Drawing and Digital Media in Archaeological Field Recording. Journal of Field Archaeology 43(2):136-151.

Morse, Dan, Jack Duncan, and James Stoutamire
1983 *Handbook of Forensic Archaeology and Anthropology*. Rose Printing Co., Tallahassee, FL.

National Research Council
2009 Strengthening Forensic Science in the United States: A Path Forward. Washington, DC. The National Academics Press. https://doi.org/10.17226/12589.

Opitz, Rachel
2015 Three Dimensional Field Recording in Archaeology: An Example from Gabii. In *Visions of Substance: 3D Imaging in Meditteranean Archaeology*, Brandon R. Olson and William Craher, editors, pp 73-87. The Digital Press @ The University of North Dakota, Grand Forks, ND.

Opitz, Rachel and W. Fred Limp
2015 Recent Developments in High-Density Survey and Measurement (HDSM) for Archaeology: Implications for Practice and Theory. *Annual Review of Anthropology* 44:347-364.

Prins, Adam B.
2016 3D Modeling for Archaeological Documentation Using the JVRP Method to Record Archaeological Excavations with Millimeter Accuracy. JVRP White Papers in Archaeological Technology.

Agisoft
2017 Agisoft Photoscan Professional Edition User Manual, Agisoft Downloads < http://www.agisoft.com/downloads/user-manuals/>. Accessed 4 April 2017.

Remondino, Fabio and Stefano Campana (editors)
2014 3*D Recording and Modelling in Archaeology and Cultural Heritage: Theory and Best Practices*. BAR International Series 2598.

Robinson, Edward M.
2012 *Crime Scene Photography, Second Edition*. Elsevier Press, Burlington, MA.

Sansoni, Giovanna, Cristina Cattaneo, Marco Trebeschi, Danielle Gibelli, Davide Porta, and Massimo Picozzi
2009 Feasibility of Contactless 3D Optical Measurement for the Analysis of Bone and Soft Tissue Lesions: new Technologies and Perspectives in Forensic Sciences. *Journal of Forensic Science* 54(3): 541-545.

Sapirstein, Philip
2016 Accurate Measurement with Photogrammetry at Large Sites. *Journal of Archaeological Science* 66:137-145.

Sapirstein, Philip and Sarah Murray
2017 Establishing Best Practices for Photogrammetric Recording During Archaeological Fieldwork. Journal of Field Archaeology 42(4):337-350.

Schultz, John J.
2012 The Application of Ground-Penetrating Radar for Forensic Grave Detection. In *A Companion to Forensic Anthropology*, Dennis C. Dirkmaat, editor, pp. 85-100.

Sigler-Eisneberg, Brenda

1985 Forensic Research: Explaining the Concept of Applied Archaeology. *American Antiquity* 50(3): 650-655.

Simons, Daniel J. and Christopher Chabris
1999 Gorillas in Our Midst: Sustained Inattentional Blindness for Dynamic Events. *Perception* 28:1059-1074.

Skinner, Mark, Djordje Alempijevic, Marija Djuric-Srejic
2003 Guidelines for International Forensic Bio-archaeology Monitors of Mass Grave Exhumations. *Forensic Science International* 134: 81-92.

Thali, Michael J., Marcel Braun, and Richard Dirnhofer
2003 Optical 3D Surface Digitizing in Forensic Medicine: 3D Documentation of Skin and Bone Injuries. *Forensic Science International* 137: 203-208.

Urbanová, Petra, Mikolas Jurda, Tomáš Vojtišek, and Jan Krajsa
2017 Using Drones for 3D On-Site Body Documentation-Experiments Inspired by Real-Life Forensic Cases. *Proceedings of the American Academy of Forensic Sciences* 23: 753.

USDA Web Soil Survey
2018 (https://websoilsurvey.nrcs.usda.gov/app/)

Volk, M.I., T.S. Hoctor, B.B. Nettles, R. Hilsenbeck, F.E. Putz, and J. Oetting
2017 Florida land use and land cover change in the past 100 years. In E.P. Chassignet, J.W. Jones, V. Misra, and J. Obeysekera (Eds.), Florida's climate: Changes, variations and impacts (pp. 51-82). Gainesville, FL: Florida Climate Institute.

Wallace, Colin
2017 Retrospective Photogrammetry in Greek Archaeology. *Studies in Digital Heritage* 1(2):507-626.

Walter, Brittany S. and John J. Schultz
2013 Mapping Simulated Scenes with Skeletal Remains Using Differential GPS in Open Environments: An Assessment of Accuracy and Practicality. *Forensic Science International* 228: 33-46.

Wolf, Paul R.
1983 Elements of Photogrammetry, Second Edition. McGraw Hill International.